Time Reparametrization Symmetry and Spatial-Temporal Fluctuations in Glasses

A dissertation presented to

the faculty of

the College of Arts and Sciences of Ohio University

In partial fulfillment

of the requirements for the degree

Doctor of Philosophy

Gcina A. Mavimbela

December 2012

© 2012 Gcina A. Mavimbela. All Rights Reserved.

This dissertation titled

Time Reparametrization Symmetry and Spatial-Temporal Fluctuations in Glasses

by

GCINA A. MAVIMBELA

has been approved for

the Department of Physics and Astronomy

and the College of Arts and Sciences by

Horacio E. Castillo

Associate Professor of Physics

Robert Frank

Dean, College of Arts and Sciences

A

MAVIMBELA, GCINA A., Ph.D., December 2012, Physics

Time Reparametrization Symmetry and Spatial-Temporal Fluctuations in Glasses (106 pp.)

Director of Dissertation: Horacio E. Castillo

In this dissertation we focus on the dynamics of glasses and other complex systems. Dynamical heterogeneity, initially proposed to explain non exponential relaxation, has been found in simulations and experiments of glassy systems. The origin of dynamical heterogeneity remains poorly understood, despite growing evidence that glass dynamics is heterogeneous. There is no consensus in the glass community on any one of the proposed theories that explains the phenomenon. Over the last decade a theoretical framework has been proposed, based on the presence of Goldstone modes associated with a broken time reparametrization symmetry in the long time dynamics of glasses. The symmetry has been shown to be present in the Edwards-Anderson model of spin glasses and in the mean field equations of p-spin models.

We study time reparametrization symmetry in p-spin models of arbitrary interaction range. Starting from the Martin-Siggia-Rose generating functional, we analytically probe the long-time dynamics by performing a renormalization group analysis where we systematically integrate over short-time scale fluctuations. We find three families of stable fixed points. The fixed points in two of these families are not time reparametrization invariant, while one family, corresponding to the low temperature dynamics, is made up of time reparametrization invariant fixed points. We hint at the possibility of doing a similar analysis on structural glasses, given the connection between p-spin models and structural glasses.

We then investigate fluctuating local phases and fluctuating local relaxation times in structural glasses. The presence of fluctuating local relaxation times, $\tau_{\neq}(t)$ has been used

for some time as a conceptual tool to describe dynamical heterogeneities in glass-forming systems. However, until now no general method is known to extract the full space and time dependent $\tau_{\vec{r}}(t)$ from experimental or numerical data. Here we introduce a new method for determining the local phase field, $\phi_{\vec{r}}(t) \equiv \int^t \frac{dt'}{\tau_{\vec{r}}(t')}$ from snapshots $\{\vec{r}(t_i)\}_{i=1...M}$ of the positions of the particles in a system, and we apply it to extract $\phi_{\vec{r}}(t)$ and $\tau_{\vec{r}}(t)$ from numerical simulations. By studying how the phase field depends on the number of snapshots, we find that it is a well defined quantity. By studying fluctuations of the phase field, we find that they describe heterogeneities well at long distance scales. We find non Gaussian distribution functions of the time derivatives of $\phi_{\vec{r}}(t)$, with more deviation from the Gaussian form in an aging system, which is at a lower temperature, than in an equilibrium system. We find power spectra that are fitted by a Lorentzian form for an equilibrium system and are fitted by a power law in an aging system.

To my Mother and Father

A

I would like to thank my advisor, Prof. H. E. Castillo, who has provided continual guidance throughout the development of the work in this dissertation. Without his constant encouragement and advice this work would not have been possible. His concern for my well being made my stay in Athens more comfortable.

I am thankful to my dissertation committee members, Profs. David Drabold, Daniel Phillips and Jeffrey Rack for making time, even when schedules were conflicting, to evaluate my work and progress.

I am thankful to all my professors in the Physics department for the knowledge I have gained during my stay. I am also thankful to the staff for being so helpful with my administrative and technical needs.

To my friends Dr. Reuben S. Dlamini and Vusi Magagula, thank you for being the brothers I can rely on. To my friend Bose Maposa, thank you for making sure I still had a reliable sister when my brothers left. And to all my friends thank you for making my stay in Athens worthwhile.

I am thankful for being a member of wonderful family. To my brother Mduduzi and his wife, thank you for constantly reminding me I have a family back home. To my father, it is with great joy that I look back and realize that your hard work was for something bigger than anyone could have imagined. I am honored by great memories of my late mother who made sure I went to the best schools the family could afford.

T C

Page

L T

L F

Figure Page

L A

MCT: Mode Coupling Theory
TTI: Time Translation Invariance
KWW: Kolrausch-William-Watts
PEL: Potential Energy Landscape
FA: Fredrickson-Andersen
AG: Adam-Gibbs
CRR: Cooperatively Rearranging Region
RFOT: Random First Order Transition
SK: Sherrington-Kirkpatrick
EA: Edwards-Anderson
MSR: Martin-Siggia-Rose
RG: Renormalization Group
TRS: Time Reparametrization Symmetry
PDF: Probability Distribution Function

1 I

The glassy state is a common feature in nature and technology [1, 2, 3]. Volcanic glass, used by Native Americans in making arrows, is one example of naturally occuring glass [1, 2]. In Astrophysics, it has been suggested that most of the water in the universe may exist as a glass that forms by condensation of the gaseous state at very low temperatures [2, 4]. Also, glass formation (virtrification) and the glassy state are critical to the preservation of living organisms, under extreme conditions, by slowing metabolism [5]. Knowledge of how nature preserves life through the glass state is used in the stabilization of labile biochemicals and the preservation of food [2, 5]. The most widely known example of a glass, window glass, is an engineered amorphous solid made up of mostly sand, lime and soda (silica) [3]. Other exapmles of glasses in technology include plastics, which have a variety of uses, and highly purified silica, which is used in the manufacturing of optical fibers. Amorphous metallic alloys (metallic glasses) are technologically important because of their soft magnetism and corrosion resistance [6].

Most of the fabrication techniques and uses of glass materials derive from empirical observations of glasses at macroscopic sizes [2]. The variety of current uses for glasses, as well as prospective uses in the future, can be greatly enhanced by understanding how the underlying microscopic dynamics gives rise to the observed macroscopic properties [2, 8, 9]. A comprehensive theory to connect microscopic and macroscopic properties remains elusive [8]. Theoretical frameworks that have been established can only describe well some aspects of glasses and there is no consensus on any one theory [9]. In this work we are concerned with properties observed in the relaxation of materials that are either close to or below the glass transition temperature. In particular, our main focus is on *dynamical heterogeneity*.

Glasses are characterized by disorder and slow dynamics [1, 2, 3, 8, 9]. The disorder manifests itself in different forms: structural disorder for structural glasses and colloidal

glasses [1]; frustrated spin orientation disorder in spin glasses [10]. As the temperature is lowered, the slowing down of the dynamics is captured by an increasing relaxation time, i.e the typical time for significant changes in the physical observables that probe the dynamics of the glass [1]. In the following sections, we give a brief discussion of the phenomenology associated with glasses. We focus our discusion on structural glass formers and discuss spin glasses in a dedicated section at the end of the Introduction.

1.1 The Glass Transition

A structural glass is a disordered solid (a solid with no crystalline order), charecterized by out of equilibrium dynamics [1, 2, 3, 8, 9]. It can be viewed as a liquid that has lost its ability to flow, because there are only modest structural changes during the transition from a liquid to a glass [1, 8]. There are many ways for making a structural glass. There are methods which start from a crystalline state, such as: cold compression of crystals; cold decompression of high-pressure stable crystals; as well as shock, irradiation and intense grinding of a crystal [2]. In addition to crystal to glass methods, there are gas to glass methods, which include vapor deposition and chemical vapor deposition [2]. Lastly, there are liquid to glass methods, which include cooling a liquid fast enough to avoid crystallization, and solvent evaporation of a solution in which a glass former is dissolved [2]. Rapid cooling of a liquid is the most common of these methods.

The right panel of Fig. (1.1) shows the change in volume, at constant pressure, during the cooling of a glass forming liquid [7]. When a liquid is cooled, it usually crystallizes at the melting temperature (T_m). If the same liquid is cooled fast enough, crystallization at T_m can be avoided and it becomes a supercooled liquid [1, 3]. As a supercooled liquid is cooled further, particle rearrangements become more difficult and it eventually falls out of liquid state equilibrium [3, 8]. This fall out of equilibrium is a gradual process that is not accompanied by singularities in the observed quantities [1]. This implies that the dynamic

glass transition is not a true phase transition. The temperature at which the fall out of equilibrium becomes apparent is one definition of the glass transition temperature (T_g). The right panel of Fig. (1.1) shows that the location of T_g is dependent on the cooling rate, i.e. different rates lead to different glassy states [7].

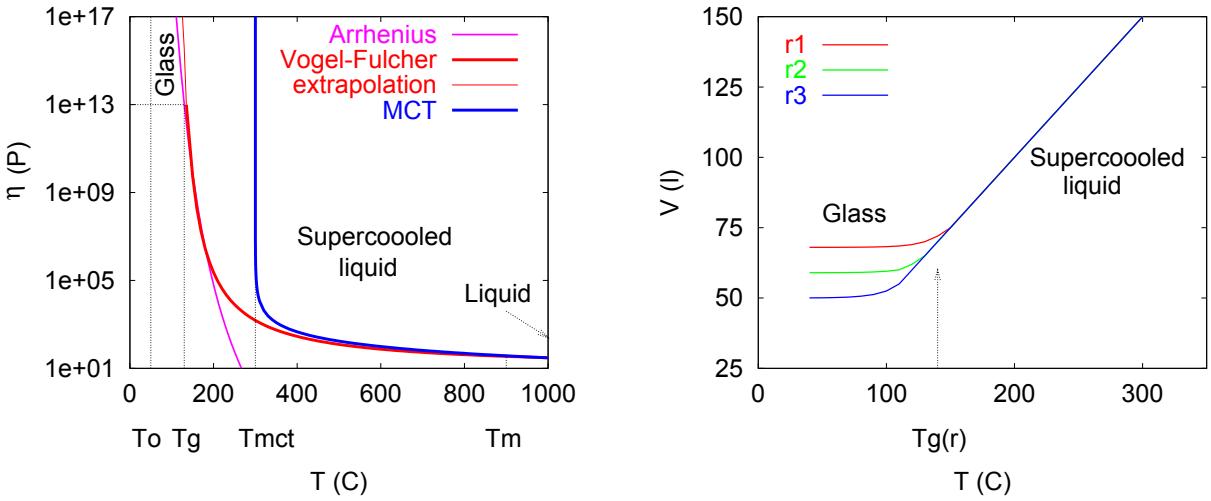

Figure 1.1: (From Ref. [7]) **Left**: A generic sketch of the viscosity against temperature in supercooled liquids, rough comparison between different functional forms. (Arrhenius: $B = 3900$C, $\eta_\infty = 10^{-6}$P. Vogel-Fulcher: $B = 500$C, $T_0 = 100.$C, $\eta_\infty = 10$P. MCT: $\eta = \eta_0(T_{mct}/(T - T_{mct}))^\gamma$ with $T_{mct} = 300$C, $\gamma = 0.7$, $\eta_0 = 1700$P.) Also shown is an extrapolation of the Vogel-Fulcher below T_g. **Right**: cooling rate r dependence of the volume in supercooled, liquids. Three colling rates are shown, $r_1 > r_2 > r_3$.

Another definition of T_g is the temperature at which the viscosity reaches 10^{13} poise [3]. In fact, as T_g is approached from the supercooled liquid state, the viscosity increases by more than 10 orders of magnitude in a temperature interval that is only a fraction of T_g [3, 8]. The left panel of Fig. 1.1 shows the increase in viscosity as the temperature is decreased. In the figure, a rough comparison between different scaling forms is shown. These scaling forms are [29]: Arrhenius

$$\eta = \eta_\infty \exp\left(\frac{B}{T}\right), \tag{1.1}$$

Vogel-Fulcher-Tammann (VFT)

$$\eta = \eta_\infty \exp\left(\frac{B}{T - T_0}\right), \tag{1.2}$$

and mode coupling theory (MCT)

$$\eta = \eta_0 \left(\frac{T_{mct}}{T - T_{mct}}\right)^\gamma. \tag{1.3}$$

Here η_∞, B, T_0, T_{mct} and γ are fitting parameters. The Arrhenius law is sometimes used to classify supercooled liquids into strong glass formers, if they are well described by this law, (for example, silica) and fragile glass formers if they deviate it, (for example, o-Terphenyl) [1, 2, 3]. There are several forms that have been used to fit the viscosity of liquids that deviate from the Arrhenius law [2], the most commonly used is the Vogel-Fulcher-Tammann (VFT) law [1, 3]. The terms strong and fragile glasses or liquids does not refer to how brittle the material is, but rather the ease with which the material changes between two energetically degenerate glass states [1]. Mode-coupling theory (MCT) is a mean field approach, valid above and around T_{mct}, a temperature that characterizes the onset of glassy behavior and is above the glass transition temperature [1, 7].

1.2 Aging

Aging, one of the universal features of glass dynamics near the glass transition, refers to the breakdown of time translation invariance (TTI) during the evolution of a glass below T_g [11]. Let's consider the situation depicted by Fig. (1.2) [7] in which a liquid is cooled and becomes a glass at time $t_0 = 0$. It is then allowed to evolve for a time t_w, the waiting time. At t_w an external field is applied and its effect is measured at time $t_m = t + t_w$. On one hand, if the material is in equilibrium, its observables measured at t_m depend only on the duration t. On the other hand, if the system is aging, its observables measured at t_m depend not only on the time interval t but also on the waiting time t_w [7, 12]. Fig. (1.3)

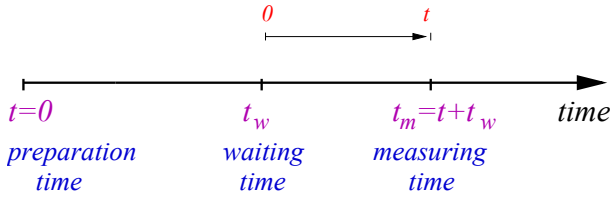

Figure 1.2: (From Ref. [7]) Characteristic times in glass experiments. The waiting and measuring times are *experimental times* t_{exp}. The equilibration time t_{eq} can be shorter or longer than them leading to equilibrium or non-equilibrium dynamics, respectively.

shows the dependence of the tensile creep compliance (response of the material to stretching) for PVC on creep time, i.e. the time duration t, and aging time, i.e. the waiting time t_w [12]. As the waiting time increases the average creep relaxation time increases as well, indicating that the waiting time influences how fast the process is. It should be noticed that when the variable in the horizontal axis is changed to the ratio t_{Creep}/t_{Aging}, the curves collapse onto a single curve. Aging can be understood to mean that older systems relax much more slowly than younger systems [7].

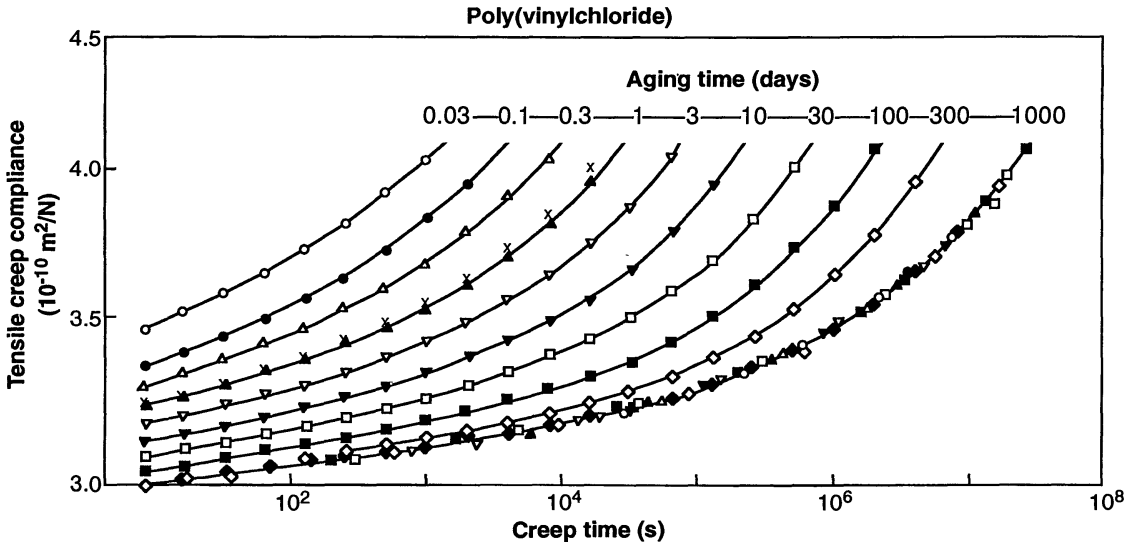

Figure 1.3: (From Ref. [12]) Tensile creep compliance in polyvinyl chloride (PVC). Each curve corresponds to a different waiting time, t_w, labeled as "aging time". The curves collapse onto a single curve when rescaled with the aging time.

1.3 Relaxation

One of the features that distinguishes glasses and supercooled liquids from ordered materials is the way they respond to changes due to external probes, such as temperature and external fields, close to and below T_g [7]. For example, the quenching of a liquid from an initial temperature T_i to a final temperature T_f results in a relaxation to a new configuration, with the relaxation process vastly different at high temperatures than close to and below T_g [3, 7]. The relaxation to the new configuration takes a characteristic time τ_{eq}, the equilibration time. For supercooled liquids the equilibration time increases dramatically with further cooling [3]. Below the glass transition, equilibration times are much larger than experimental timescales and the liquid appears frozen [3, 8]. Next, we describe the relaxation process of glass forming systems close to T_g as a function of temperature.

Let's consider, as an example, the relaxation in a glass forming liquid. At higher temperatures, the relaxation is exponential, a direct consequence of Brownian-like motion; by contrast, at lower temperatures the relaxation is a two step process [3, 13]. Fig. (1.4) shows the decay of the self part of the intermediate scattering function $F_s(q,t)$, a function that describes the decay of density fluctuations [2], for an 80 : 20 binary Lennard-Jones mixture [3]. $F_s(q,t'+t,t')$ is defined by [14]

$$F_s(\vec{q},t'+t,t') \equiv \frac{1}{N}\sum_{j=1}^{N} \exp\left[i\vec{q}\cdot(\vec{r}_j(t+t') - \vec{r}_j(t'))\right], \tag{1.4}$$

where N is the number of particles, $\vec{q}$ is a wave vector, $\vec{r}_i$ is the position vector of particle i and $F_s(q,t)$ is obtained by setting $t' = 0$ in $F_s(q,t+t',t')$. The figure shows the evolution of $F_s(q,t)$ with temperature, at a fixed magnitude of the wave vector q corresponding to the first peak of the static structure factor $S(q)$ of the majority particle species in the mixture. As the temperature is decreased, $F_s(q,t)$ begins to show two step relaxation in which exponential behavior, corresponding to fast dynamics, is observed only at the early

times [2, 3]. At intermediate times, a plateau emerges, due to the caging effect, i.e. the trapping of particles by their neighbors. The plateau is followed by a non exponential decay of $F_s(q,t)$ at later times, which in many cases is described well by the Kohlrausch-Williams-Watts (KWW, or "stretched exponential") function $g(t) = \exp\left(-(t/\tau)^{\beta}\right)$, where τ is the characteristic temperature dependent relaxation time and β is the stretching exponent, which is sometimes referred to as the "Kohlrausch exponent" [3, 15]. The observed two-step relaxation is described qualitatively well by

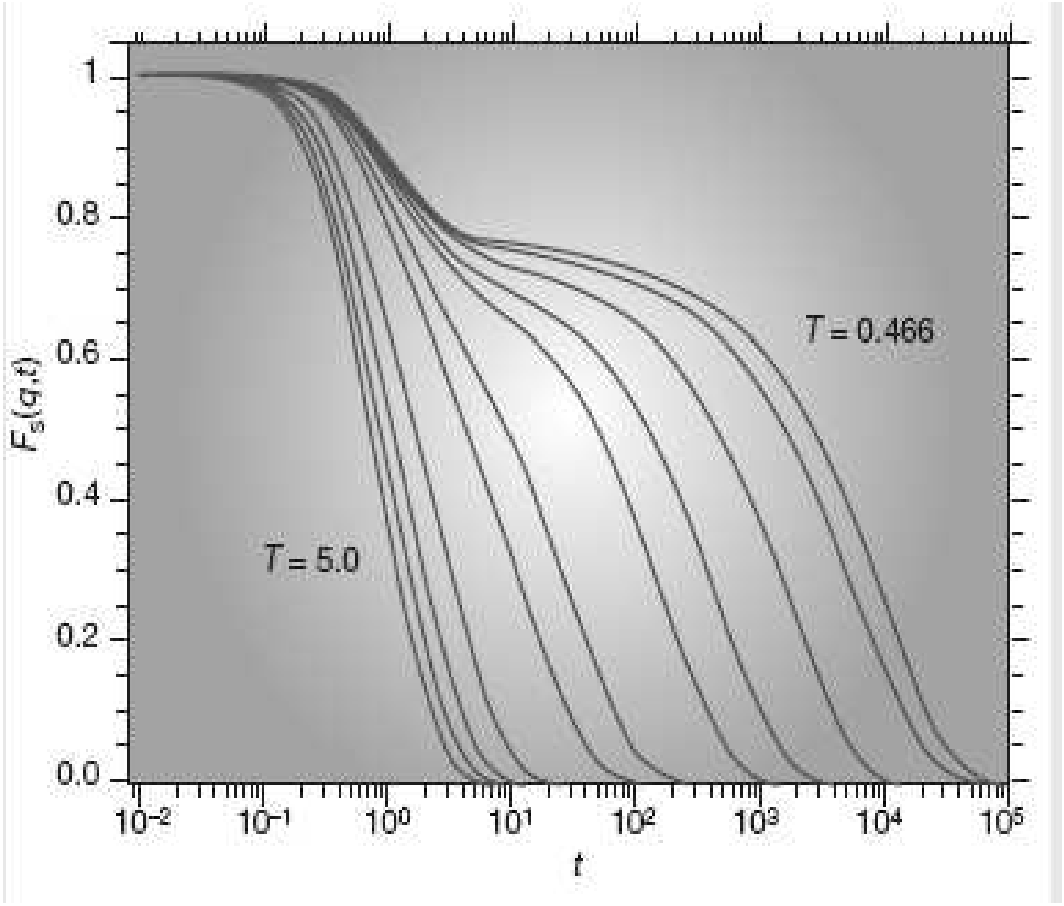

Figure 1.4: (From Ref. [3]) Evolution of the self-intermediate scattering function, $F_s(q,t)$ for a supercooled 80 : 20 binary Lennard-Jones mixture at $q = 7.251$, corresponding to the first peak of the static structure factor of the majority species in the mixture. Temperature and time are in reduced units.

Mode-Coupling Theory (MCT), which predicts the presence of three regimes at sufficiently low temperatures [3, 15]. The three MCT regimes appear after the exponential relaxation at the early times. The first regime is described by a power law decay towards a plateau, given by $F(t) = f + At^{-a}$; the second regime, which appears before the non exponential relaxation at late times, is described by a second power law decay away from the plateau, given by $F(t) = f - Bt^{b}$; and lastly, a regime of slow relaxation at very long times described by the KWW function $F = \exp(-(t/\tau)^{\beta})$ [15]. Here f is the plateau value; A,B,a and b are constants determined by fits.

1.4 The Energy Landscape

The potential energy landscape (PEL) provides an intuitive picture in which the slowdown of dynamics close to T_g can be understood [1, 3]. For an N-body system, the landscape is a hyper-surface described by the potential energy function $\Phi(\mathbf{r}_1, \cdots, \mathbf{r}_N)$, where the $\mathbf{r}_i$ are phase space vectors representing position, orientation and vibration coordinates [1, 3]. In the simplest case of N structureless particles, i.e. particles without any internal degrees of freedom, the PEL is a $3N + 1$ dimensional object [3]. The potential energy function contains all the information about the interactions of the constituents of a system [16] and is independent of temperature [1]. The system is represented by points moving at a temperature dependent $d \times N$ dimensional velocity, where d is the dimension, on the surface of the PEL [1].

The left panel of Fig. (1.5) is a schematic representation of an energy landscape [3]. In general, the landscape is rugged, with a lot of local potential energy minima [3], which are sometimes referred to as inherent structures [1, 16]. Each inherent structure is surrounded by states that spontaneously transform to it if the energy is suddenly minimized, and together they form a *basin of attraction* [16]. Between the basins of attraction are the transition states (potential energy barriers). The shape of the landscape is

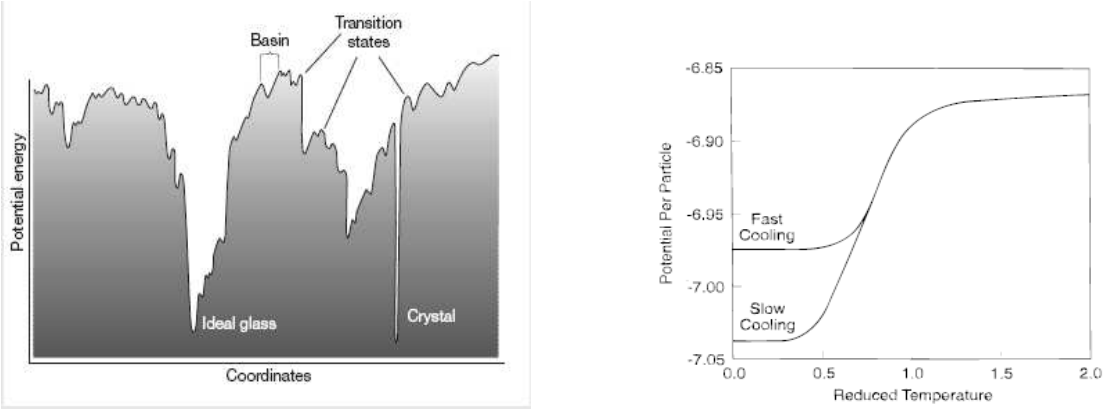

Figure 1.5: **Left**: (From Ref. [3]) A schematic representation of an energy landscape. **Right**: (From Ref. [16]) Mean inherent structure energy per particle vs initial liquid temperature (reduced units) for the 80 : 20 binary Lennard-Jones system. Two cooling rates are shown.

determined by the density because changes in the interaction strength are a result of changes in inter-particle distances[16, 17, 18]. The temperature determines how the system explores the landscape [16, 17, 18]. At high temperatures the system's kinetic energy is large and the dynamics is only weakly influenced by the landscape [3, 16, 17, 18]. At lower temperatures the landscape dominates the dynamics, and the system spends longer times trapped in local minima [3, 16, 17, 18]. The sampling of the energy landscape also depends on the cooling rate [16]. A slowly cooled system has more time to explore the landscape and find deeper minima than a rapidly cooled system [3, 16]. The right panel of Fig. (1.5) is from a simulation of a glass forming binary (80:20) Lennard-Jones system [3, 16, 19]. The inherent structure energy per particle is plotted against reduced temperature for a slow cooling rate r_{slow} and a fast cooling rate $r_{fast} = 324 r_{slow}$. Fast cooling reduces the likelyhood of finding the deepest minimum, representing the crystalline state [16]. The system finds other deep minima -metastable states- and continues to relax by transitioning among the different metastable states [17]. The relaxation slows down because of increasing time scales for basin to basin transitions,

which are the transitions associated with significant structural changes [17]. In liquids that readily crystallize, the inherent structure energy distribution is a narrow distribution around the depth of the crystal minimum, hence the ease with which they crystallize [16].

1.5 Dynamical Heterogeneity

Some time ago, two extreme scenarios were proposed to explain non-exponential relaxation in supercooled liquids and glasses [8, 9, 13]. In one scenario, we understand non-exponential relaxation by thinking of the relaxation function as a sum of a large number of exponential contributions, each with a different relaxation time; with each contribution corresponding to a particular region in the system [8, 9]. That is, the system has a distribution of relaxation times $P(\tau)$, and the relaxation function is given by

$$C(t-t') = \int_0^\infty d\tau P(\tau) \exp\left(-\frac{t-t'}{\tau}\right). \tag{1.5}$$

In the other scenario, the dynamics of the liquid is homogeneous, the distribution of the relaxation times is a delta function but the relaxation in all regions is described by a unique function $g(x)$, which is non-exponential:

$$C(t-t') = \int_0^\infty d\tau \delta(\tau-\tau_0) g\left(\frac{t-t'}{\tau}\right). \tag{1.6}$$

A distribution of relaxation times is one feature of the picture of *dynamical heterogeneity*, in which mesoscopic regions evolve differently from each other and from the bulk; and local relaxation times $\tau_{\vec{r}}(t)$ evolve, so that "fast" regions become "slow", and viceversa [8, 9, 20, 21, 22, 23, 24, 25, 26, 27, 28]. Fig. (1.6) is a schematic illustration of spatial dynamical heterogeneity [8].

Non-exponential relaxation provides indirect evidence that the dynamics of supercooled liquids and glasses is heterogeneous. More indirect evidence for dynamical heterogeneity is provided by the decoupling of diffusion from viscosity, i.e. the

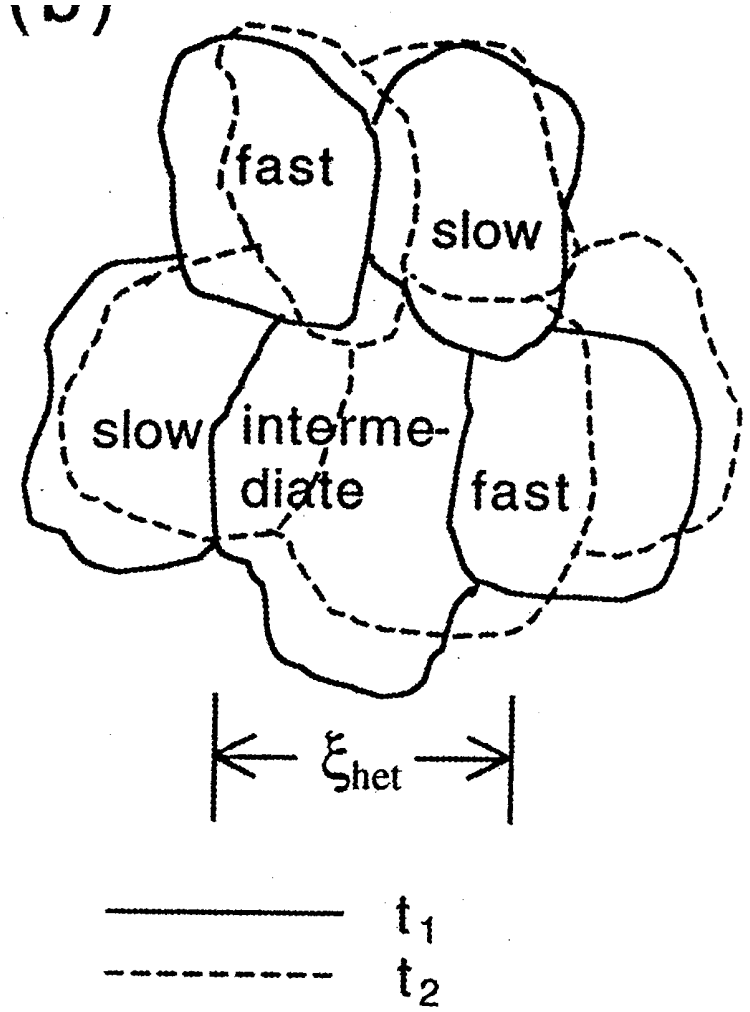

Figure 1.6: (From Ref. [8]) Schematic picture of spatially heterogeneous dynamics near the glass transition. The regions are on a scale of ξ_{het} which is a few nanometers (a few particle diameters). Slow and fast regions are continuously evolving.

breakdown of the Stoke-Einstein relation [29]. The Stoke-Einstein relation relates the diffusion constant D, the viscosity η and the temperature T:

$$D\eta T^{-1} = k, \tag{1.7}$$

where k is a constant. This relation is valid for liquids at higher temperatures but begins to break down close to the glass transition. Fig. (1.7) shows experimental results on the breakdown of the Stoke-Einstein relation for six molecular glass forming liquids [29]. The

deviation from the Stoke-Einstein line grows by almost an order of magnitude between 1.25 T_g and 1.15 T_g. Diffusivity decreases less rapidly than the viscosity grows. In a system with fast and slow regions, particles can diffuse more rapidly only by flowing around slow regions using paths of connected fast regions [29].

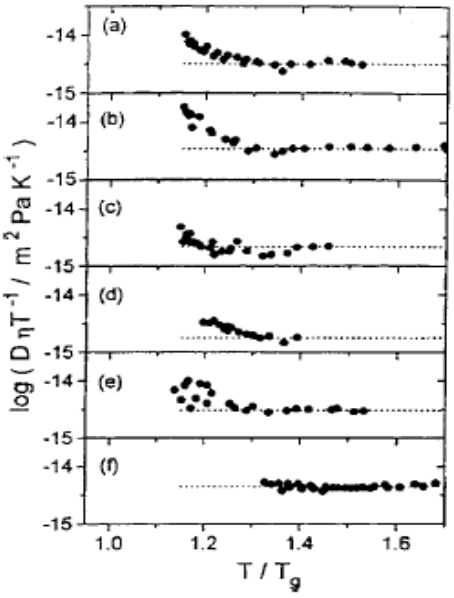

Figure 1.7: (From Ref. [29]) The decoupling of diffusivity from viscosity. The vertical axis is the product $D\eta T^{-1}$ and the horizontal axis is the ratio T/T_g. The points are experimental data and the dotted line is the prediction from the Stokes-Einstein relation. Results for six molecular liquids are shown: (a)-(f) are OTP, salol, CDE, m-tricresyl and glycerol, respectively. Notice the logarithmic scale in the vertical axis.

Direct evidence for dynamical heterogeneity has been found in particle tracking experiments in glassy colloidal systems [21, 22, 23] and granular systems [25], and in numerical simulations [26, 27]. Fig. (1.8) shows a result from a particle tracking experiment using confocal microscopy in a colloidal glass [23]. Shown are snapshots showing the 10 percent most mobile particles for three different waiting times. In each snapshot, there are clusters of high mobility particles (as well as clusters of low mobility

particles) and the location of the clusters is changing with time, indicating that the observed heterogeneity is dynamic.

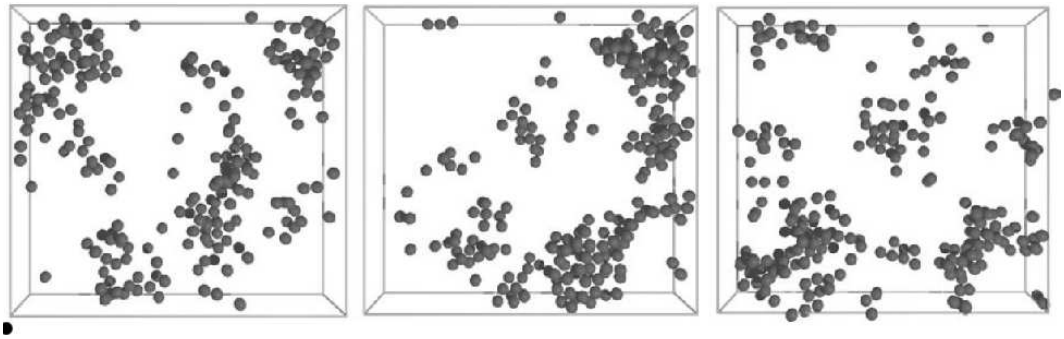

Figure 1.8: (From Ref. [23]) Confocal microscopy results from a colloidal glass. Shown are snapshots of the 10 percent most mobile particles at different waiting times. Left, t_w = 10 mins; center, t_w = 55 mins; right, t_w = 95 mins.

The cause of the change from homogeneous to heterogeneous dynamics, as T_g is approached, is not fully understood. Understanding the onset of heterogeneities without an apparent structural trigger is believed to be key to an understanding of the glass transition [8]. Since no microscopic theory in which there is consensus has been developed, I present in the following subsections, three theories that provide possible explanations for the presence of heterogeneities in supercooled liquids as well as in the glass state.

1.5.1 Geometrical Explanation

The geometrical explanation for the presence of dynamical heterogeneities comes from kinetically constrained models, in which trivial Hamiltonians are used together with dynamical rules to reproduce complex dynamical features [30, 31]. To illustrate how the geometrical structures develop, we consider the kinetically constrained

Fredrickson-Andersen (FA) model and the East model[1]. The constraints induce nontrivial structure in the space of transition trajectories of these systems [30, 31]. The left panel of Fig. (1.9) shows the difference in the space of trajectories between unconstrained dynamics (left) and constrained dynamics (middle and right) [30]. When there are no constraints, the space is evenly filled with trajectories but constraints put limitations on possible trajectories. The extensive regions of down spins seen in Fig. (1.9) impose four different type of boundaries that are allowed between regions of up and down spins (Fig. (1.9) top right panel) [30]. The resulting shape of domains for the FA and East models are shown on the bottom of the right panel of Fig. (1.9). Spins in the interior of a region of down spins cannot flip, hence these regions are the slow domains. Spins in the regions of up spins and at boundaries can flip, hence these regions are fast domains [30]. Therefore the presence of extensive regions of down spins is a source of dynamical heterogeneities [30]. Comparing kinetically constrained models to real glasses, we immediately realize that the Hamiltonians of real systems are not trivial and therefore reproducing the dynamical features using complex rules does not provide a true microscopic origin of dynamical heterogeneities. In principle, we still need to determine a microscopic origin of these rules and how they will change when they are used together with real system's Hamiltonians.

1.5.2 Random First Order Transition Theory

Random First Order Transition (RFOT) theory is based on entropic driving of a system rather than free energy gain, and in this regard it is closely related to the Adam-Gibbs (AG) theory [1, 32, 33, 34]. In the AG theory, the system is assumed to be

[1] The FA and East models have the trivial Hamiltonian, $H = \sum_i s_i$, where $s_i = \pm 1 \quad i = 1, \cdots, N$ are spin variables. There is no thermodynamic phase transition at nonzero temperature in either model because the Hamiltonian is simple. In both models, however, nontrivial dynamical rules are postulated. In the FA model a spin can flip if either of its neighbors is an up spin and in the East model a spin can flip if the spin to the right is an up spin.

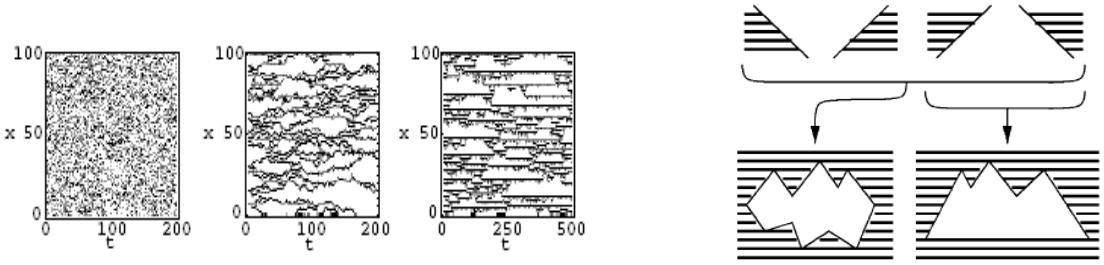

Figure 1.9: (From Ref. [30]) **Left panel**: Equilibrium trajectories for the unconstrained case (left), the FA (middle) and the East Model (right). The vertical direction is space and the horizontal direction is time. Black/white corresponds to up/down spins. **Right panel**: Geometry imposed by slow dynamics. Allowed boundaries of up and down spins (Top) and shapes of domains in the FA (bottom left) and in the East model (bottom right)

characterized by cooperatively rearranging regions (CRRs) $C(n)$, of n particles and linear size ψ, which have ω preferred configurations [1]. The VFT law is obtained by assuming that ω is independent of ξ after the CRR's have grown to a critical size ξ^* and that there is a free energy barrier that scales with the volume of the CRR's [1]. Both assumptions of the AG theory are not reasonable: taking $\omega = 2$, the assumption made by Adams and Gibbs, it is found that the critical number $n^* < 1$ for most liquids; and assuming a barrier that continually grows with the volume will make it impossible for cooperative rearrangements to occur eventually [1].

In RFOT theory, the transition from a homogeneous liquid at higher temperatures to a mosaic structure at lower temperatures is likened to the first order transition from a liquid into a periodic crystal [32]. The mosaic pieces (CRRs) are each in an aperiodic minimum separated by domain walls [32, 33, 34]. Fig. (1.10) shows an illustration of the mosaics [32]. In principle, there are many metastable states, which are almost of the same free energy but are structurally not the same, and the transformation of CRRs results in the system hoping between the metastable states, hence dynamical heterogeneity [1, 32, 33, 34]. The nucleation and growth of CRRs is not driven by free energy gain because the states have almost the same energy, instead the very large number of these

states provides an entropic driving force, which is opposed by a surface tension term [1, 32, 33, 34].

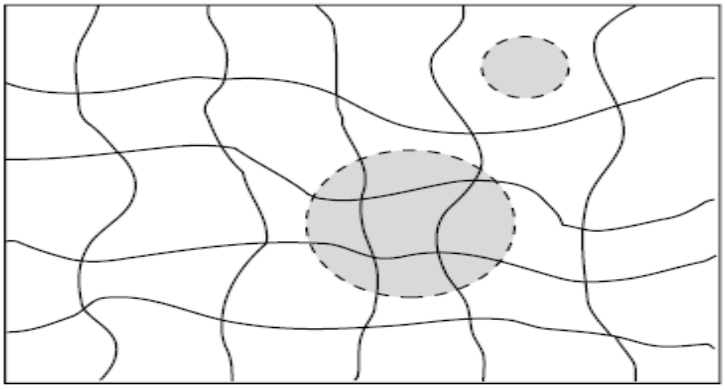

Figure 1.10: (From Ref. [32]) An illustration of the ”mosaic structure” of supercooled liquids. The mosaic pieces have random sizes due to fluctuations in the driving force, the configurational entropy.

1.5.3 Time Reparametrization Group Theory

Another theoretical avenue to explain dynamical heterogeneities is based on time reparametrization symmetry (TRS) in glasses. Time reparametrization symmetry refers to an invariance under transformations of the time variable $t \rightarrow \phi(t)$, where $\phi(t)$ is a continuous and monotonically increasing function of t. This symmetry has been shown to be present in mean field spin glass models [35, 36] and in short range spin glass models [37, 39, 40, 45]. Numerical studies in spin glasses [39] and structural glasses [41, 46] have given evidence supporting the presence of this symmetry. The symmetry starts to be spontaneously broken by correlations and relaxation functions as the glass transition is approached. We can illustrate the breaking of the symmetry by considering the two time correlation function $C(t - t')$ between the state of the system at t' and at t. If $C(t - t')$ was symmetric under time reparametrizations , then

$C(t-t') = C[\phi(t) - \phi(t')]$ for *all* mappings $t \to \phi(t)$, which is only possible if the correlation is independent of time. But we know that in the long time limit the correlation function of a glass forming liquid decays from its plateau value, therefore the symmetry is broken by $C(t-t')$. The broken reparametrization symmetry is expected to give rise to Goldstone modes [37, 38, 39, 40, 41, 42, 43, 44, 45, 46] associated with smooth variations in space of the reparametrized variable, that is $t \to \phi_{\vec{r}}(t)$. In Refs. [37, 38, 39], the authors use the analogy of Goldstone modes in the $O(N)$ model to describe Goldstone modes of a system with time reparametrization symmetry. The $O(N)$ model's hamiltonian in d dimensions is

$$H = \int d^d r \left[(\nabla \cdot \vec{m}(\vec{r}))^2 + \vec{h} \cdot \vec{m}(\vec{r}) + V(m) \right], \tag{1.8}$$

where $\vec{m}(\vec{r})$ is a N dimensional vector whose components are *real variables*, $\vec{h}$ is an external field and $V(\vec{m}) = \frac{r_0}{2} m^2(\vec{r}) + \frac{u_0}{4} m^4(\vec{r})$ is a potential with one minimum when $r_0 > 0$ and infinitely degenerate minima when $r_0 < 0$ [39, 48]. The authors of Refs. [37, 38, 39] note that in the $O(N)$ model, the ground state vector $\vec{m}_0(\vec{r})$ has longitudinal fluctuations corresponding to changes of the length of the vector and transverse fluctuations corresponding to spatial variations in rotations of the ground state. The transverse fluctuations are energetically favorable and are the Goldstone modes of the system. The authors of Refs. [37, 38, 39] then argue that in the theory of time reparametrization symmetry, the Goldstone modes are spatially varying transverse modes of the time reparametrizations $\phi_{\vec{r}}(t) = \phi(t) + \delta\phi_{\vec{r}}(t)$. The spatio-temporal fluctuations of $\phi_{\vec{r}}(t)$ imply that different regions of a sample relax differently from each other, that the relaxation of the different regions is advanced (or retarded) with respect to each other and the bulk, and that "advanced" and "retarded" regions can switch roles in the course of the relaxation. Hence, the spatial-temporal fluctuations of the broken reparametrization symmetry are connected to dynamical heterogeneities in glass forming and glassy systems.

1.6 Spin Glasses

Spin glasses are disordered magnetic systems in which the spins' interactions are frustrated [10]. When cooling ferromanetic or antifferomagnetic systems, a critical temperature T_c is found beyond which the spins are ordered [10]. Spin glasses do not exhibit such long range order and instead, their spins freeze in random directions below a freezing temperature T_f, i.e.

$$\langle s_i \rangle_t \neq 0, \tag{1.9}$$

$$N^{-1} \sum_i \langle s_i \rangle_t \exp(i\mathbf{k} \cdot \mathbf{R}_i) = 0, \tag{1.10}$$

where $\langle \cdots \rangle_t$ denotes an average over observation time t, s_i are the spin variables, $\mathbf{k}$ an arbitrary wave vector, $\mathbf{R}_i$ are the position vectors and the sum over spins is taken in the thermodynamic limit ($N \to \infty$) [10]. In the study of spin glasses two commonly used functions are the two time correlation $C(t, t')$ and response function $G(t, t')$, defined by

$$C(t, t') \equiv \frac{1}{N} \sum_i^N \overline{\langle s_i(t) s_i(t') \rangle} \tag{1.11}$$

$$G(t, t') \equiv \frac{1}{N} \sum_i^N \overline{\frac{\delta \langle s_i(t) \rangle}{\delta h_i(t')}}, \tag{1.12}$$

where h_i is a space dependent magnetic field [39]. Here the angle brackets $\langle \cdots \rangle$ represent an average over noise and the bar $\overline{\cdots}$ represents an average over random couplings. In theoretical studies, the integrated response function $\chi(t, t')$ is sometimes used instead of the response function

$$\chi(t, t') \equiv \int_{t'}^{t} dt'' G(t, t''). \tag{1.13}$$

At the spin glass transition T_f, there is a frequency dependent cusp in the ac-susceptibility $\chi(\omega)$, i.e. the response to an alternating current field such as $h_{ac} = h \cos(\omega t)$ [10, 49]. Fig. (1.11) shows the real part ($\chi'(w)$) of the ac-susceptibility as a function of temperature for the spin glass $CuMn$ [50]. The insert in the figure is an expanded view of the transition

point T_f. The different curves are for measurements of the $\chi'(w)$ at different frequencies. As the frequency decreases the value of T_f decreases [50].

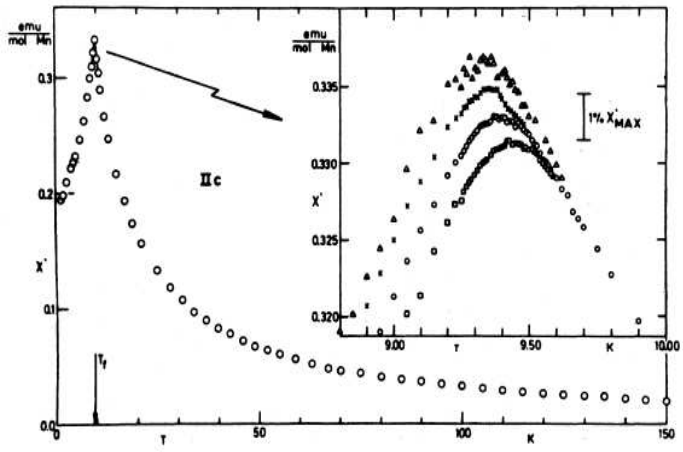

Figure 1.11: (From Ref. [50]) The figure shows the real part χ' of the susceptibility χ as a function of temeprature for a sample of CuMn with 0.94% Mn powder. The insert is an expanded view of the cusp at T_f and it shows frequency dependence. From the curve with the lowest peak to the curve with the highest peak, the measuring frequencies are: 1.33 kHz, 234 Hz, 104 Hz and 2.6 Hz.

Aging is observed below the spin glass transition. The left panel of Fig. (1.12) shows the decay with the time difference $t - t' \geq 0$ of the thermoremanent magnetization (integrated response) and the right panel shows the decay of the two time correlation in a thiospinel insulator spin glass [7]. The different curves correspond to different waiting times t', in both panels, with the waiting time increasing from left to right. The inset in each panel of Fig. (1.12) shows that both the correlations and integrated response curves collapse to a single curve when the horizontal axis is changed to $\frac{t^{1-\mu}-t'^{1-\mu}}{1-\mu}$, where the scaling exponent $\mu = 0.87$ [7].

Some of the most extensively studied models of spin glasses are the Sherington-Kirkpatrick (SK) model, the Edwards-Anderson (EA) model and the p-spin

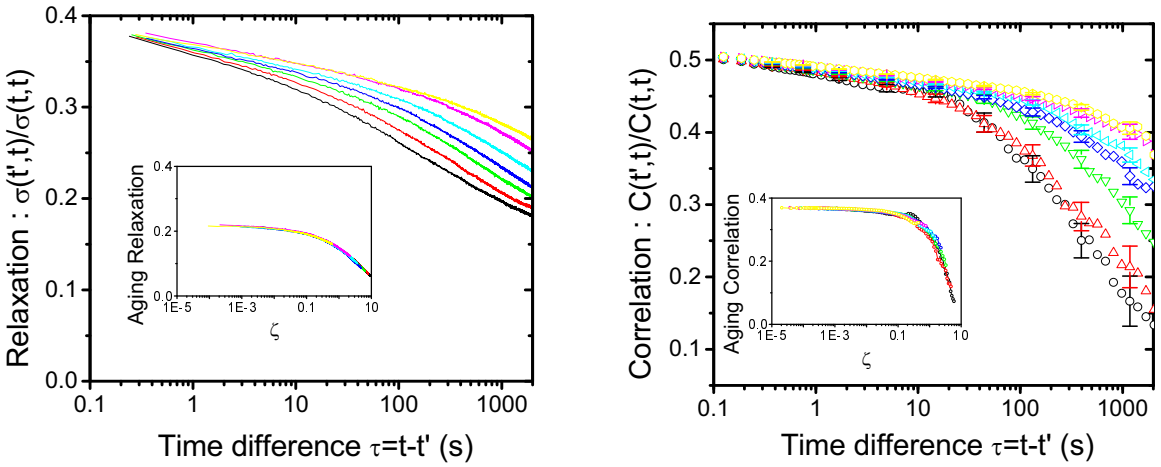

Figure 1.12: (From Ref. [7]) Aging in a thiospinel insulator spin-glass. Decay of the thermoremanent magnetization (left) and correlations between magnetic fluctuations (right). From left to right curves for increasing waiting-times. Inset: scaling. Here $\zeta = \frac{t^{1-\mu}-t'^{1-\mu}}{1-\mu}$ with $\mu = 0.87$ is the scaling variable and $\sigma(t,t') = \chi(t,t')$ is the thermoremanent magnetization

model[51]. Let's consider the simple Hamiltonian with two spin interactions

$$H = \sum_{ij} J_{ij} s_i s_j, \tag{1.14}$$

where the couplings, J_{ij}'s are time independent (quenched) random variables, usually assumed to be Gaussian distributed, and the $\{s_i\}_{i=1\cdots,N}$ are Ising variables (i.e. $s_i = \pm 1 \quad i = 1, \cdots, N$) [7]. There are two extreme cases that we consider for this Hamiltonian. One of them describes the SK model, in which every spin interacts with all other spins, i.e., all J_{ij}'s can be different from zero [7]. The other extreme case is realized if a spin interacts only with its nearest neighbors, i.e., J_{ij} is non zero only if i and j are nearest neighbors. This case describes the EA model [7].

The p-spin model is given by interactions of groups of p-spins instead of the pair interactions of the SK and EA models [36]. It is described by the Hamiltonian

$$H = -\sum_{1\le i_1\le\ldots\le i_p\le N} J_{i_1\ldots i_p}\phi_{i_1}\ldots\phi_{i_p}, \tag{1.15}$$

in which $p \geq 3$. We will consider the case in which the spins are real variables (soft spins) and satisfy the spherical constraint $\sum_{i=1}^{N}[\phi_i(t)]^2 = N$. The couplings $J_{i_1 \ldots i_p}$ are disordered and are usually chosen to be uncorrelated, zero-mean Gaussian random variables, i.e.

$$P\{J\} = \prod_{i_1 < \ldots < i_p} \frac{1}{\sqrt{2\pi K_{i_1 \ldots i_p}}} \exp[-J^2_{i_1 \ldots i_p}/2K_{i_1 \ldots i_p}]. \tag{1.16}$$

Here $K_{i_1 \ldots i_p}$ is the variance of the distribution of $J_{i_1 \ldots i_p}$. We let the dynamics be given by the Langevin equation,

$$\Gamma_0^{-1}\partial_t \phi_i(t) = -\beta \frac{\delta H}{\delta \phi_i(t)} + \eta_i(t). \tag{1.17}$$

Here Γ_0 sets the time scale and $\eta_i(t)$ is a Gaussian distributed white noise with $\langle \eta_i(t) \rangle = 0$ and $\langle \eta_i(t)\eta_j(t') \rangle = 2T\delta_{ij}\delta(t - t')$, which represents the coupling to a thermal reservoir at temperature T.

Early studies on the p-spin model were carried out mainly through mean field approaches. In one of these studies, Cugliandolo and Kurchan analytically obtained an off-equilibrium dynamical solution in the asymptotic long time limit [36]. In other studies, it was shown that the long range p-spin model has a thermodynamic critical temperature (T_c) and a dynamic critical temperature(T_d) with $0 < T_d < T_c$ [52, 53]. The p-spin model is known to share certain features with structural glasses at the level of mean field theory [52, 54]. At the dynamic transition, the Edwards-Anderson parameter q_{EA} is discontinuous. Likewise, the density correlation for a structural glass, $\langle \rho(t)\rho(t') \rangle$, is discontinuous at the MCT transition temperature (T_{MCT}) [15].

1.7 Organization of the Dissertation

The work we present here covers two areas of dynamics: explaining the presence of dynamical heterogenities using time reparametrization symmetry in glasses and developing a method for reducing the degrees of freedom in a complex system. The dissertation is organized as follows, In Chapter (2), we present our proof that p-spin

models, in which the interaction range is arbitrary, are time reparametrization invariant in the long time limit. In Chapter (3), we introduce a method for extracting the actual time reparametrization fluctuations from data, we establish a connection between those fluctuations and local fluctuations of the relaxation time, and we apply the method to analyze existing numerical data for structural glasses.

2 TRIAR-M:SN-D

The work presented in this chapter has been published in: G. A. Mavimbela and H. E. Castillo, J. Stat. Mech. (2011) P05017.

2.1 Introduction

Time reparametrization symmetry, i.e. the symmetry under the transformation $t \to h(t)$ with $h(t)$ a monotonic increasing function, has been shown some time ago to be present in the mean field equations for the correlation function $C(t, t')$ and response function $G(t, t')$ of the SK spin glass model [7, 35]. The symmetry is found when taking the long time limit of the mean field equations. By contrast, the full equations contain explicit symmetry breaking terms that affect the short time dynamics [7, 35]. The symmetry has also been shown to be present in the long time dynamics of the short ranged EA spin glass model in two studies that go beyond mean field analysis [37, 40], by using the Martin-Siggia-Rose (MSR) formalism and the Renormalization Group (RG) to study the long time dynamics. The MSR formalism is used to write a generating functional, and the RG is used to show that the symmetry holds for this model in the long time limit, at the level of the generating functional, including all fluctuations. However, not all models of interacting spins under Langevin dynamics are time reparametrization invariant. For example, in a study of the O(N) model it was shown that the symmetry is not present, even for the long time limit of the low temperature dynamics [55]. In this chapter we follow a procedure similar to the one in Ref. [40] to prove that the long time dynamics of p-spin models of arbitrary range is time reparametrization invariant.

As mentioned before, time reparametrization symmetry has been shown to be present in the long time dynamics of infinite range p-spin models [36]. The authors of Ref. [36]

analyze the mean field equations describing the eveolution of the two time correlation function $C(t,t')$ and the two time response function $G(t,t')$:

$$\begin{aligned}\frac{\partial C(t,t')}{\partial t} &= -\left[1-p\beta\epsilon(t)\right]C(t,t')+2G(t,t')+\mu\int_0^{t'}dt''C^{p-1}(t,t'')G(t',t'')\\ &\quad+\mu(p-1)\int_0^{t}dt''G(t,t'')C^{p-2}(t,t'')C(t'',t'), \qquad (2.1)\\ \frac{\partial G(t,t')}{\partial t} &= -\left[1-p\beta\epsilon(t)\right]G(t,t')+\delta(t-t')\\ &\quad+\mu(p-1)\int_0^{t}dt''G(t,t'')C^{p-2}(t,t'')G(t'',t'). \qquad (2.2)\end{aligned}$$

Here $\beta=(k_BT)^{-1}$, $\epsilon(t)$ is the energy per spin and $\mu=p\beta^2/2$. In the long time limit $t-t'\to\infty$, the delta function term is negligible, the time derivatives are negligible and the energy per spin is a constant. The term $2G(t,t')$ in the correlation equation is negligible because we have the scaling $G(t,t')\sim\frac{C(t,t')}{|t-t'|}$. Therefore, the asymptotic equations are

$$\begin{aligned}0 &= -\left[1-p\beta\epsilon\right]C(t,t')+\mu\int_0^{t'}dt''C^{p-1}(t,t'')G(t',t'')\\ &\quad+\mu(p-1)\int_0^{t}dt''G(t,t'')C^{p-2}(t,t'')C(t'',t') \qquad (2.3)\\ 0 &= -\left[1-p\beta\epsilon\right]G(t,t')+\mu(p-1)\int_0^{t}dt''G(t,t'')C^{p-2}(t,t'')G(t'',t'). \qquad (2.4)\end{aligned}$$

Let's transform these equations by reparametrizing the time variable $t\to h(t)$ such that the correlation and response functions transform to $C(t,t')\to\tilde{C}(t,t')$ and $G(t,t')\to\tilde{G}(t,t')$, respectively. We name the right hand side of the correlation equation RHS1 and the right hand side of the response equation RHS2, hence:

$$\begin{aligned}RHS\,1 &= -\left[1-p\beta\epsilon\right]\tilde{C}(t,t')+\mu\int_0^{t'}dt''\tilde{C}^{p-1}(t,t'')\tilde{G}(t',t'')\\ &\quad+\mu(p-1)\int_0^{t}dt''\tilde{G}(t,t'')\tilde{C}^{p-2}(t,t'')\tilde{C}(t'',t') \qquad (2.5)\\ RHS\,2 &= -\left[1-p\beta\epsilon\right]\tilde{G}(t,t')+\mu(p-1)\\ &\quad\times\int_0^{t}dt''\tilde{G}(t,t'')\tilde{C}^{p-2}(t,t'')\tilde{G}(t'',t'). \qquad (2.6)\end{aligned}$$

Letting the transformed correlation and response be $\tilde{C}(t,t') = C[h(t),h(t')]$ and $\tilde{G}(t,t') = G[h(t),h(t')]\frac{\partial h}{\partial t'}$, respectively, we obtain the transformed evolution equations:

$$\begin{aligned} RHS\,1 &= -\left[1-p\beta\epsilon\right]C[h(t),h(t')] \\ &\quad +\mu\int_0^{h(t')} dt'' C^{p-1}[h(t),h(t'')]G[h(t'),h(t'')]\frac{\partial h''}{\partial t''} \\ &\quad +\mu(p-1)\int_0^{h(t)} dt'' G[h(t),h(t'')]\frac{\partial h''}{\partial t''}C^{p-2}[h(t),h(t'')]C[h(t''),h(t')] \quad (2.7) \\ RHS\,2 &= -\left[1-p\beta\epsilon\right]G[h(t),h(t')]\frac{\partial h'}{\partial t'} + \mu(p-1) \\ &\quad \times\int_0^{h(t)} dt'' G[h(t),h(t'')]\frac{\partial h''}{\partial t''}C^{p-2}[h(t),h(t'')]G[h(t''),h(t')]\frac{\partial h'}{\partial t'}. \quad (2.8) \end{aligned}$$

Here we define $h' \equiv h(t')$ and we use the chain rule, $dh = \frac{dh}{dt}dt$ to get

$$\begin{aligned} RHS\,1 &= -\left[1-p\beta\epsilon\right]C[h,h'] + \mu\int_0^{h'} dh'' C^{p-1}[h,h'']G[h',h''] \\ &\quad +\mu(p-1)\int_0^{h} dh'' G[h,h'']C^{p-2}[h,h'']C[h'',h'] \quad (2.9) \\ RHS\,2 &= -\left[1-p\beta\epsilon\right]G[h,h'] \\ &\quad +\mu(p-1)\int_0^{h} dh'' G[h,h'']C^{p-2}[h,h'']G[h'',h'], \quad (2.10) \end{aligned}$$

where we have factored out $\frac{\partial h'}{\partial t'}$ in the last equation. RHS1 and RHS2 are the right hand side to the asymptotic correlation and response equations, respectively, with t replaced by h. Hence, the resultant asymptotic equations are invariant under time reparametrizations, with the correlation and response functions transforming as $C(t,t') \to \tilde{C}(t,t') = C[h(t),h(t')]$ and $G(t,t') \to \tilde{G}(t,t') = G[h(t),h(t')]\frac{\partial h}{\partial t'}$, respectively. In this chapter, we go beyond mean field and prove that the symmetry is present in the long time limit of the full dynamics (with all fluctuations) in arbitrary ranged models.

We consider a system of soft spins on a lattice, with p-spin interactions. The spin couplings are assumed to be uncorrelated Gaussian random variables with zero mean. We assume Langevin dynamics for the spins with a white noise term that represents the coupling of the spins to a thermal reservoir. We set up the calculation by writing the

generating functional of the spin correlations and responses using the MSR approach and introduce two-time fields that are associated with the spin correlations and responses. The formalism provides a general tool for field theory calculations of classical systems [56]. In other studies of p-spin models, the action derived from the generating functional has been used to determine mean field equations describing the evolution of the correlation and response functions in spin glass models [36, 57, 58, 59, 60]. To study the long time dynamics we start the renormalization group procedure by introducing a short time cutoff τ_0 to the time difference $t - t'$ [37, 40]. We introduce the cutoff in this manner because we are probing the dynamics of two time functions, the correlations, which are the observables that reveal the freezing of the glass state. We systematically integrate over two-time fields associated with the shortest time difference followed by an increase in the short time cutoff , thus following a procedure analogous to Wilson's approach to the RG. In our case, however, we integrate over fluctuations that are fast in *time*, not in space. In general, the integration over fast fluctuations can have one of two possible results: one, the integration changes the structure of the action; two, the integration preserves the structure of the action but the coupling constants change [61, 62, 63, 64]. The p-spin action we find falls under the second family, in which only the coupling constants change during the RG step.

We find Gell-Mann-Low equations, i.e. equations describing the evolution of the coupling constants with the RG process, which give three families of stable fixed points. First, we find a family of stable fixed point actions containing the coupling to the thermal bath. This family of fixed points is not time reparametrization invariant. A second family of stable fixed points, that are not time reparametrization invariant, corresponds to fixed point actions containing two marginal terms: the coupling to the thermal bath and the spin-spin interactions. Intuitively, the second family of fixed points corresponds to the effective dynamics at intermediate temperatures, where a transition occurs between the

high and low temperature regimes. Finally, we have the case in which only the spin-spin interaction term is marginal. The fixed points in this last family are time reparametrization invariant, and we believe that they represent the low temperature glassy dynamics of the model.

The rest of the chapter is organized as follows: in Sec. 2.2 we derive the generating functional; in Sec. 2.3 we show how we use Wilson's approach to the renormalization group to get stable fixed points; in Sec. 2.4 we study the stable fixed point generating functionals and determine which ones are invariant under reparametrizations of the time variable; and in Sec. 2.5 we end with a discussion of our results and conclusions.

2.2 Model and MSR generating functional

We recall from Section (1.6) the p-spin Hamiltonian, given by

$$H = -\frac{1}{p!}\sum_{i_1\ldots i_p} J_{i_1\ldots i_p}\phi_{i_1}\ldots\phi_{i_p}. \tag{2.11}$$

Starting from the Langevin equation, we let the dynamics be given by the Langevin equation,

$$\Gamma_0^{-1}\partial_t\phi_i(t) = -\beta\frac{\delta H}{\delta\phi_i(t)} + \eta_i(t). \tag{2.12}$$

we use the Martin-Siggia-Rose formalism [56] to write down the noise averaged generating functional

$$\begin{aligned}\langle Z[\{l_i\},\{h_i\}]\rangle = \int D\phi D\hat{\phi} D\hat{\varphi} D\hat{N}\exp\Bigg\{L[\phi,\hat{\phi}] + \sum_{i=1}^{N}\int_{t_0}^{t_f} dt[l_i(t)\phi_i(t) \\ + ih_i(t)\hat{\phi}_i(t)] + i\sum_{i=1}^{N}\hat{\varphi}_i[\phi_i(t_0)-\varphi_i] + i\int_{t_0}^{t_f} dt\hat{N}(t)\left[\sum_{i=1}^{N}\phi_i^2(t) - N\right]\Bigg\},\end{aligned} \tag{2.13}$$

where l and h are source fields and the last two terms in the exponent are due to the initial condition and spherical constraint, respectively. In this formalism, the spin variable ϕ_i gets elavated to a field variable $\phi_i(t)$ and a conjugate field $\hat{\phi}_i(t)$ gets coupled to the dynamics operator to give the action $L[\phi,\hat{\phi}]$. Details of the MSR formalism are given in

Appendix (A). The action $L[\phi, \hat{\phi}]$ is given by

$$L[\phi, \hat{\phi}] = -i \sum_{i=1}^{N} \int_{t_0}^{t_f} dt\ \hat{\phi}_i(t) \left[\Gamma_0^{-1} \partial_t \phi_i(t) - iT \hat{\phi}_i(t) - \frac{p}{p!} \sum_{i_1 \ldots i_{p-1}} J_{i,i_1 \ldots i_{p-1}} \phi_{i_1} \ldots \phi_{i_{p-1}} \right]. \quad (2.14)$$

We average the generating functional over the disorder in the system. We note that the action contains only one term with an explicit dependence on the disorder, the spin-spin interaction term ,which we call $L_J[\phi, \hat{\phi}]$,

$$L_J[\phi, \hat{\phi}] = i \frac{p}{p!} \sum_{i_1 \ldots i_p} \int_{t_0}^{t_f} dt J_{i_1 \ldots i_p} \hat{\phi}_{i_1}(t) \phi_{i_2}(t) \cdots \phi_{i_p}(t). \quad (2.15)$$

Therefore, we average over disorder by computing the part of the generating functional affected by the disorder,

$$\overline{\exp(L_J[\phi, \hat{\phi}])} = \int DJ P\{J\} \exp[L_J], \quad (2.16)$$

with $DJ \equiv \prod_{i_1 < \cdots < i_p} dJ_{i_1 \ldots i_p}$. The distribution of the disorder, which is assumed Gaussian, simplifies this integration. The result of the integration is to replace the $p-1$ real fields plus 1 auxiliary field with $2(p-1)$ real fields plus 2 auxiliary fields in the interaction term. From the point of view of time variables, we have now introduced two times, t and t', in the action. After integrating over the disorder we get $\overline{\exp(L_J[\phi, \hat{\phi}])}$ given by

$$\overline{\exp(L_J[\phi, \hat{\phi}])} = \exp\left[-\frac{p^2}{p!} \sum_{i_1 \ldots i_p} K_{i_1 \ldots i_p} \int_{t_0}^{t_f} \int_{t_0}^{t_f} dt dt' \times \sum_{\alpha_{i_r}, \alpha'_{i_r} \in \{0,1\}}^{C=1, C'=1} \sum_{i_1 \ldots i_p} \prod_{r=1}^{p} \phi_{i_r}^{\alpha_{i_r}}(t) \phi_{i_r}^{\alpha'_{i_r}}(t') \right], \quad (2.17)$$

where we have re-labeled the fields using the definitions $\phi_i^0(t) \equiv \hat{\phi}_i(t)$ and $\phi_i^1(t) \equiv \phi_i(t)$. The constrained variables C and C' are given by $C \equiv \sum_{r=1}^{p} (1 - \alpha_{i_r})$, $C' \equiv \sum_{r=1}^{p} (1 - \alpha'_{i_r})$, and the constraints $C = C' = 1$ enforce the condition that for each of the two times t and t', there is a product of fields, of which only one is a $\hat{\phi}$ and all others are ϕ fields. We are also interested in explicitly introducing two-time fields $Q_i^{\alpha,\alpha'}(t_1, t_2)$, physically associated with two-time correlations and responses. It should be noticed that the Hubbard-Stratonovich transformation allows for an intuitive way of introducing two time fields in the EA model,

but it is unlikely to be useful for the p-spin model because it involves completing squares in the exponent. Instead, we introduce two-time fields by writing the number one as an integral of delta function products that enforce the condition $Q_i^{\alpha,\alpha'}(t_1,t_2) = \phi_i^{\alpha}(t_1)\phi_i^{\alpha'}(t_2)$,

$$1 = \int DQ \prod_{i,t_1,t_2} \prod_{\alpha_i,\alpha_i' \in \{0,1\}} \delta\left[Q_i^{\alpha_i,\alpha_i'}(t_1,t_2) - \phi_i^{\alpha_i}(t_1)\phi_i^{\alpha_i'}(t_2)\right]. \tag{2.18}$$

By writing the delta function in exponential form we get

$$1 = \int DQD\hat{Q} \exp\left\{ i \sum_i \sum_{\alpha_i,\alpha_i' \in \{0,1\}} \int\int dt_1 dt_2 \hat{Q}_i^{\overline{\alpha_i},\overline{\alpha_i'}}(t_1,t_2) \times \left[Q_i^{\alpha_i,\alpha_i'}(t_1,t_2) - \phi_i^{\alpha_i}(t_1)\phi_i^{\alpha_i'}(t_2)\right]\right\}, \tag{2.19}$$

where we have introduced the auxiliary two-time fields $\hat{Q}_i^{\alpha_i,\alpha_i'}(t_1,t_2)$ and the notation $\overline{0} = 1$, $\overline{1} = 0$. This procedure of introducing two time fields is similar to combining the Lagrange multiplier method with the method of steepest descent, as used to obtain mean field equations [57, 58]. We now obtain the noise and disorder averaged generating functional

$$\begin{aligned} \overline{\langle Z[\{l_i\},\{h_i\}]\rangle} &= \int DQD\hat{Q}D\phi^0 D\phi^1 D\hat{\varphi} D\hat{N} \exp(\mathcal{S}), \\ \mathcal{S} &= S_1 + S_J + S_{spin} + S_{ext} + S_{BC} + S_{SC}. \end{aligned} \tag{2.20}$$

Here we have written the different terms of the action separately:

$$S_1[Q,\hat{Q},\phi^0,\phi^1] = i \sum_i \sum_{\alpha_i,\alpha_i' \in \{0,1\}} \int_{t_0}^{t_f}\int_{t_0}^{t_f} dt_1 dt_2 \hat{Q}_i^{\overline{\alpha_i},\overline{\alpha_i'}}(t_1,t_2) \times \left(Q_i^{\alpha_i,\alpha_i'}(t_1,t_2) - \phi_i^{\alpha_i}(t_1)\phi_i^{\alpha_i'}(t_2)\right), \tag{2.21}$$

$$S_J[Q] = -\frac{p^2}{p!} \sum_{i_1\ldots i_p} K_{i_1\ldots i_p} \int_{t_0}^{t_f}\int_{t_0}^{t_f} dt_1 dt_2 \sum_{\alpha_{i_r},\alpha_{i_r}' \in \{0,1\}}^{C=1,C'=1} \prod_{r=1}^{p} Q_{i_r}^{\alpha_{i_r},\alpha_{i_r}'}(t_1,t_2), \tag{2.22}$$

$$\begin{aligned} S_{spin}[\phi^0,\phi^1] \;=\; & -i \sum_{i=1}^{N} \int_{t_0}^{t_f} dt \phi_i^0(t)\left[\Gamma^{-1}\partial_t \phi_i^1(t) + \gamma_{00}\phi_i^0(t)\right] - \frac{p^2}{p!} \sum_{i_1\ldots i_p} K_{i_1\ldots i_p} \\ & \times \int_{t_0}^{t_f}\int_{t_0}^{t_f} dt_1 dt_2 g(t_1-t_2) \sum_{\alpha_{i_r},\alpha_{i_r}' \in \{0,1\}}^{C=1,C'=1} \prod_{r=1}^{p} \phi_{i_r}^{\alpha_{i_r}}(t_1)\phi_{i_r}^{\alpha_{i_r}'}(t_2), \end{aligned} \tag{2.23}$$

$$S_{ext}[\phi^0, \phi^1; l, h] = \int_{t_0}^{t_f} dt \left[l_i(t)\phi_i^0(t) + ih_i(t)\phi_i^1(t) \right], \tag{2.24}$$

$$S_{BC}[\phi^1, \hat{\varphi}; \varphi] = i \sum_{i=1}^{N} \hat{\varphi}_i \left[\phi_i^1(t_0) - \varphi_i \right], \tag{2.25}$$

$$S_{SC}[\phi^1, \hat{N}; N] = i \int_{t_0}^{t_f} dt \hat{N}(t) \left[\sum_{i=1}^{N} (\phi_i^1(t))^2 - N \right], \tag{2.26}$$

and we have the coupling constants $\Gamma = \Gamma_0$, $\gamma_{00} = -iT$ and $g(t - t') = 0$ at the start of the RG flow. In general, these constants are described by flow equations, the Gell-Mann-Low equations, when the RG transformation is applied to the generating functional. The flow equations give information about fixed points, *if any*, of the action.

2.3 Renormalization group analysis

2.3.1 Renormalization Group Transformation

We perform a renormalization group analysis on the time variables. For simplicity we take $t_0 = 0$ and $t_f = \infty$ from now on. Focusing on the two-time fields, first, we introduce a cutoff in their integration, $\tau_0 \leq |t_1 - t_2|$. We are mostly interested in the limit $t_1 - t_2 \to \infty$, in which time translation invariance and exponential behavior starts to break down with decreasing temperature. We then write the terms of the action affected by the cutoff:

$$S_1[Q, \hat{Q}] = i \sum_i \int_{\substack{0 \leq t_1, t_2 < \infty \\ \tau_0 \leq |t_1 - t_2|}} dt_1 dt_2 \sum_{\alpha_i, \alpha_i'} \hat{Q}_i^{\overline{\alpha_i}, \overline{\alpha_i'}}(t_1, t_2) \times \left[Q_i^{\alpha_i, \alpha_i'}(t_1, t_2) - \phi_i^{\alpha_i}(t_1)\phi_i^{\alpha_i'}(t_2) \right], \tag{2.27}$$

$$S_J[Q] = -\frac{p^2}{p!} \sum_{i_1 \ldots i_p} K_{i_1 \ldots i_p} \int_{\substack{0 \leq t_1, t_2 < \infty \\ \tau_0 \leq |t_1 - t_2|}} dt_1 dt_2 \sum_{\alpha_{i_r}, \alpha_{i_r}' \in \{0,1\}}^{C=1, C'=1} \prod_{r=1}^{p} Q_{i_r}^{\alpha_{i_r}, \alpha_{i_r}'}(t_1, t_2). \tag{2.28}$$

We define fast and slow fields respectively by $Q_{>i}^{\alpha_i, \alpha_i'}(t_1, t_2) = Q_i^{\alpha_i, \alpha_i'}(t_1, t_2)$, for $\tau_0 \leq |t_1 - t_2| < b\tau_0$ and $Q_{<i}^{\alpha_i, \alpha_i'}(t_1, t_2) = Q_i^{\alpha_i, \alpha_i'}(t_1, t_2)$, for $b\tau_0 \leq |t_1 - t_2|$, with $b > 1$. Applying

these definitions of slow and fast fields, we find that the terms $S_1[Q, \hat{Q}, \phi^0, \phi^1]$ and $S_J[Q]$ separate into slow and fast terms, i.e

$$S_1[Q, \hat{Q}, \phi^0, \phi^1] = S_1[Q_>, \hat{Q}_>, \phi^0, \phi^1] + S_1[Q_<, \hat{Q}_<, \phi^0, \phi^1], \tag{2.29}$$

$$S_J[Q] = S_J[Q_>] + S_J[Q_<]. \tag{2.30}$$

Next we calculate the integral over fast fields, $I_>$. The absence of cross terms between slow and fast terms makes the calculation of $I_>$ trivial:

$$\begin{aligned} I_> = & \int DQ_> D\hat{Q}_> \exp\left\{ i \sum_i \int_{\substack{\tau_0 \le |t_1 - t_2| < b\tau_0 \\ 0 \le t_1, t_2 < \infty}} dt_1 dt_2 \sum_{\alpha_i, \alpha_i'} \hat{Q}_{>i}^{\overline{\alpha_i}, \overline{\alpha_i'}}(t_1, t_2) \right. \\ & \times \left[Q_{>i}^{\alpha_i, \alpha_i'}(t_1, t_2) - \phi_i^{\alpha_i}(t_1) \phi_i^{\alpha_i'}(t_2) \right] \\ & \left. - \frac{p^2}{p!} \sum_{i_1 \ldots i_p} K_{i_1 \ldots i_p} \int_{\substack{\tau_0 \le |t_1 - t_2| < b\tau_0 \\ 0 \le t_1, t_2 < \infty}} dt_1 dt_2 \sum_{\alpha_{i_r}, \alpha_{i_r}' \in \{0,1\}}^{C=1, C'=1} \prod_{r=1}^{p} Q_{>i_r}^{\alpha_{i_r}, \alpha_{i_r}'}(t_1, t_2) \right\}. \end{aligned} \tag{2.31}$$

Calculating the delta function integral constitutes undoing the transformation that introduced the two-time fields, via integrals of delta functions, for the fast modes. Hence, we recover

$$I_> = \exp\left\{ -\frac{p^2}{p!} \sum_{i_1 \ldots i_p} K_{i_1 \ldots i_p} \int_{\substack{\tau_0 \le |t_1 - t_2| < b\tau_0 \\ 0 \le t_1, t_2 < \infty}} dt_1 dt_2 \sum_{\alpha_{i_r}, \alpha_{i_r}' \in \{0,1\}}^{C=1, C'=1} \prod_{r=1}^{p} \phi_{i_r}^{\alpha_{i_r}}(t_1) \phi_{i_r}^{\alpha_{i_r}'}(t_2) \right\}, \tag{2.32}$$

for the fast modes. Next we re-scale all the two-time as well as the one-time fields, which were not directly affected by the *coarse graining in time*. The rescaling is described by

$$Q_{<i}^{\alpha_i,\alpha_i'}(bt_1', bt_2') = b^{\lambda_{\alpha_i\alpha_i'}} Q'^{\alpha_i,\alpha_i'}_i(t_1', t_2'), \tag{2.33}$$

$$\hat{Q}_{<i}^{\alpha_i,\alpha_i'}(bt_1', bt_2') = b^{\hat{\lambda}_{\alpha_i\alpha_i'}} \hat{Q}'^{\alpha_i,\alpha_i'}_i(t_1', t_2'), \tag{2.34}$$

$$bt' = t, \tag{2.35}$$

$$\phi_i^{\alpha_i}(bt') = b^{\lambda_{\alpha_i}} \phi'^{\alpha_i}_i(t'), \tag{2.36}$$

$$l_i(bt') = b^{\lambda_l} l_i'(t'), \tag{2.37}$$

$$h_i(bt') = b^{\lambda_h} h_i'(t'), \tag{2.38}$$

$$\hat{\varphi}_i = b^{\lambda_\varphi} \hat{\varphi}_i'. \tag{2.39}$$

The effect of the rescaling is to ensure that the transformed slow fields fluctuate on the time scale set by the original cutoff, i.e $\tau_0 < t_2' - t_1'$, given that $b > 1$. From the definition of the two time fields in Eq. (2.18) and the transformation of the fields we get the condition

$$\lambda_{\alpha_i,\alpha_i'} = \lambda_{\alpha_i} + \lambda_{\alpha_i'}. \tag{2.40}$$

By rescaling the fields in the part of the action arising from the disorder average (S_J) we get

$$S_J[Q] = -\frac{p^2}{p!} b^{\lambda_J} \sum_{i_1 \ldots i_p} K_{i_1 \ldots i_p} \int_{\tau_0 \le |b(t_1' - t_2')|} dt_1' dt_2' \times \sum_{\alpha_{i_r},\alpha_{i_r}' \in \{0,1\}}^{C=1,C'=1} \sum_{i_1 \ldots i_p} \prod_{r=1}^{p} Q'^{\alpha_{i_r},\alpha_{i_r}'}_{i_r}(t_1', t_2'). \tag{2.41}$$

Using the relation between $\lambda_{\alpha,\alpha'}$, λ_α and $\lambda_{\alpha'}$ given by Eq. (2.40) together with the constraints $C = C' = 1$ we get

$$\lambda_J \equiv 2\lambda_0 + 2(p-1)\lambda_1 + 2. \tag{2.42}$$

Rescaling the fields in the source terms, we get

$$S'_{ext}[\phi^0, \phi^1; l, h] = \sum_{i=1}^{N} \int_0^\infty dt' \left[b^{1+\lambda_l+\lambda_1} l_i'(t') \phi'^0_i(t') + b^{1+\lambda_h+\lambda_0} i h_i'(t') \phi'^1_i(t') \right]. \tag{2.43}$$

The source terms are marginal by virtue of being derived from external fields, hence

$$\lambda_l = -1 - \lambda_1, \tag{2.44}$$

$$\lambda_h = -1 - \lambda_0. \tag{2.45}$$

Rescaling the fields in the boundary term we get;

$$S'_{BC}[\phi^1, \hat{\varphi}; \varphi] = i \sum_{i=1}^{N} b^{\lambda_\varphi} \hat{\varphi}'_i \left[b^{\lambda_1} {\phi'}^1_i(t_0) - \varphi'_i \right] \tag{2.46}$$

If this term is marginal we obtain $\lambda_\phi = -\lambda_1$. Next we consider the constraint term and obtain

$$S'_{CS}[\phi^1, \hat{N}; N] = ib^{1+\lambda_N} \int_0^\infty dt' \hat{N}'(t) \left[\sum_{i=1}^{N} (b^0 {\phi'}^1_i(t))^2 - N' \right]. \tag{2.47}$$

There is no condition on this term. But requiring this term to be marginal so that the constraint is still enforced at long times gives $\lambda_N = -1$. Also, the constraint term is constant in the long time limit because the constraints are still valid in this limit. Finally we re-scale the fields in the spin term

$$S_{spin}[\phi^0, \phi^1] = -i \sum_{i=1}^{N} \int_0^\infty dt' {\phi'}^0_i(t') \left[b^{\lambda_{vel}} \Gamma^{-1} \partial_{t'} {\phi'}^1_i(t') + b^{\lambda_T} \gamma_{00} {\phi'}^0_i(t') \right] \tag{2.48}$$

$$-\frac{p^2}{p!} \sum_{i_1 \ldots i_p} K_{i_1 \ldots i_p} \int\int_0^\infty dt'_1 dt'_2 b^{\lambda_J} g(t'_1 - t'_2) \sum_{\alpha_{i_r}, \alpha'_{i_r} \in \{0,1\}}^{C=1, C'=1} \prod_{r=1}^{p} {\phi'}^{\alpha_{i_r}}_{i_r}(t'_1) {\phi'}^{\alpha'_{i_r}}_{i_r}(t'_2)$$

The result is the following set of flow equations

$$\Gamma^{-1} \to \Gamma'^{-1} = \Gamma^{-1} b^{\lambda_{vel}}, \tag{2.49}$$

$$\gamma_{00} \to \gamma'_{00} = \gamma_{00} b^{\lambda_T}, \tag{2.50}$$

$$g(t_1 - t_2) \to g'(t'_1 - t'_2) = b^{\lambda_J} \left[g(b(t'_1 - t'_2)) + C_{\tau_0 \le |bt'_1 - bt'_2| < b\tau_0} \right], \tag{2.51}$$

where $C_{\mathcal{P}}$ is defined by $C_{\mathcal{P}} = 1$ if $\mathcal{P}$ is true and $C_{\mathcal{P}} = 0$ if $\mathcal{P}$ is not true, and

$$\lambda_{vel} = \lambda_0 + \lambda_1, \tag{2.52}$$

$$\lambda_T = 1 + 2\lambda_0. \tag{2.53}$$

By now we have applied the RG procedure once and we have shifted the short time cutoff by the parameter b to a higher cutoff value, $\tau_0 \to \tau_0' \equiv b\tau_0$ and restored it to its original value. Repeating the procedure several times and if we let $b = e^{dl} \cong 1 + dl$ then we find the flow equations for Γ and γ_{00} and g:

$$\frac{d\Gamma}{dl} = -\lambda_{vel}\Gamma, \tag{2.54}$$

$$\frac{d\gamma_{00}}{dl} = \lambda_T\gamma_{00}, \tag{2.55}$$

$$\frac{dg}{dl} = \lambda_J g. \tag{2.56}$$

In oder to determine the nature of the fixed points we need to choose values for the scaling exponents λ_0 and λ_1. Details of Wilson's approach to the RG are given in Appendix (B).

2.3.2 Choice of Scaling Exponents

In traditional RG calculations one determines an engineering dimension for the field variable by requiring that the action of the free theory be marginal. In our case, there is an ambiguity in fixing engineering dimensions for ϕ_i^0 and ϕ_i^1 because none of the terms in the action is of the same form as the gradient squared term that is usually considered to be the unperturbed part of the action and assumed to be marginal. The only systematic way to proceed is to consider what happens when each of the terms in the action is marginal. We start by noting that the spherical constraint $\sum_{i=1}^{N}[\phi_i(t)]^2 = N$ imposes an upper bound on the correlation function $C(t,t') \sim Q^{11}(t,t')$, i.e we have the constraint $\lambda_1 \leq 0$. The case of $\lambda_1 = 0$ means that the correlation function transforms as $C(t,t') \to \tilde{C}(t,t') \equiv C(t,t')$ or equivalently $C(t,t') = k$, with k a constant and hence freezing. The strict inequality means that the correlation function transforms as $C(t,t') \to b^{-2|\lambda_1|}C(t,t')$, which corresponds to a decaying correlation because $b > 1$. The terms in the action that are of interest for our analysis are the three terms contained in S_{spin}: the spin-spin interaction term, the time

derivative term and the term representing the coupling to the thermal bath. As indicated in Eqs. (2.42), (2.52) and (2.53), these three terms have the scaling exponents $\lambda_J = 2(1 + \lambda_0 + (p-1)\lambda_1)$, $\lambda_{vel} = \lambda_0 + \lambda_1$ and $\lambda_T = 1 + 2\lambda_0$, respectively. By considering the cases in which only one of the terms is marginal we get the results summarized in Fig. (2.1).

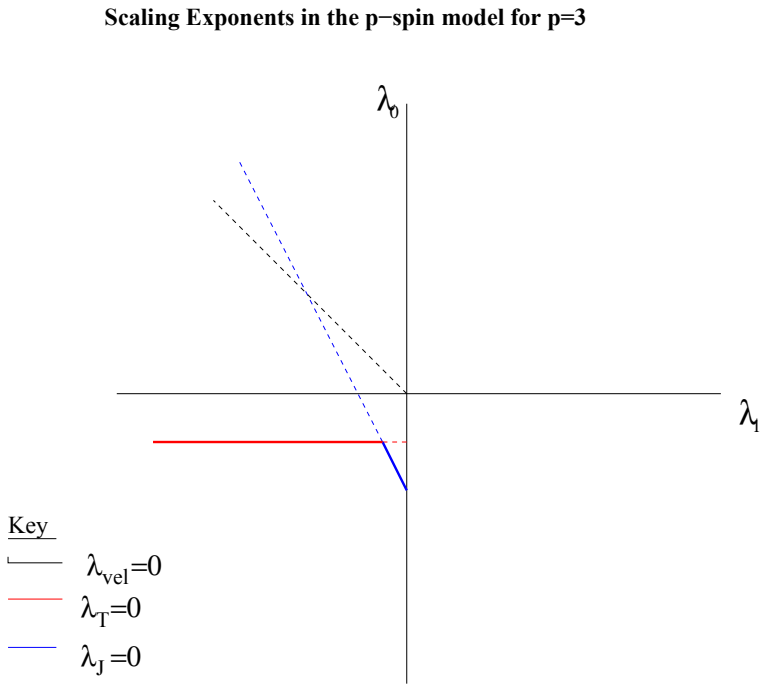

Figure 2.1: The figure shows the different lines along which each one of the three terms in S_{spin} is marginal for $p = 3$. The red line corresponds to a marginal coupling to the thermal bath ($\lambda_T = 0$), the black line corresponds to a marginal time-derivative term ($\lambda_{vel} = 0$), and the blue line corresponds to a marginal spin-spin interaction term ($\lambda_J = 0$).

In the case in which the coupling to the thermal bath is marginal, $\lambda_T = 0$, we have a line $\lambda_0 = -1/2$ in the (λ_1, λ_0) plane. The line divides the plane into three distinct subsets. One, the line is a subset of (λ_1, λ_0) plane on which the coupling to the thermal bath does not flow with the changing time scale. Two, below this line is a subset of the plane in which $\lambda_T < 0$, and the coupling to the thermal bath decays with increasing time scales, i.e

the subset of *irrelevant* couplings. Three, above this line is a subset of the plane in which $\lambda_T > 0$ and the coupling to the thermal bath grows with increasing time scales, i.e the subset of *relevant* couplings. Considering only the subset in which the coupling to the thermal bath is marginal, we make a comparison with the other two couplings, the time derivative term's coupling and the spin-spin interaction term's coupling. Given the constraint $\lambda_1 \leq 0$ and the values of λ_J and λ_{vel}, we find that there is an interval on this line, $\lambda_1 < \frac{-1}{2(p-1)}$, in which both the spin-spin interactions and the time derivative term are irrelevant. Since the coupling to the thermal bath is marginal then we have a family of stable high temperature fixed points, i.e the effective dynamics is given by this term.

Next, considering only the case when the time derivative term is marginal, corresponding to the line $\lambda_0 = -\lambda_1$ in the (λ_1, λ_0) plane, we make a comparison to the thermal bath term's coupling and the spin-spin interaction term's coupling. Since we have $\lambda_1 \leq 0$, the exponent λ_T of Eq. (2.53) is always positive, i.e. the coupling to the thermal bath is always a relevant term along this line. Hence the thermal coupling always grows faster than the marginal time derivative coupling. Thus, any fixed points containing only the time derivative term are always unstable, i.e the derivative term is unable to fully determine dynamics without the other terms overshadowing its influence in the long time limit. Finally, we consider the case where the spin-spin term is marginal and compare it to the other two terms. This happens on the line described by $\lambda_0 = -1 - (p-1)\lambda_1$. In the interval $\frac{-1}{2(p-1)} < \lambda_1 \leq 0$ the time derivative term and coupling to the thermal bath are irrelevant. Therefore in this interval we have stable low temperature fixed points, in which the effective dynamics is given by the spin-spin interactions.

The above analysis shows that there is a subset of the (λ_1, λ_0) plane for which a high temperature dynamical fixed point family is present. The effective generating functional

for this fixed point family is

$$\mathcal{Z}_{fp}[l,h;T] = \overline{\langle Z[\{l_i\},\{h_i\}]\rangle}_{fp} = \int DQD\hat{Q}D\phi^0 D\phi^1 D\hat{\varphi}D\hat{N}$$
$$\times \exp\left\{ i\sum_i \int\int_0^\infty dt_1 dt_2 \sum_{\alpha_i,\alpha_i'} \hat{Q}_i^{\overline{\alpha_i},\overline{\alpha_i'}}(t_1,t_2)\left[Q_i^{\alpha_i,\alpha_i'}(t_1,t_2) - \phi_i^{\alpha_i}(t_1)\phi_i^{\alpha_i'}(t_2)\right]\right.$$
$$-T\sum_{i=1}^N \int_0^\infty dt\left[\phi_i^0(t)\right]^2 + \int_0^\infty dt[l_i(t)\phi_i^0(t) + ih_i(t)\phi_i^1(t)]$$
$$\left. +i\sum_{i=1}^N \hat{\varphi}_i[\phi_i^1(t_0) - \varphi_i] + i\int_0^\infty dt\hat{N}(t)\left[\sum_{i=1}^N (\phi_i^1(t))^2 - N\right]\right\}. \qquad (2.57)$$

There is another subset of the (λ_1, λ_0) plane for which a low temperature interaction-dominated fixed point family is present. The effective generating functional for this family of fixed points is

$$\mathcal{Z}_{fp}[l,h;J] = \overline{\langle Z[\{l_i\},\{h_i\}]\rangle}_{fp} = \int DQD\hat{Q}D\phi^0 D\phi^1 D\hat{\varphi}D\hat{N}$$
$$\times \exp\left\{ i\sum_i \int\int_0^\infty dt_1 dt_2 \sum_{\alpha_i,\alpha_i'} \hat{Q}_i^{\overline{\alpha_i},\overline{\alpha_i'}}(t_1,t_2)\left[Q_i^{\alpha_i,\alpha_i'}(t_1,t_2) - \phi_i^{\alpha_i}(t_1)\phi_i^{\alpha_i'}(t_2)\right]\right.$$
$$-\frac{p^2}{p!}\sum_{i_1\ldots i_p} K_{i_1\ldots i_p}\int\int_0^\infty dt_1 dt_2 \sum_{\alpha_{i_r},\alpha_{i_r}'\in\{0,1\}}^{C=1,C'=1}\prod_{r=1}^p Q_{i_r}^{\alpha_{i_r},\alpha_{i_r}'}(t_1,t_2)$$
$$+\int_0^\infty dt[l_i(t)\phi_i^0(t) + ih_i(t)\phi_i^1(t)]$$
$$\left. +i\sum_{i=1}^N \hat{\varphi}_i[\phi_i^1(t_0) - \varphi_i] + i\int_0^\infty dt\hat{N}(t)\left[\sum_{i=1}^N (\phi_i^1(t))^2 - N\right]\right\}. \qquad (2.58)$$

We note that the subset representing stable low temperature fixed points in the (λ_1, λ_0) plane includes the point $\lambda_1 = 0$ and $\lambda_0 = -1$. This is the only point in the plane that represents freezing of the correlation, a property of glasses. We also note that the point $\lambda_0 = -1/2$ and $\lambda_1 = \frac{-1}{2(p-1)}$ corresponds to a third family of stable fixed point actions, in which there are two marginal terms: the spin-spin interactions term and the coupling to the thermal bath.

2.4 Time reparametrization symmetry

We now evaluate the effect of a reparametrization $t \to s(t)$ of the time variable on the families of stable fixed point generating functionals. For this purpose we consider a monotonically increasing function with the boundary conditions $s(0) = 0$ and $s(\infty) = \infty$, which induces the following transformations on the sources,

$$\tilde{l}_i(t) = \frac{\partial s}{\partial t} l_i(s(t)), \tag{2.59}$$

$$\tilde{h}_i(t) = h_i(s(t)). \tag{2.60}$$

First we consider the effective generating functional of the high temperature fixed points. We evaluate the fixed point generating functional of the new sources

$$\begin{aligned}
\mathcal{Z}_{fp}[\tilde{l}, \tilde{h}; T] = \int D\tilde{Q} D\tilde{\hat{Q}} D\psi^0 D\psi^1 D\tilde{\varphi} D\tilde{N} \\
\times \exp\left\{ i \sum_i \int_0^\infty dt_1 dt_2 \sum_{\alpha_i, \alpha_i'} \tilde{\hat{Q}}_i^{\overline{\alpha_i}, \overline{\alpha_i'}}(t_1, t_2) \left[\tilde{Q}_i^{\alpha_i, \alpha_i'}(t_1, t_2) - \psi_i^{\alpha_i}(t_1) \psi_i^{\alpha_i'}(t_2) \right] \right. \\
-T \sum_{i=1}^N \int_0^\infty dt \left[\psi_i^0(t) \right]^2 + \int_0^\infty dt [\tilde{l}_i(t) \psi_i^0(t) + i \tilde{h}_i(t) \psi_i^1(t)] \\
\left. + i \sum_{i=1}^N \tilde{\hat{\varphi}}_i [\psi_i^1(t_0) - \tilde{\varphi}_i] + i \int_0^\infty dt \tilde{N}(t) \left[\sum_{i=1}^N (\psi_i^1(t))^2 - N \right] \right\}.
\end{aligned} \tag{2.61}$$

Here we have used new dummy variables ψ^α, $\tilde{\hat{\varphi}}$, $\tilde{\hat{Q}}$, $\tilde{Q}$ and $\tilde{N}$, instead of ϕ^α, $\hat{\varphi}$, $\hat{Q}$, Q and $\hat{N}$, respectively, in the functional integral. We now perform the following change of variables

$$\psi_i^\alpha(t) = \left(\frac{\partial s}{\partial t} \right)^{\overline{\alpha}} \phi_i^\alpha(s(t)), \tag{2.62}$$

$$\tilde{Q}_i^{\alpha, \alpha'}(t, t') = \left(\frac{\partial s}{\partial t} \right)^{\overline{\alpha}} \left(\frac{\partial s}{\partial t'} \right)^{\overline{\alpha'}} Q_i^{\alpha, \alpha'}(s(t), s(t')), \tag{2.63}$$

$$\tilde{\hat{Q}}_i^{\alpha, \alpha'}(t, t') = \left(\frac{\partial s}{\partial t} \right)^{\alpha} \left(\frac{\partial s}{\partial t'} \right)^{\alpha'} \hat{Q}_i^{\alpha, \alpha'}(s(t), s(t')), \tag{2.64}$$

$$\tilde{N}(t) = \frac{\partial s}{\partial t} \hat{N}(s(t)), \tag{2.65}$$

$$\tilde{\hat{\varphi}} = \hat{\varphi}. \tag{2.66}$$

The change of variables results in Jacobians in the differentials,

$$D\tilde{Q}D\hat{\tilde{Q}} = DQD\hat{Q}\mathcal{J}_1\left[\frac{D\tilde{Q}}{DQ}\frac{D\hat{\tilde{Q}}}{D\hat{Q}}\right], \tag{2.67}$$

$$D\psi^0 D\psi^1 D\tilde{N} = D\phi^0 D\phi^1 D\hat{N}\mathcal{J}_2\left[\frac{D\psi^0}{D\phi^0}\frac{D\psi^1}{D\phi^1}\frac{D\tilde{N}}{D\hat{N}}\right], \tag{2.68}$$

$$D\tilde{\hat{\varphi}} = D\hat{\varphi}. \tag{2.69}$$

Since the field transformations are linear, the Jacobians depend only on the reparametrization $s(t)$. Therefore, they are independent of the fields and sources, and can be taken outside the integral as common factors.

By inserting the values of the transformed sources and dummy variables back into the fixed point generating functional we obtain,

$$\begin{aligned}\mathcal{Z}_{fp}[\tilde{l},\tilde{h};T] = \mathcal{J}_1\mathcal{J}_2\int DQD\hat{Q}D\phi^0 D\phi^1 D\hat{\varphi}D\hat{N}\\ \exp\left\{i\sum_i\int_0^\infty dtdt'\sum_{\alpha_i,\alpha_i'}\left(\frac{\partial s}{\partial t}\right)^{\overline{\alpha_i}+\alpha_i}\left(\frac{\partial s}{\partial t'}\right)^{\overline{\alpha_i'}+\alpha_i'}\hat{Q}_i^{\overline{\alpha_i},\overline{\alpha_i'}}(s(t),s(t'))\right.\\ -T\int_0^\infty dt\left[\frac{\partial s}{\partial t}\phi_i^0(s(t))\right]^2+\int_0^\infty dt\left(\frac{\partial s}{\partial t}l_i(s(t))\phi_i^0(s(t))+ih_i(s(t))\frac{\partial s}{\partial t}\phi_i^1(s(t))\right)\\ \left.+i\sum_{i=1}^N\hat{\varphi}_i[\phi_i^1(s(0))-\varphi_i]+i\int_0^\infty dt\frac{\partial s}{\partial t}\hat{N}(s(t))\left[\sum_{i=1}^N(\phi_i^1(s(t)))^2-N\right]\right\}.\end{aligned} \tag{2.70}$$

So then the transfomed fixed point generating functional is

$$\begin{aligned}\mathcal{Z}_{fp}[\tilde{l},\tilde{h};T] = \mathcal{J}_1\mathcal{J}_2\int DQD\hat{Q}D\phi^0 D\phi^1 D\hat{\varphi}D\hat{N}\\ \exp\left\{i\sum_i\int_0^\infty dsds'\sum_{\alpha_i,\alpha_i'}\hat{Q}_i^{\overline{\alpha_i},\overline{\alpha_i'}}(s,s')\left(Q_i^{\alpha_i,\alpha_i'}(s,s')-\phi_i^{\alpha_i}(s)\phi_i^{\alpha_i'}(s')\right)\right.\\ -T\int_0^\infty ds\left[\phi_i^0(s)\right]^2\frac{\partial s}{\partial t}+\int_0^\infty ds[l_i(s)\phi_i^0(s)+ih_i(s)\phi_i^1(s)]\\ \left.+i\sum_{i=1}^N\hat{\varphi}_i[\phi_i^1(0)-\varphi_i]+i\int_0^\infty ds\hat{N}(s)\left[\sum_{i=1}^N(\phi_i^1(s))^2-N\right]\right\}.\end{aligned} \tag{2.71}$$

Here we have used the fact that $\alpha+\overline{\alpha}=1$. We notice that the term describing the coupling to the bath is not invariant with respect to the transformation $t\to s(t)$. So the high

temperature fixed points are not invariant under reparametrizations of the time variable. For the same reason, the family of fixed point actions containing both the coupling to the thermal bath and the spin-spin interaction is not invariant under time reparametrizations.

Finally, we consider the fixed point generating functional for the low temperature fixed point family. We evaluate the fixed point generating functional for the new sources

$$\mathcal{Z}_{fp}[\tilde{l},\tilde{h};J] = \int D\tilde{Q}D\tilde{\hat{Q}}D\psi^0 D\psi^1 D\tilde{\hat{\varphi}}D\tilde{N}$$
$$\times \exp\left\{ i\sum_i \int_0^\infty dt_1 dt_2 \sum_{\alpha_i,\alpha_i'} \tilde{\hat{Q}}_i^{\overline{\alpha_i},\overline{\alpha_i'}}(t_1,t_2)\left(\tilde{Q}_i^{\alpha_i,\alpha_i'}(t_1,t_2) - \psi_i^{\alpha_i}(t_1)\psi_i^{\alpha_i'}(t_2)\right)\right.$$
$$-\frac{p^2}{p!}\sum_{i_1\ldots i_p} K_{i_1\ldots i_p}\int_0^\infty dt_1 dt_2 \sum_{\alpha_{i_r},\alpha_{i_r}'\in\{0,1\}}^{C=1,C'=1}\prod_{r=1}^{p}\tilde{Q}_{i_r}^{\alpha_{i_r},\alpha_{i_r}'}(t_1,t_2)$$
$$+\int_0^\infty dt[\tilde{l}_i(t)\psi_i^0(t) + i\tilde{h}_i(t)\psi_i^1(t)]$$
$$\left. +i\sum_{i=1}^N \tilde{\hat{\varphi}}_i[\psi_i^1(t_0) - \tilde{\varphi}_i] + i\int_0^\infty dt\tilde{N}(t)\left[\sum_{i=1}^N(\psi_i^1(t))^2 - N\right]\right\}. \qquad (2.72)$$

Here we have used the dummy variables used in the analysis of the high temperature fixed point. Doing the same change of variables we get the Jacobians $\mathcal{J}_1$ and $\mathcal{J}_2$.

By inserting the values of the transformed sources and dummy variables back into the fixed point generating functional we obtain,

$$\mathcal{Z}_{fp}[\tilde{l},\tilde{h};J] = \mathcal{J}_1\mathcal{J}_2\int DQD\hat{Q}D\phi^0 D\phi^1 D\hat{\varphi}D\hat{N}$$
$$\exp\left\{ i\sum_i\int_0^\infty dtdt'\sum_{\alpha_i,\alpha_i'}\left(\frac{\partial s}{\partial t}\right)^{\overline{\alpha_i}+\alpha_i}\left(\frac{\partial s}{\partial t'}\right)^{\overline{\alpha_i'}+\alpha_i'}\hat{Q}_i^{\overline{\alpha_i},\overline{\alpha_i'}}(s(t),s(t'))\right.$$
$$\left.\times\left(Q_i^{\alpha_i,\alpha_i'}(s(t),s(t')) - \phi_i^{\alpha_i}(s(t))\phi_i^{\alpha_i'}(s(t'))\right)\right.$$
$$-\frac{p^2}{p!}\sum_{i_1\ldots i_p}K_{i_1\ldots i_p}\int_0^\infty dtdt'\sum_{\alpha_{i_r},\alpha_{i_r}'\in\{0,1\}}^{C=1,C'=1}\prod_{r=1}^{p}\left(\frac{\partial s}{\partial t}\right)^{\overline{\alpha_{i_r}}}\left(\frac{\partial s}{\partial t}\right)^{\overline{\alpha_{i_r}'}}Q_{i_r}^{\alpha_{i_r},\alpha_{i_r}'}(s(t),s(t'))$$
$$+\int_0^\infty dt\left(\frac{\partial s}{\partial t}l_i(s(t))\phi_i^0(s(t)) + ih_i(s(t))\frac{\partial s}{\partial t}\phi_i^1(s(t))\right)$$
$$\left.+i\sum_{i=1}^N\hat{\varphi}_i[\phi_i^1(s(0)) - \varphi_i] + i\int_0^\infty dt\frac{\partial s}{\partial t}\hat{N}(s(t))\left[\sum_{i=1}^N(\phi_i^1(s(t)))^2 - N\right]\right\}. \qquad (2.73)$$

We now use the fact that $\alpha + \bar{\alpha} = 1$ and that the constraints C and C' ensure that $\prod_{r=1}^{p} \left(\frac{\partial s}{\partial t}\right)^{\bar{\alpha}_{i_r}} \left(\frac{\partial s}{\partial t'}\right)^{\bar{\alpha}'_{i_r}} = \frac{\partial s}{\partial t}\frac{\partial s}{\partial t'}$, to write the transformed fixed point generating functional

$$\mathcal{Z}_{fp}[\tilde{l},\tilde{h};J] = \mathcal{J}_1\mathcal{J}_2 \int DQD\hat{Q}D\phi^0 D\phi^1 D\hat{\varphi}D\hat{N}$$
$$\exp\left\{ i\sum_i \int_0^\infty dsds' \sum_{\alpha_i,\alpha'_i} \hat{Q}_i^{\bar{\alpha}_i,\bar{\alpha}'_i}(s,s')\left(Q_i^{\alpha_i,\alpha'_i}(s,s') - \phi_i^{\alpha_i}(s)\phi_i^{\alpha'_i}(s')\right)\right.$$
$$-\frac{p^2}{p!}\sum_{i_1\ldots i_p} K_{i_1\ldots i_p}\int_0^\infty dsds' \sum_{\alpha_{i_r},\alpha'_{i_r}\in\{0,1\}}^{C=1,C'=1} \prod_{r=1}^{p} Q_{i_r}^{\alpha_{i_r},\alpha'_{i_r}}(s,s')$$
$$+\int_0^\infty ds[l_i(s)\phi_i^0(s) + ih_i(s)\phi_i^1(s)]$$
$$\left. +i\sum_{i=1}^{N}\hat{\varphi}_i[\phi_i^1(0)-\varphi_i] + i\int_0^\infty ds\hat{N}(s)\left[\sum_{i=1}^{N}(\phi_i^1(s))^2 - N\right]\right\}. \tag{2.74}$$

In other words, we have shown that

$$\mathcal{Z}_{fp}[\tilde{l},\tilde{h};J] = \mathcal{J}_1\mathcal{J}_2\mathcal{Z}_{fp}[l,h;J]. \tag{2.75}$$

We know that in the absence of sources, the transformation leaves the generating functional unchanged. This implies that $\mathcal{J}_1\mathcal{J}_2 = 1$, but since $\mathcal{J}_1$ and $\mathcal{J}_2$ are independent of the values of the sources, then for *any* value of the sources the fixed point generating functional is unchanged by the transformation, i.e.,

$$\mathcal{Z}_{fp}[\tilde{l},\tilde{h}] = \mathcal{Z}_{fp}[l,h]. \tag{2.76}$$

Therefore, the long-time fixed point dynamics of the spin-spin interactions in the p-spin model is invariant under time reparametrizations.

2.5 Discussion and conclusion

We have shown that there are three families of stable fixed points for the time RG applied to the MSR generating functional of the p-spin model: (i) a family of high temperature fixed point actions that are not invariant under global reparametrizations of

the time variable, characterized by the presence of the coupling to the thermal bath and the absence of the spin interaction term; (ii) a family of low temperature fixed points that are invariant under global time reparametrizations in the long time limit, for which the action contains the spin interaction term but not the coupling to the bath; and (iii) a third family of stable fixed points, for which both terms are present in the action, and the action is not invariant under time reparametrizations. Since not all the stable fixed point actions in the model are invariant, it is clear that the time reparametrization symmetry is a nontrivial property of the low temperature, interaction dominated dynamics. It should also be pointed out that in another interacting spin model, the O(N) ferromagnet model with Langevin dynamics, the symmetry is not present even in the low temperature effective dynamics [55].

The proof of invariance only assumes that the couplings $J_{i_1 \ldots i_p}$ are uncorrelated Gaussian random variables with zero mean, but no condition is imposed on the variance $K_{i_1 \ldots i_p}$ of the couplings, thus allowing them to have an arbitrary space dependence. In particular, the proof applies to both short-range and long-range models. Since some versions of the p-spin model share some of the main features of structural glass phenomenology [54, 65], we expect that analytical tools similar to the ones used here may be able to uncover the presence of time reparametrization symmetry in models of structural glass systems. We recall, from Section (1.5.3), that time reparametrization symmetry is a spontaneously broken symmetry in glasses and we expect Goldstone modes associated with smooth spatial variations of the reparametrizations, $t \to h_{\vec{r}}(t)$. In the next chapter we present a method to determine the phases $\phi_{\vec{r}}(t) \equiv h_{\vec{r}}(t)$, and demonstrate it on existing data.

3 F P F R T G S

Part of the material presented in this chapter has been submitted for publication: G. A. Mavimbela, H. E. Castillo and A. Parsaeian, arxiv:1210.1249. The rest of the material is included in a second manuscript, which is in preparation.

3.1 Introduction

Developing quantitative approaches for studying local dynamics has become more important nowadays because of the growing evidence for dynamical heterogeneity which has been found in particle tracking experiments in glassy colloidal systems [21, 22, 23] and granular systems [25], and in numerical simulations [26, 27]. A quantitative description of dynamical heterogeneity in terms of the presence of locally fluctuating relaxation times $\tau_{\vec{r}}(t)$ has in principle some strong advantages. One of them is its simplicity and intuitive appeal. Another one is that the basic quantities that appear in this description are intrinsically instantaneous, as opposed to other common descriptions for which the basic quantities describe changes in the system over a finite time interval, which complicates their interpretation. Despite those advantages, however, such a description has proved elusive. For example, even the question of experimentally determining the relationship between the lifetime τ_{ex} of regions of heterogeneous dynamics and the bulk α-relaxation time τ_α has proved controversial, with some results indicating that $\tau_{\text{ex}}/\tau_\alpha \sim 1$, and other results indicating that $\tau_{\text{ex}}/\tau_\alpha \gg 1$ [8].

In this chapter, our goal is twofold. On one hand, we establish a connection between the presence of time reparametrization fluctuations and the presence of fluctuating local relaxation times $\tau_{\vec{r}}(t)$. Starting from the intuitive picture of spatial heterogeneity in the relaxation times [8], we show that phases that are local in time and space emerge. The

same local phases are naturally present if one assumes that there is a time reparametrization symmetry which is spontaneously broken, and therefore, there are Goldstone modes [37, 38, 39, 40, 41, 42, 43, 44, 45, 46, 47]. In addition, we show that under certain circumstances the time derivatives of the phases can in some cases be interpreted as spatial-temporal fluctuating local relaxation rates. Additionally, we introduce a new method to extract the actual values of those relaxation times $\tau_{\vec{r}}(t)$ from experimental or numerical data, and test this method on existing data from numerical simulations.

The chapter is organized as follows. In Sec. 3.2 we discuss the connection between the presence of time reparametrization fluctuations and a description of the system in terms of fluctuating local relaxation times. In Sec. 3.3 we explain our proposed method to extract local relaxation times from numerical or experimental data. In Sec. 3.4 we discuss the details of the numerical simulations that we have used to test the method, and we present the results of those tests. In Sec. 3.5 we use the method to study probability distributions and power spectra. Finally, in Sec. 3.6, we summarize our results.

3.2 Connection between fluctuating local relaxation times and time reparametrization fluctuations

In this section we present arguments that lead to the identification of fluctuating local phases, and show that the time derivatives of the phases may sometimes be interpreted as instantaneous local relaxation rates. We begin our discussion by considering the two extreme scenarios that were proposed to explain the non-exponential relaxation behavior in glass formers close to the glass transition [8, 13]. We recall that in one of them, the liquid is heterogeneous, the relaxation is exponential in each small region, there is a

spatial distribution of relaxation times $P(\tau)$, and the relaxation function is given by

$$C(t-t') = \int_0^\infty d\tau P(\tau) \exp\left(-\frac{t-t'}{\tau}\right) = \int \frac{d^d r}{V} C_{\vec{r}}(t,t') \quad \text{with } C_{\vec{r}}(t,t') = C_0 \exp\left(-\frac{t-t'}{\tau_r}\right), \tag{3.1}$$

where $C_{\vec{r}}(t,t')$ is the local two-time correlation in a small region around point $\vec{r}$ and τ_r is the corresponding relaxation time for the small region. In the other extreme scenario, the dynamics of the liquid is homogeneous, the distribution of the relaxation times is a delta function, and the relaxation in all regions is described by a unique function $g(x)$, which is non-exponential:

$$C(t-t') = \int_0^\infty d\tau \delta(\tau-\tau_0) g\left(\frac{t-t'}{\tau}\right) = \int \frac{d^d r}{V} C_{\vec{r}}(t,t') \quad \text{with } C_{\vec{r}}(t,t') = g\left(\frac{t-t'}{\tau_0}\right). \tag{3.2}$$

Eqs. (3.1) and (3.2) can be generalized to allow for the simultaneous presence of both heterogeneous relaxation times and non-exponential local relaxation functions [66]:

$$C(t-t') = \int_0^\infty d\tau P_g(\tau) g\left(\frac{t-t'}{\tau}\right) = \int \frac{d^d r}{V} C_{\vec{r}}(t,t') \quad \text{with } C_{\vec{r}}(t,t') = g\left(\frac{t-t'}{\tau_{\vec{r}}}\right), \tag{3.3}$$

where $P_g(\tau)$ is the probability density of relaxation times compatible with the local relaxation function $g(x)$.

If we allow the time difference $t-t'$ to be long enough, we cannot assume that each local region is characterized by a time independent relaxation time $\tau_{\vec{r}}$, because $\tau_{\vec{r}}$ could in principle have fluctuated over this time interval. To take this effect into account, let us divide the time interval $[t',t)$ into $n-1$ sub-intervals $\{[t_{i-1},t_i)\}_{i=2,\ldots,n}$ such that for each sub-interval the fluctuations in $\tau_{\vec{r}}(t)$ are negligible. Hence, for long time intervals, the local correlation is given by

$$C_{\vec{r}}(t,t') = g\left[\sum_{i=2}^{n} \frac{t_i - t_{i-1}}{\tau_{\vec{r}}(t_{i-1})}\right], \tag{3.4}$$

where $t_n = t$ and $t_1 = t'$. In the limit of infinitesimal time intervals we get $t_i - t_{i-1} \to dt$ and the sum becomes an integral,

$$C_{\vec{r}}(t,t') = g\left[\int_{t'}^{t} \frac{dt''}{\tau_{\vec{r}}(t'')}\right]. \tag{3.5}$$

In this general expression for $C_{\vec{r}}(t,t')$, the relaxation is allowed to be locally non-exponential, and the relaxation time is allowed to fluctuate both in space and time.

Another way of looking at local correlations is to consider first the exponential relaxation case where

$$\frac{dC(t,t')}{dt} = -\frac{1}{\tau}C(t,t') \qquad \Rightarrow C(t,t') = C_0 \exp\left(-\frac{t-t'}{\tau}\right). \tag{3.6}$$

If we allow τ to fluctuate in space and time but postulate that the same differential equation still holds, then we have

$$\frac{dC_{\vec{r}}(t,t')}{dt} = -\frac{1}{\tau_{\vec{r}}(t)}C_{\vec{r}}(t,t') \qquad \Rightarrow C_{\vec{r}}(t,t') = C_0 \exp\left[-\int_{t'}^{t}\frac{dt''}{\tau_{\vec{r}}(t'')}\right], \tag{3.7}$$

where $C_{\vec{r}}(t,t')$ and $\tau_{\vec{r}}(t)$ are defined as before and we have used the initial condition $C_0 = \lim_{t\to t'^+} C(t,t')$. Eq. (3.7) can be extended to describe the more general case of non-exponential relaxation. For example, we can modify the right hand-side of the differential equation in Eq. (3.7) to

$$\frac{dC_{\vec{r}}(t,t')}{dt} = -\frac{1}{\tau_{\vec{r}}}G[C_{\vec{r}}(t,t')]. \tag{3.8}$$

Here the function $G[C_{\vec{r}}(t,t')]$ represents the effect of non-exponential relaxation. The solution of the new differential equation is of the form

$$C_{\vec{r}}(t,t') = C\left[\phi_{\vec{r}}(t) - \phi_{\vec{r}}(t')\right], \tag{3.9}$$

where $\phi_{\vec{r}}(t) \equiv \int^{t}\frac{dt'}{\tau_{\vec{r}}(t')}$, and $C(x)$ is a monotonous decreasing function that satisfies $C'(x) = -G[C(x)]$ and $0 \le C(x) \le 1$.

By comparing Eq. (3.5) with Eq. (3.9) we find that $g(x) = C(x)$ and

$$\phi_{\vec{r}}(t) - \phi_{\vec{r}}(t') = \int_{t'}^{t}\frac{dt''}{\tau_{\vec{r}}(t'')}. \tag{3.10}$$

A completely different way of deriving Eq. (3.9) is based on the presence of time reparametrization symmetry. We recall, from Section 1.5.3, that time reparametrization is

a broken continuous symmetry and is expected to give rise to Goldstone modes [37, 38, 39, 40, 41, 42, 43, 44, 45, 46, 47]. The Goldstone modes are associated with smooth variations in space of the reparametrized variable, that is $t \rightarrow \phi_{\vec{r}}(t)$ and the spatial-temporal fluctuations of $\phi_{\vec{r}}(t)$ lead to recovering Eq. (3.9) if we ignore longitudinal fluctuations [37, 38, 39]. As discussed in Refs. [37, 38, 39], longitudinal fluctuations should be suppressed by coarse graining in larger regions because at long distances they are less correlated than transverse fluctuations [68]. It should be noticed that the phase difference that appears in the argument in Eq. (3.9) can also be written as an integral of the time derivative of the phases $\dot{\phi}_{\vec{r}}(t) = \frac{\partial \phi_{\vec{r}}}{\partial t}$, evaluated at the two times, i.e

$$\phi_{\vec{r}}(t) - \phi_{\vec{r}}(t') \equiv \int_{t'}^{t} dt'' \dot{\phi}_{\vec{r}}(t''). \tag{3.11}$$

Finally, it should be noticed that there is a symmetry under time-independent shifts of the reparametrization variable $\phi_{\vec{r}}(t)$, that is in Eq. (3.9), the local correlation is unchanged by the transformation $\phi_{\vec{r}}(t) \rightarrow \phi_{\vec{r}}(t) + \rho_{\vec{r}}$. Consequently, when we analyze data we cannot determine an absolute $\phi_{\vec{r}}(t)$. To work with invariant quantities, we either have to go back to studying two-time quantities like $\phi_{\vec{r}}(t) - \phi_{\vec{r}}(t')$ or we must work with time derivatives of $\phi_{\vec{r}}(t)$.

3.3 Method to extract phases and instantaneous relaxation rates from numerical or experimental data

Our method for the extraction of $\phi_{\vec{r}}(t)$ from local two-time correlations is inspired by the work in Refs. [46, 47]. Refs. [46, 47] use a functional form $g_{\text{global}}(x) = q_{EA} \exp\left(-|x|^{\beta}\right)$, where q_{EA} and β are fitting parameters, to fit global correlations in molecular dynamics simulations of glass forming particle systems and polymer systems. They find functions $\phi(t)$ for the different systems such that the data are described by

$$C(t, t') = g_{\text{global}}[\phi(t) - \phi(t')], \tag{3.12}$$

As discussed in Sec. (3.2), two different lines of argument lead to the prediction that local fluctuations can be described in terms of fluctuating phases $\phi_{\vec{r}}(t)$, such that

$$C_{\vec{r}}(t, t') \approx g[\phi_{\vec{r}}(t) - \phi_{\vec{r}}(t')]. \tag{3.13}$$

In principle, the functions $g_{\text{global}}(x)$ and $g(x)$, respectively describing global two-time correlations and local two-time correlations, could have completely different forms. For example, as discussed in Sec. 3.2, some of the initial motivation for the picture of dynamical heterogeneity came from the idea that non-exponential relaxation in a macroscopic sample is due to the combined effect of local exponential relaxations with different relaxation times. In this picture, $g_{\text{global}}(x) \propto \exp(-|x|^{\beta})$ and $g(x) \propto \exp(-|x|)$. In Refs. [46, 47], as a simplifying assumption, the two functions were taken to be equal. In the present work, we focus exclusively on the local function $g(x)$. However, we will consider different coarse graining sizes when determining $C_{\vec{r}}(t, t')$. Each of these coarse graining sizes will give rise to a different form for $g(x)$. In practice, to simplify the determination of $g(x)$, we will restrict it to be a member of a family of functional forms $g(x; \vec{\alpha})$, parametrized by a vector $\vec{\alpha}$ of p components, and for each coarse graining size both the parameter vector $\vec{\alpha}$ and the fluctuating phases $\phi_{\vec{r}}(t)$ will be determined by fitting $C_{\vec{r}}(t, t')$ according to Eq. (3.13). For technical reasons, we impose the condition that g be an even function, $g(-x) = g(x)$.

Let's consider a data set containing "snapshots" of the relevant degrees of freedom of the system, taken at times $\{t_i\}_{i=1,\ldots,M}$. In our case the positions of the particles are recorded at each time step. For a given coarse graining region centered at a point $\vec{r}$ in the sample, our data points will be the $M(M-1)/2$ two-time local correlations $C_{\vec{r}}(t_i, t_j)$ calculated from the recorded data. Considering for the moment a fixed parameter vector $\vec{\alpha}$, we have M fitting parameters $\{\phi_{\vec{r}}(t_i)\}_{i=1,\ldots,M}$, thus giving us a fitting problem with $\sim M/2$ data points per fitting parameter. However, since the function $g(x)$ is nonlinear, this becomes a

nonlinear fitting problem with a large number M of fitting parameters. In order to make this problem manageable, we want to convert it into a linear fitting problem. To do this, we expand the rhs of Eq. (3.13) to linear order in the local fluctuations

$$g[\phi_{\vec{r}}(t) - \phi_{\vec{r}}(t')] \approx g[\phi(t) - \phi(t')] + g'[\phi(t) - \phi(t')][\delta\phi_{\vec{r}}(t) - \delta\phi_{\vec{r}}(t')] \tag{3.14}$$

where $\phi(t)$ is a global phase, still to be determined, and the local fluctuations of the phase are given by

$$\delta\phi_{\vec{r}}(t) \equiv \phi_{\vec{r}}(t) - \phi(t). \tag{3.15}$$

At this point, we have simplified the problem by converting it into a linear fitting problem, at the price of introducing the extra phase variables $\{\phi(t_i)\}_{i=1,\cdots,M}$.

Before we describe the method for determining the phases, we define three quantities to measure fluctuations in the two-time local correlations. The *total fluctuations* are defined by

$$\delta C_{\vec{r}}(t,t') \equiv C_{\vec{r}}(t,t') - g[\phi(t) - \phi(t')] \tag{3.16}$$

and contain complete information about the space dependence of the local two time correlations. We decompose the total fluctuations as the sum of a transverse component $\delta C^T_{\vec{r}}(t,t')$ and a longitudinal component $\delta C^L_{\vec{r}}(t,t')$,

$$\delta C_{\vec{r}}(t,t') = \delta C^T_{\vec{r}}(t,t') + \delta C^L_{\vec{r}}(t,t'). \tag{3.17}$$

The transverse component is associated with time reparametrization fluctuations, and it is defined by the linear term in Eq. (3.14), namely

$$\delta C^T_{\vec{r}}(t,t') \equiv g'[\phi(t) - \phi(t')]\left[\delta\phi_{\vec{r}}(t) - \delta\phi_{\vec{r}}(t')\right]. \tag{3.18}$$

To satisfy Eq. (3.17), the longitudinal component is defined by

$$\delta C^L_{\vec{r}}(t,t') \equiv \delta C_{\vec{r}}(t,t') - \delta C^T_{\vec{r}}(t,t') \tag{3.19}$$

$$\equiv C_{\vec{r}}(t,t') - \{g[\phi(t) - \phi(t')] + g'[\phi(t) - \phi(t')]\left[\delta\phi_{\vec{r}}(t) - \delta\phi_{\vec{r}}(t')\right]\}. \tag{3.20}$$

In what follows we explain how to perform a least squares fit of the local correlation $C_{\vec{r}}(t,t')$ by the rhs of Eq. (3.14). In the case of numerical data, we normally have not only data for different coarse grained regions inside the sample, but also data for different independent runs. If we have N_R independent simulation runs for a system of volume V, we can imagine juxtaposing the configurations for all the runs, thus creating a larger volume $\mathcal{V} = N_R V$. Assuming that each coarse graining region $B_{\vec{r}}$ centered around point $\vec{r}$ has a volume V_{cg}, the total number of non-overlapping regions per run is $\omega = [V/V_{cg}]$, and the total number of non-overlapping regions including all runs is $\Omega = N_R\omega = N_R[V/V_{cg}]$, where in this context $[V/V_{cg}]$ denotes the integer part of V/V_{cg}.

The fit we want to perform corresponds to minimizing the quantity

$$E \equiv \frac{1}{\Omega}\sum_{\vec{r}} \epsilon\left[\{\delta\phi_{\vec{r}}(t_i)\}_{i=1,\cdots,M}, \vec{\alpha}; \{C_{\vec{r}}(t_j,t_i)\}_{1\le i<j\le M}\right] \tag{3.21}$$

with respect to all phase fluctuations $\delta\phi_{\vec{r}}(t_i)$ and with respect to $\vec{\alpha}$. Here

$$\begin{aligned}
&\epsilon\left[\{\delta\phi_{\vec{r}}(t_i)\}_{i=1,\cdots,M}, \vec{\alpha}; \{C_{\vec{r}}(t_j,t_i)\}_{1\le i<j\le M}\right] \\
&\equiv \eta^{-1}(M) \sum_{1\le i<j\le M} \left[\delta C^L_{\vec{r}}(t_j,t_i)\right]^2, \\
&= \frac{1}{\eta(M)} \sum_{1\le i<j\le M} \Big(C_{\vec{r}}(t,t_i) - \Big\{g[\phi(t_j)-\phi(t_i);\vec{\alpha}] + g'[\phi(t_j)-\phi(t_i);\vec{\alpha}] \\
&\times\left[\delta\phi_{\vec{r}}(t_j) - \delta\phi_{\vec{r}}(t_i)\right]\Big\}\Big)^2,
\end{aligned} \tag{3.22}$$

is the residual corresponding to the region centered at $\vec{r}$,

$$\eta(M) \equiv \frac{M(M-1)}{2} - M + 1 = \frac{M(M-3)+2}{2} \tag{3.23}$$

is the number of degrees of freedom in the fit of the data corresponding to one particular coarse graining region, and $\sum_{\vec{r}}$ denotes a sum over non-overlapping coarse graining regions. From now on we consider only times belonging to the set $\{t_i\}_{i=1,\cdots,M}$, and we simplify our notation by indicating times as subindices, i.e. $\delta\phi_{i\vec{r}} \equiv \delta\phi_{\vec{r}}(t_i)$, $\delta C^L_{ji\vec{r}} \equiv \delta C^L_{\vec{r}}(t_j,t_i)$, and similarly for all other one- and two-time variables.

To minimize E, we observe that for a fixed parameter vector $\vec{\alpha}$, the determination of the local fluctuations $\{\delta\phi_{i\vec{r}}\}$ for a specific region centered at $\vec{r}$ can be performed by separately minimizing the corresponding $\epsilon\left(\{\delta\phi_{i\vec{r}}\}_{i=1,\cdots,M}, \vec{\alpha}; \{C_{ji\vec{r}}\}_{1\le i<j\le M}\right)$ for that particular region. For this reason, instead of minimizing with respect to all variables in one step, the problem becomes significantly simplified if we perform an iterated minimization,

$$\min_{\{\delta\phi\};\vec{\alpha}} E = \min_{\vec{\alpha}} \epsilon_\phi(\vec{\alpha}), \tag{3.24}$$

$$\epsilon_\phi(\vec{\alpha}) \equiv \frac{1}{\Omega}\sum_{\vec{r}} \min_{\{\delta\phi_{i\vec{r}}\}} \epsilon\left(\{\delta\phi_{i\vec{r}}\}, \vec{\alpha}; \{C_{ji\vec{r}}\}_{1\le i<j\le M}\right). \tag{3.25}$$

In other words, we first keep $\vec{\alpha}$ fixed and separately minimize with respect to the phase fluctuations in each coarse graining region, and then minimize the result with respect to $\vec{\alpha}$. The minimization with respect to the phases, at fixed $\vec{\alpha}$, is performed in two steps. In the first step we determine global phases. In the second step, we use the global phases from the first step to determine local phases. Next, we describe these steps in detail, but without derivations. The details of the derivations can be found in Appendix C.

3.3.1 Step One: determining global phases at fixed $\vec{\alpha}$

The global phases $\{\phi_i\}_{i=1,\ldots,M}$ define the point around which the Taylor expansion in Eq. (3.14) is performed. The only requirement on them is to be close enough to the values of $\phi_{i\vec{r}}$ such that the expansion is accurate to first order in the fluctuations. In particular, we only need to determine them to within an error of the order of the fluctuations in the $\phi_{i\vec{r}}$. There is more than one possible way to satisfy these conditions, and for simplicity we do it by choosing them to be the phases that best represent the *global* correlations for the given value of $\vec{\alpha}$. We define the quantity $\bar{\epsilon}$

$$\bar{\epsilon}(\{\phi_1, \cdots, \phi_M\}; \vec{\alpha}) \equiv \eta^{-1}(M) \sum_{1\le i<j\le M} \left[C_{ji} - g^{(1)}(\phi_j - \phi_i; \vec{\alpha})\right]^2, \tag{3.26}$$

where $C_{ji} \equiv C(t_j, t_i)$, and $g^{(1)}(\phi_j - \phi_i; \vec{\alpha})$ is the first order Taylor expansion of $g(\phi_j - \phi_i; \vec{\alpha})$ with respect to the phase difference, taken about

$$\Phi_{ji} \equiv \Big[\mathrm{sgn}(t_j - t_i)\Big] g^{-1}\Big[C(t_j, t_i)\Big]. \tag{3.27}$$

To minimize $\bar{\epsilon}$ we impose the condition that all derivatives of $\bar{\epsilon}$ with respect to ϕ_k must be zero. Additionally, we fix the gauge with the condition

$$0 = \sum_{i=1}^{M} \phi_i. \tag{3.28}$$

Thus we obtain the matrix equation

$$\vec{w} = \bar{A}\,\vec{\phi} \tag{3.29}$$

where

$$\bar{w}_k \equiv \begin{cases} 0 & \text{for} \quad k = 1 \\ \sum_{j=1}^{M} \Phi_{jk}\, g'^2(\Phi_{jk}; \vec{\alpha}) & \text{for} \quad k \neq 1 \end{cases} \tag{3.30}$$

$$\bar{A}_{ki} \equiv \begin{cases} 1 & \text{for} \quad k = 1 \\ -\delta_{ki} \sum_{j=1}^{M} g'^2(\Phi_{jk}; \vec{\alpha}) + g'^2(\Phi_{ki}; \vec{\alpha}) & \text{for} \quad k \neq 1. \end{cases} \tag{3.31}$$

The solution to Eq. (3.29) is the set of global phases $\{\phi_i\}_{i=1,\ldots,M}$ which minimizes $\bar{\epsilon}$ for the given $\vec{\alpha}$. We use the global phases as input in the second step, which we describe next.

3.3.2 Step Two: determining the local phases at fixed α

In the second step, we minimize $\epsilon(\{\delta\phi_{i\vec{r}}\}; \vec{\alpha})$ with respect to the local phase fluctuations $\{\delta\phi_{1\vec{r}}, \cdots, \delta\phi_{M\vec{r}}\}$, for each coarse graining region, while keeping $\vec{\alpha}$ fixed at the values used in the first step. By Taylor expanding $g(\phi_{i\vec{r}} - \phi_{j\vec{r}}; \vec{\alpha})$ about the global phase differences, $\phi_i - \phi_j$, imposing the condition that all derivatives of $\epsilon(\{\delta\phi_{i\vec{r}}\}; \vec{\alpha})$ with respect to the phase fluctuations $\{\delta\phi_{1\vec{r}}, \cdots, \delta\phi_{M\vec{r}}\}$ should be zero, and fixing the gauge with the condition

$$0 = \sum_{i=1}^{M} \delta\phi_{i\vec{r}}, \tag{3.32}$$

we obtain the matrix equation

$$\vec{w}_{\vec{r}} = A\ \delta\vec{\phi}_{\vec{r}}, \tag{3.33}$$

where

$$w_{k\vec{r}} \equiv \begin{cases} 0 & \text{for} \quad k = 1 \\ \sum_{j=1}^{M} g'(\phi_k - \phi_j; \vec{\alpha})\ \delta C_{kj\vec{r}} & \text{for} \quad k \neq 1 \end{cases} \tag{3.34}$$

$$A_{ki} \equiv \begin{cases} 1 & \text{for} \quad k = 1 \\ \delta_{ki} \sum_{j=1}^{M} g'^2(\phi_k - \phi_j; \vec{\alpha}) - g'^2(\phi_k - \phi_i; \vec{\alpha}) & \text{for} \quad k \neq 1. \end{cases} \tag{3.35}$$

The solution to this matrix equation is the vector $\delta\vec{\phi}_{\vec{r}} = (\delta\phi_{1\vec{r}}, \cdots, \delta\phi_{M\vec{r}})$ containing the local fluctuating phase differences that minimize ϵ for the given value of the parameter vector $\vec{\alpha}$ and for the region $B_{\vec{r}}$. By averaging the minimum values of $\epsilon(\{\delta\phi_{i\vec{r}}\}; \vec{\alpha})$ for all regions, we obtain $\epsilon_\phi(\vec{\alpha})$.

3.3.3 Minimization with respect to α

The optimum value of $\vec{\alpha}$ is obtained by numerically minimizing $\epsilon_\phi(\vec{\alpha})$ with respect to it. Once the optimum $\vec{\alpha}$ has been obtained, the solutions of Eq. (3.33) for that specific value of $\vec{\alpha}$ and for each region B_r give the optimal choice for the fluctuating phases $\delta\phi_{i\vec{r}}$.

3.4 Testing the method with data from numerical simulations of glass-forming model systems

We tested the method on the results of classical Molecular Dynamics simulations of two glass forming systems, each one consisting of an 80 : 20 binary mixture of 1000 particles interacting via purely repulsive Weeks-Chandler-Andersen (WCA) potentials. These simulations were performed by Parsaeian [67]. The systems were quenched from an initial temperature T_i much higher than the Mode Coupling critical temperature T_c. One of the systems was quenched to a temperature T below the mode coupling critical temperature T_c such that $T/T_c \sim 0.9$ and it did not reach equilibrium during the

simulation. We call this system the *aging system*. The other system was quenched to a temperature T such that $T/T_c \sim 1.1$ and it reached equilibrium within the duration of the simulation. In our studies we use the data corresponding to times after the system reached equilibrium and we call this system the *equilibrium system*. After the quench, the systems were allowed to evolve for times much longer than the typical vibrational periods of the particles. Snapshots of the systems were taken periodically during the evolution and the positions of the particles were stored.

To probe a system, we divide it into coarse graining boxes $B_{\vec{r}}$, centered at the space points $\vec{r}$. The local correlation for each box is calculated using

$$C_{\vec{r}}(t,t') \equiv \frac{1}{N_{B_{\vec{r}}}} \sum_{\vec{r}_i(t')\in B_{\vec{r}}} \cos\{\vec{q}\cdot[\vec{r}_i(t)-\vec{r}_i(t')]\}. \tag{3.36}$$

Here $N_{B_{\vec{r}}}$ is the number of particles in the coarse graining box $B_{\vec{r}}$ at time t', and $|\vec{q}|$ is chosen to be the value given by the location of the main peak of the static structure factor $S(q)$. $C_{\vec{r}}(t,t')$ measures the extent to which the configuration in the coarse graining region has changed between the times t' and t. If the particles that are initially in the region have not moved much then $C_{\vec{r}}(t,t')$ is larger than $1/2$, and if the particles have moved a significant distance then $C_{\vec{r}}(t,t') \ll 1$. In the first case, we say the the region is "slow", and in the second, that it is "fast".

To implement the method, we choose the fit function to be the stretched exponential

$$g(x;\vec{\alpha}) = q_{EA}\exp\left(-|x|^{\beta}\right). \tag{3.37}$$

In this case the vector of parameters is $\vec{\alpha} \equiv (q_{EA},\beta)$, where q_{EA} is the plateau value of the correlation function and β is the stretching exponent. We begin the analysis by determining the optimal values of $\vec{\alpha}$ at different coarse graining sizes; the results are summarized in Fig. (3.1) for both systems. Each one of the curves is drawn using two colors: one part is drawn in black and the other in a color other than black. The part that is

drawn in black is the part where longitudinal fluctuations, *i.e.* the fit residuals, account for more than 40% of the total variance of the fluctuations. We observe that the optimal β decreases with increasing coarse graining volume and the optimal q_{EA} increases with coarse graining volume. Both quantities approach constant values at high coarse graining volumes. The trend of q_{EA} appears to be an artifact of the fact that fluctuations are stronger for smaller coarse graining volumes. Since fluctuations that increase $C_{\vec{r}}(t, t')$ above a value given by the Debye-Waller factor are unlikely, there is a bias for fluctuations to reduce, rather than increase, the value of $C_{\vec{r}}(t, t')$ for times when $C_{\vec{r}}(t, t')$ is high. Since the largest values that $C_{\vec{r}}(t, t')$ takes are associated to the optimal q_{EA}, this bias will push q_{EA} down, particularly when fluctuations are stronger due to the small size of the coarse graining regions. The trend of β is reminiscent of one of the initial motivations for the proposal that dynamics must be heterogeneous, i.e. the idea [8, 9] that in systems for which the bulk relaxation is non-exponential, local regions have exponential relaxation - $\beta \approx 1$ - with heterogeneous timescales, and this translates into a lower exponent β for the system as a whole. However, as we will discuss below, for smaller coarse graining volumes the majority of the fluctuations are captured by the fit residuals and not by the fitting function itself, so it is unclear whether or not this trend in the optimal value of the fit parameter β has any physical significance.

3.4.1 Fluctuations

As we mentioned in Sec. 3.2 we expect longitudinal fluctuations to be less correlated at long distances, and consequently to be more strongly suppressed by coarse graining, than transverse fluctuations [68]. It is not immediately obvious how to quantify the strength of the fluctuations, since they are functions of the position and of two times. However, in this context it becomes natural to think of them as vectors in an Euclidean

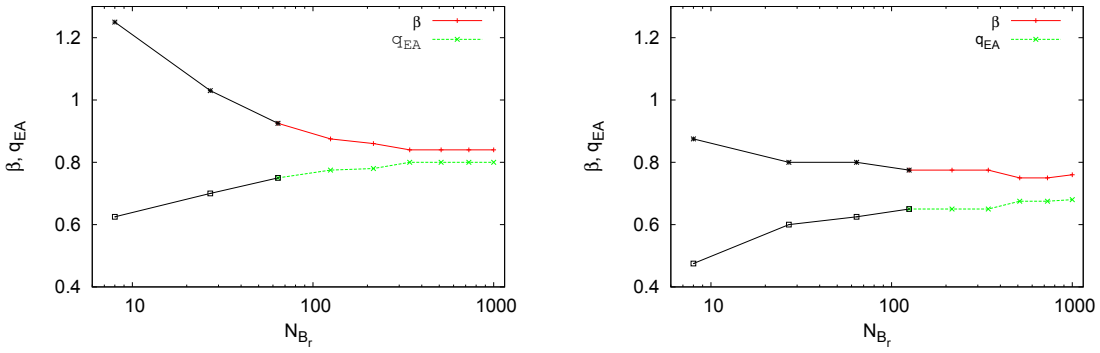

Figure 3.1: Variation of the optimal values for the fitting parameters β and q_{EA} with coarse graining size, in the equilibrium system with $M = 94$ snapshots and $N_R = 10$ independent runs (right panel), and in the aging system with $M = 100$ and $N_R = 10$ (left panel). The part that is drawn in black for each curve corresponds to the range of coarse graining sizes for which longitudinal fluctuations account for more than 40% of the total fluctuations.

vector space, with the inner product defined by

$$(f|g) \equiv \frac{2}{\omega M(M-1)} \sum_{1 \le j < i \le M} \sum_{\vec{r}} \langle f_{\vec{r}}(t_i, t_j) g_{\vec{r}}(t_i, t_j) \rangle, \tag{3.38}$$

and the Euclidean norm defined by

$$||f|| \equiv (f|f)^{1/2} . \tag{3.39}$$

Here M is the number of snapshots, $\{\vec{r}\}$ are the centers of each one of the ω non-overlapping coarse-graining boxes $B_{\vec{r}}$ in the volume V of the system, and $\langle \cdots \rangle$ denotes an average over thermal fluctuations, which in the case of quantities obtained from numerical simulations corresponds to an average over independent simulation runs. The only slightly unusual aspect in these definitions is the prefactor $2/\omega M(M-1)$, which was included so that the square of the norm is an "intensive" quantity, which gives the average over positions and over time pairs of the variance of the fluctuations for one coarse graining box and one time pair. This makes it easier to compare results for different snapshot numbers M and different numbers ω of coarse graining boxes. With these definitions, and as a direct consequence of the minimization conditions that determine the

values of the phases $\{\phi_{\vec{r}}(t_i)\}$, we show in Appendix C.1 that the transverse and longitudinal fluctuation vectors are orthogonal, *i.e.*

$$\left(\delta C^T | \delta C^L\right) = 0, \tag{3.40}$$

and therefore they satisfy the Pythagorean condition

$$||\delta C||^2 = ||\delta C^T||^2 + ||\delta C^L||^2. \tag{3.41}$$

In Fig. (3.2) we show how the strengths of the fluctuations vary with the average number of particles $N_{B_{\vec{r}}}$ per coarse graining box. In the figure, the two top panels correspond to the aging system and the two bottom ones correspond to the equilibrium system. For each system, the left panel shows the magnitudes $||\delta C||$, $||\delta C^T||$, and $||\delta C^L||$ of the total fluctuations, their transverse component and their longitudinal component; and the right panel shows the ratios $||\delta C^T||/||\delta C||$, and $||\delta C^L||/||\delta C||$. Due to the Pythagorean condition, the sum of the squares of these two ratios is unity in all cases.

We expect that as the coarse graining is increased, all fluctuations will be suppressed by the effect of averaging. Indeed, we find that the magnitudes of all three kinds of fluctuations decrease as we increase the coarse graining volume, both for the aging system and for the equilibrium system. The magnitude of the longitudinal fluctuations decreases at a faster rate than the total fluctuations while the magnitude of the transverse fluctuations decreases at a slower rate. Indeed at small coarse graining volumes the ratio $||\delta C^T||/||\delta C||$ is smaller than the ratio $||\delta C^L||/||\delta C||$, but the first one increases and the second one decreases as the coarse graining volume increases. For the aging system the two ratios cross at $N_{B_{\vec{r}}} \approx 30$ and for the equilibrium system they cross at $N_{B_{\vec{r}}} \approx 100$. This is consistent with our expectation that longitudinal fluctuations should be more strongly suppressed by coarse graining than transverse fluctuations. We also observe that transverse fluctuations are dominant for a wider range of coarse graining sizes in the case of the aging system than in the case of the equilibrium system. This is indeed what should

be expected if the transverse fluctuations are the Goldstone fluctuations associated with time reparametrization symmetry. Since time reparametrization symmetry is a long time asymptotic effect, and in the case of the equilibrium system, which is at higher temperature than the aging system, the relaxation time provides a cutoff for long timescales, we expect that the transverse fluctuations associated with this symmetry will manifest themselves less strongly in the equilibrium system than in the aging one.

Table 3.1: Optimal Fit Parameters for the Analyzed Systems

System	$N_{B_{\vec{r}}}$	q_{EA}	β
Equilibrium	216	0.65	0.775
Aging	125	0.775	0.875

From now on, we consider in detail one coarse graining volume for each system. We choose in each case the smallest coarse-graining volume for which transverse fluctuations capture 60% of the total variance of the fluctuations, *i.e.* $||\delta C^T||^2 \geq 0.6\ ||\delta C||^2$. This corresponds to $N_{B_{\vec{r}}} = 125$ for the aging system and $N_{B_{\vec{r}}} = 216$ for the equilibrium system. Table 3.1 contains a summary of the fitting parameters for those coarse graining volumes.

Since the number of snapshots M used in the analysis cannot be increased indefinitely, it is important to test that the results are robust with respect to changes in M, and that meaningful results can be obtained even for relatively small values of M. There are two aspects to this question: one is to show that the phases $\phi_{\vec{r}}(t)$ are well defined, by showing that their determination is robust with respect to changes in the number of snapshots M, and the other is to show that the magnitudes of the transverse, longitudinal and total fluctuations are not singular as a function of M. With regards to the first aspect, we find that as the number of snapshots is increased, $\phi_{\vec{r}}(t)$ quickly converges to a relatively smooth function. Fig. (3.3) shows that $\phi_{\vec{r}}(t)$ changes very little if the number of snapshots

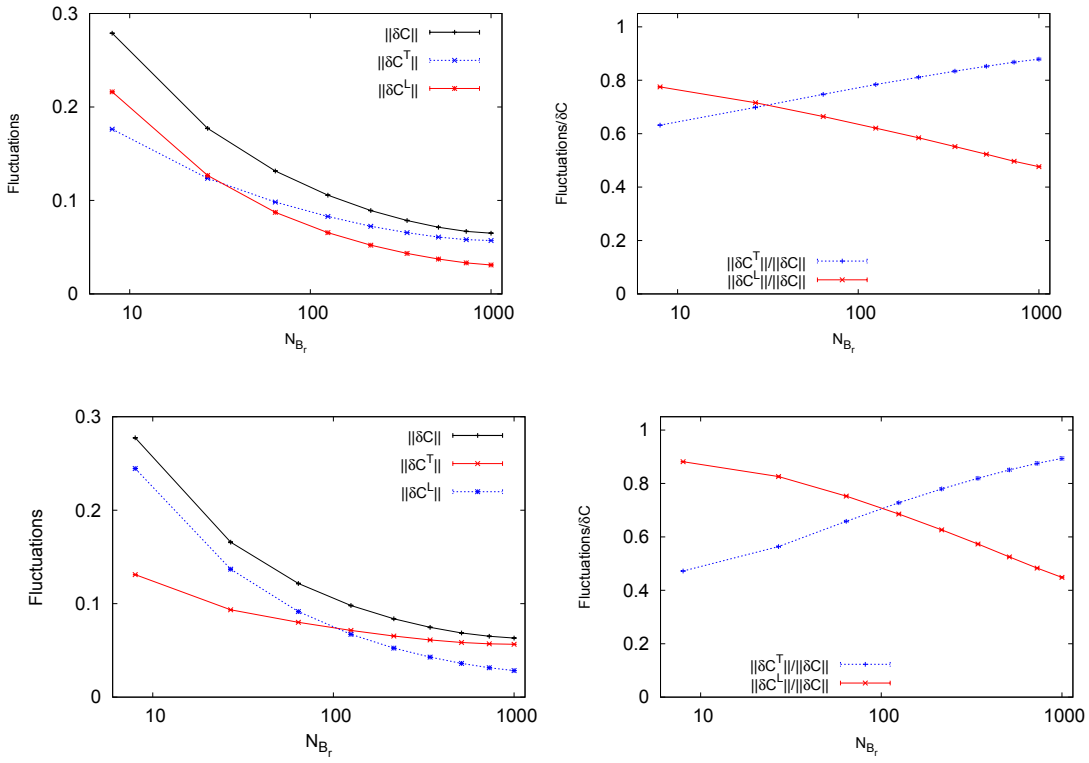

Figure 3.2: Dependence of fluctuation strengths on the average number of particles $N_{B_{\vec{r}}}$ per coarse graining box, in the aging system with $M = 100$ and $N_R = 100$ (top panels) and in the system in equilibrium with $M = 94$ and $N_R = 100$ (bottom panels). For each system, the left panel shows the magnitude $||\delta C||$ of the total fluctuations, the magnitude $||\delta C^T||$ of the transverse fluctuations, and the magnitude $||\delta C^L||$ of the longitudinal fluctuations; and the right panels show the ratios $||\delta C^T||/||\delta C||$ and $||\delta C^L||/||\delta C||$. The ratio $||\delta C^T||/||\delta C||$ increases and the ratio $||\delta C^L||/||\delta C||$ decreases with increasing coarse graining size. For both systems, the first ratio is smaller than the second one at small coarse grainings, and larger than the second one at large coarse grainings. The two ratios cross at $N_{B_{\vec{r}}} \approx 30$ for the aging system and at $N_{B_{\vec{r}}} \approx 100$ for the equilibrium system.

M used to compute it is 7 or larger in the case of the aging system or if it is 24 or larger in the case of the equilibrium system. It is noticeable that the minimum number M_{st} of snapshots needed for a stable determination of $\phi_{\vec{r}}(t)$ is comparable to the total variation $\Delta\phi$ of the global phase over the interval considered: in the aging case $M_{st} \approx 7$ and $\Delta\phi \approx 4$, while in the equilibrium case $M_{st} \approx 24$ and $\Delta\phi \approx 18$. It is tempting to speculate that at

least one or two configurations per relaxation time are needed in order to capture a minimum of information about the α relaxation in the system, and this would lead to the prediction that $M_{st}/\Delta\phi \sim 1$–2. However at this point the data we have available are insufficient to draw any definite conclusions.

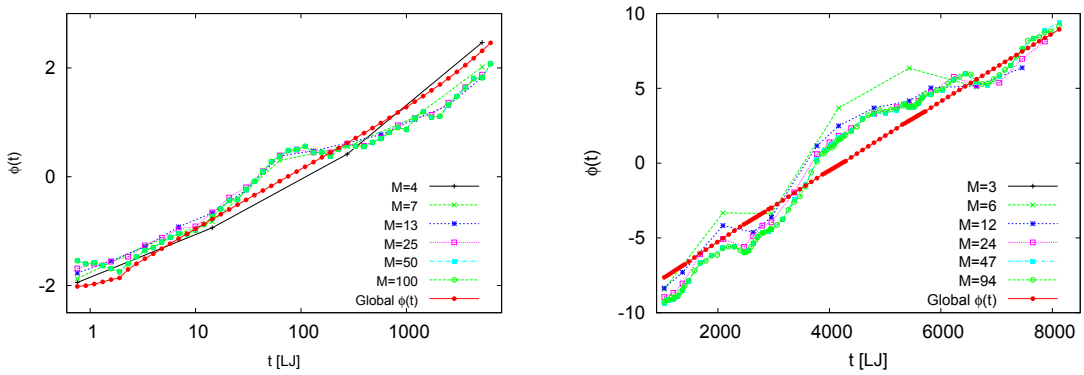

Figure 3.3: Dependence of the function $\phi_{\vec{r}}(t)$ on the number of snapshot M used to compute it, for the aging system with $N_{B_{\vec{r}}} = 125$ (left panel), and for the system in equilibrium with $N_{B_{\vec{r}}} = 216$ (right panel).

We now consider the issue of the smoothness of the dependence of the magnitudes of the different kinds of fluctuations on the number M of snapshots. In Fig. (3.4) we plot the magnitude $||\delta C||$ of the total fluctuations, the magnitude $||\delta C^T||$ of the transverse fluctuations, and the magnitude $||\delta C^L||$ of the longitudinal fluctuations as functions of $1/M$. We find that all three fluctuation magnitudes are gently increasing functions of M, and that each of them appears to approach a constant as $M \to \infty$. For the specific coarse graining sizes shown in the figure, the longitudinal fluctuations are always weaker than the transverse ones, but the opposite case is found for small enough coarse graining sizes.

3.4.2 Local Phases and Local Relaxation Times

Up to this point we have presented evidence in favor of the statement that the method we are introducing leads to a robust determination of the transverse and longitudinal

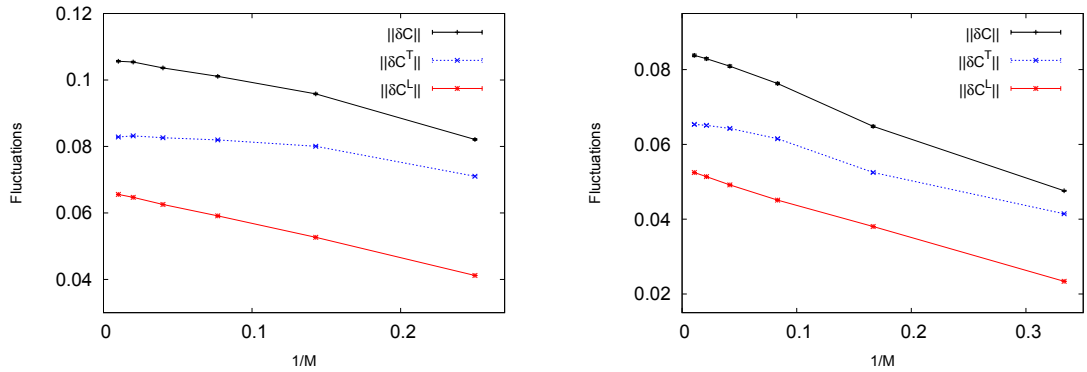

Figure 3.4: Dependence of the magnitude $||\delta C||$ of the total fluctuations, the magnitude $||\delta C^T||$ of the transverse fluctuations, and the magnitude $||\delta C^L||$ of the longitudinal fluctuations on the number M of snapshots used in their evaluation, for the aging system with $N_{B_{\vec{r}}} = 125$ and $N_R = 100$ (left panel), and for the system in equilibrium with $N_{B_{\vec{r}}} = 216$ and $N_R = 100$ (right panel). In all cases, the magnitude of each kind of fluctuation is a gently increasing function of M that appears to extrapolates to a well-defined value as $M \to \infty$.

components δC^T and δC^L of the fluctuations and of the fluctuating phases $\phi_{\vec{r}}(t)$. We now use the method to show some examples of the phases $\phi_{\vec{r}}(t)$ and their time derivatives $\dot{\phi}_{\vec{r}}(t) \equiv d\phi_{\vec{r}}(t)/dt$. The time derivatives are particularly interesting, not only because they are gauge invariant, but also because, according to Eq. (3.10), they can in principle be interpreted as local relaxation rates or inverse local relaxation times $\tau_{\vec{r}}^{-1}(t)$.

In Fig. (3.5) we show the time evolution of the local phases $\phi_{\vec{r}}(t)$ at a fixed point $\vec{r}$ in the sample for different thermal histories, for both the aging system and the equilibrium system. For comparison, we also show the evolution of the global phase $\phi(t)$, and we indeed find that for different thermal histories the local phase $\phi_{\vec{r}}(t)$ gently fluctuates around the global value.

In Figs. (3.6) and (3.7) we show the time evolution of the time derivative $\dot{\phi}_{\vec{r}}(t)$ of the local phase at the same point in space and for the same thermal histories as in the previous figure. In Fig. (3.6), $\dot{\phi}_{\vec{r}}(t)$ is rescaled so that the instantaneous global relaxation rate is unity, and results are shown both for the aging and the equilibrium cases. In the case of

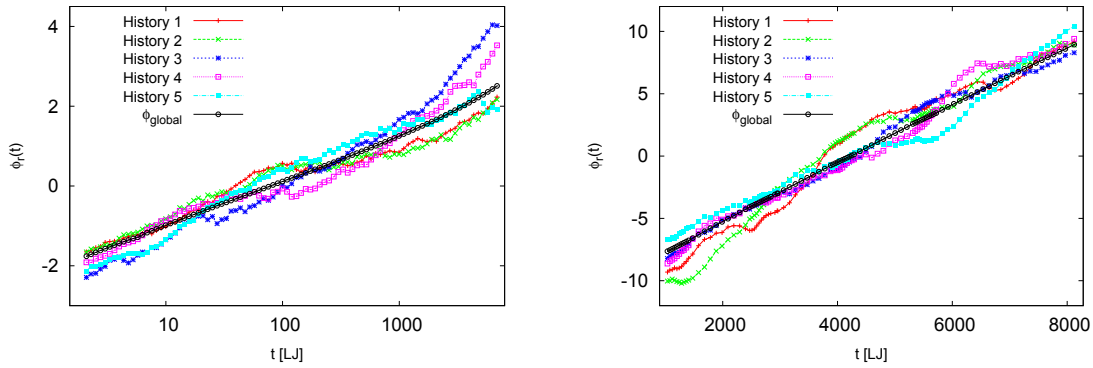

Figure 3.5: Comparison between the local phase $\phi_{\vec{r}}(t)$ as a function of time at a fixed point in space for different thermal histories and the global phase $\phi(t)$. Shown for the aging system, with $N_{B_{\vec{r}}} = 125$ and $M = 100$ (left panel), and for the equilibrium system, with $N_{B_{\vec{r}}} = 216$ and $M = 94$ (right panel).

the equilibrium system, the rescaling is done approximately, by multiplying the time derivative of the phase by the α-relaxation rate $\tau_\alpha \equiv 1/\overline{d\phi/dt}$, where $\overline{\cdots}$ denotes a time average, and the fluctuating values of $\dot{\phi}_{\vec{r}}(t)$ are plotted as functions of the rescaled time t/τ_α, which is approximately equal to the global phase plus a constant. In the case of the aging system, the rescaling is done by dividing by $d\phi/dt$, and the scaled values of $\dot{\phi}_{\vec{r}}(t)$ are plotted as functions of the global phase $\phi(t)$. In both cases the time derivative of the local phase fluctuates strongly, often becoming more than twice as large as the global relaxation rate $d\phi/dt$, or even becoming negative. It should be pointed out that at the times when $\dot{\phi}_{\vec{r}}(t)$ becomes negative, its interpretation as a local relaxation rate $1/\tau_{\vec{r}}(t)$ becomes problematic. However, from a more general point of view, it is not surprising that transient fluctuations in a small region of the sample may give rise to changes that make the configuration of the region temporarily become closer to what it was in the past, thus making the two time correlation $C_{\vec{r}}(t, t')$ increase over time instead of decreasing, with the effect that, for some time at least, $\dot{\phi}_{\vec{r}}(t)$ becomes negative. In Fig. (3.7) we plot the time derivative of the local phase in the aging system, without rescaling it, as a function of time in Lennard-Jones units. For times longer than 2.5 Lennard-Jones time units, the global relaxation rate $d\phi/dt$

decreases as a function of time, which is a direct consequence of the aging in the system, namely the fact that the dynamics becomes slower as the relaxation progresses. In this figure we can notice again the strong fluctuations of the time derivative of the local phase with respect to the global value, but we also notice that both the typical value and the fluctuations of $\dot{\phi}_{\vec{r}}(t)$ decrease together with the decrease of $d\phi/dt$. Also shown in the same figure is a fit of the global relaxation rate by the form $d\phi/dt = \left(\frac{t}{t_0}\right)^{\alpha}$, where $t_0 \approx 3.4 \times 10^{-4}$ and $\alpha \approx -0.91$, a result that is in agreement with the results in Refs. [46, 47].

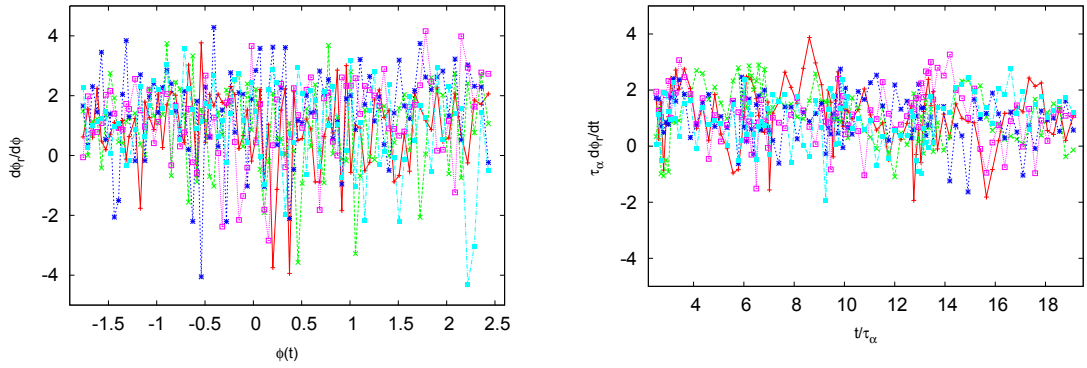

Figure 3.6: Time evolution of the time derivative of the local phases $\dot{\phi}_{\vec{r}}$, rescaled so that the time derivative of the global phase is unity. In the left panel, corresponding to the aging system with $N_{B_{\vec{r}}} = 125$ and $M = 100$, the time derivative of the local phases is rescaled by dividing by the global time dependent relaxation rate $\frac{d\phi}{dt}$, and it is plotted as a function of the global phase $\phi(t)$. In the right panel, corresponding to the equilibrium system with $N_{B_{\vec{r}}} = 216$ and $M = 94$, the rescaling of $\dot{\phi}_{\vec{r}}$ is performed approxmately by multiplying it with the α-relaxation rate $\tau_\alpha \equiv 1/\overline{d\phi/dt}$, and the rescaled time derivative is plotted as a function of the rescaled time t/τ_α, which is approximately equal to the global phase $\phi(t)$ plus a constant.

3.5 Probability Distribution Functions and Power Spectra of $\dot{\phi}_{\vec{r}}$

In Section (3.3) we presented a method for extracting the local fluctuating phases $\phi_{\vec{r}}(t)$, and demonstrated in Section (3.4) that it works, by using it on existing data. We have also shown that the time derivatives of the phases $\dot{\phi}_{\vec{r}}$ can be determined, and in

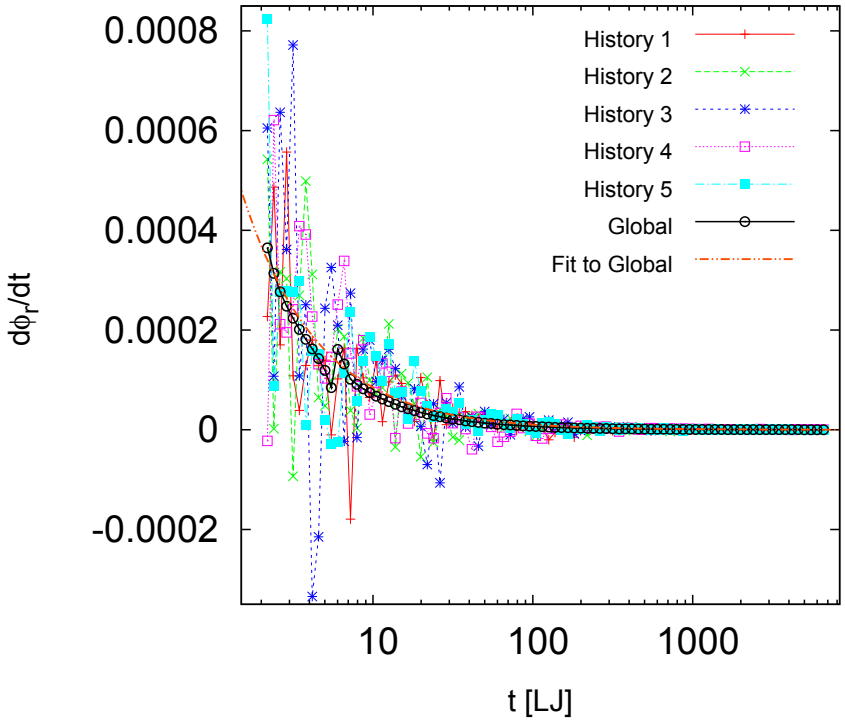

Figure 3.7: Time evolution of the time derivative of the local phase, $\dot{\phi}_{\vec{r}}$, for the aging system with $N_{B_{\vec{r}}} = 125$ and $M = 100$, with no rescaling. The global relaxation rate is also shown, together with a fit of the form $d\phi/dt = (t/t_0)^{\alpha}$, where $t_0 \approx 3.4 \times 10^{-4}$ and $\alpha \approx -0.91$.

certain cases may be interpreted as local fluctuating relaxation rates. In this section we apply the method to obtain statistical properties of the time derivatives $\dot{\phi}_{\vec{r}}$ of the phases. We present results on probability distribution functions (PDFs) and power spectra of $\dot{\phi}_{\vec{r}}$ for the same data sets that we used to test the method.

3.5.1 Probability Distribution Functions

We determine probability distribution functions $\rho(\dot{\phi})$, of $\dot{\phi}_{\vec{r}}$ for the two systems. For the aging system, $\dot{\phi}_{\vec{r}}$ has time dependent average and variance, hence we subtract the average $\langle\dot{\phi}_{\vec{r}}\rangle$ from the data and scale it by dividing by its standard deviation σ, in order to compare the shapes of the distributions at different times. Fig. (3.8) shows the time dependence of $\langle\dot{\phi}_{\vec{r}}\rangle$ and σ for the aging system. The plot is logarithmic in both axes.

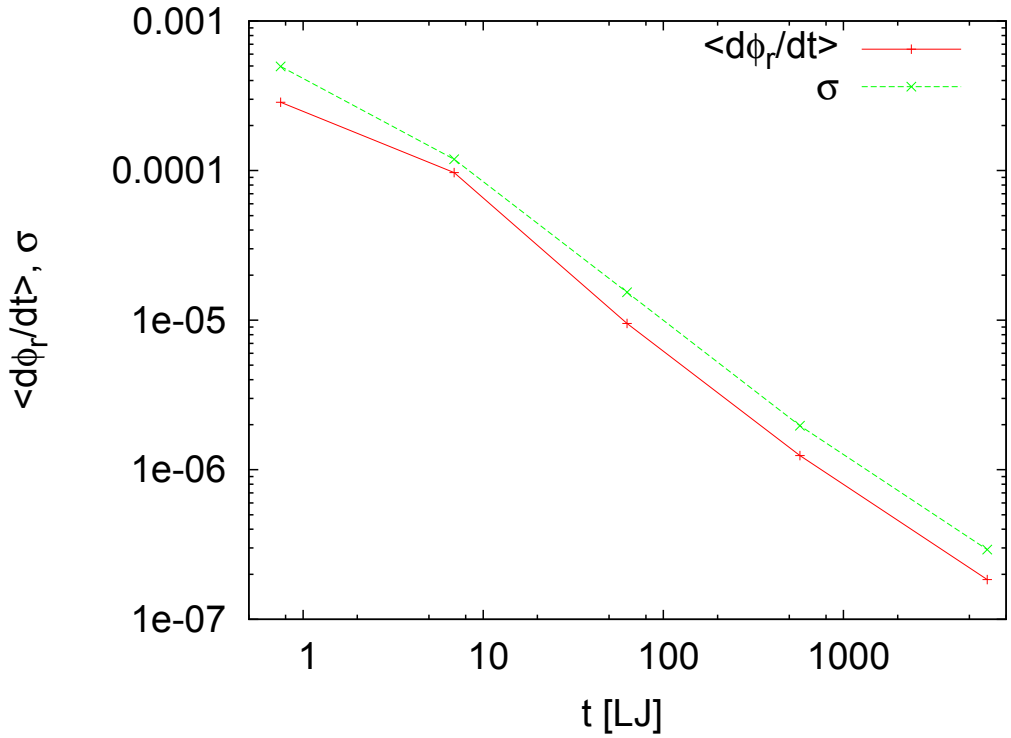

Figure 3.8: Time dependence of $\langle \dot{\phi}_{\vec{r}} \rangle$ and σ for the aging system with $N_{B_{\vec{r}}} = 125$, $M = 100$ and $N_R = 400$.

Figs. (3.9) summarizes our findings for the rescaled probability distributions. The top panels show results for the aging system, with the left panel showing fits to a generalized Gumbel form, and the right panel showing the same fits but with a logarithmic scale on the vertical axis to emphasize the tail of the distributions. The bottom panel is for the equilibrium system, with the left and right panels as described for the top panels. The generalized Gumbel form is described by [69]

$$f_a(x) = \frac{|\alpha| a^a}{\Gamma(a)} \exp\left\{a\left[\alpha(x - x_0) - e^{\alpha(x-x_0)}\right]\right\}, \tag{3.42}$$

where $\Gamma(a)$ is a gamma function, x_0 contols the center of the distribution and α controls the width of the distribution. In the limit $a \to \infty$ while the product $\alpha^2 a = 1/\sigma^2$ is fixed,

the Gumbel form approaches a Gaussian form of variance σ^2 [69]

$$\lim_{a\to\infty,\alpha^2 a=1} f_a(x) = \frac{1}{\sqrt{2\pi}} \exp\left[-\frac{1}{2\sigma^2}(x-x_0)^2\right]. \tag{3.43}$$

In the limit $a \to 0$ with $a|\alpha| = \lambda > 0$ fixed, it approaches an exponential form [69]

$$\lim_{a\to 0,|\alpha|a=1} P_a(x) = \theta[-(\mathrm{sgn}\alpha)(x-x_0)] \exp[(\mathrm{sgn}\alpha)(x-x_0)]. \tag{3.44}$$

Appendix (D) contains a description of the generalized Gumbel distribution and its relationship with the Gaussian and exponential distributions.

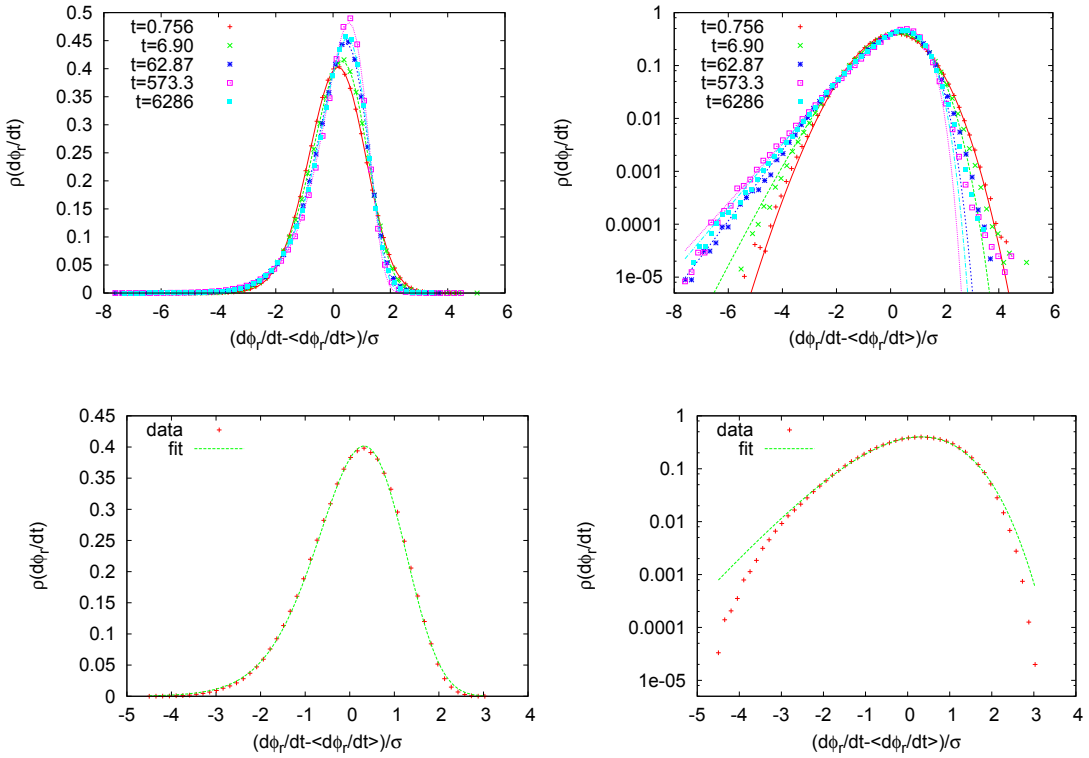

Figure 3.9: Evolution of PDF with time for the aging system with $N_{B_{\vec{r}}} = 125$, $M = 100$ and $N_R = 1000$ (top panels), and the PDF of the equilibrium system with $N_{B_{\vec{r}}} = 216$, $M = 94$ and $N_R = 1000$. The distributions are fitted to Gumbel forms. The top panels are for the aging system and the bottom panels are for the equilibrium system. In each case, the left and right panels are the same figure, with a logarithmic vertical axis in the right panel to emphasize the tails.

The PDF of the equilibrium system is fitted by $a = 3.97$ with $a|\alpha| = 2.048$ and $a\alpha^2 = 1.057$. It is skewed to the left with tails that are not fitted well by the Gumbel form. In the aging system the rescaled probability distibution gradually changes, with both the shape and skewness changing as time increases. At the earliest time, $\rho(\dot{\phi})$ is less skewed and gradually becomes more skewed as the system evolves, but appears to become approximately constant at larger times. In contrast to the case of the equilibrium system, the tails of $\rho(\dot{\phi})$ in the aging system are better fitted by the generalized Gumbel form. Fig. (3.10) summarizes our findings on the skewness parameter a of the Gumbel fit for the two systems, with the left part showing the value for the equilibrium system and the right part showing its time evolution for the aging system. Also shown are the quantities $a|\alpha|$ and $\alpha^2 a$. We remark that the parameter a for the aging system at $T \approx 0.9T_c$ decreases significantly as the system ages, and at time$\sim 10[LJ]$ it becomes smaller than in the equilibrium system at $T \approx 1.1T_c$.

In Ref. [69], Chamon *et al.* propose an effective theory that explains the deviation of the PDF's from the Gaussian form. The theory is based on the Goldstone modes of the broken time reparametrization symmetry discussed in Refs. [37, 38, 39, 40, 41, 42, 43, 44, 45, 46, 47]. The proposal is for an effective action that is local, invariant under time reparametrizations, gauge invariant and positive definite. They find that the simplest action with the least spatial derivatives satisfying these conditions is described by [69]

$$S_{EFF} = K \int d^d\vec{r} \int dt \frac{\left[\nabla\dot{\phi}_{\vec{r}}(t)\right]^2}{\dot{\phi}_{\vec{r}}(t)}, \tag{3.45}$$

where K is a constant and $\dot{\phi}_{\vec{r}} \geq 0$. From this form, we have that $\dot{\phi}_{\vec{r}}$ are uncorrelated random variables for t and t' different, and for critical finite systems, the distributions of correlators of $\int dt\dot{\phi}_{\vec{r}}(t)$ are non Gaussian [69]. Even though the authors' discusion centered around two time quantities, the argument that the skewness of the PDFs is a

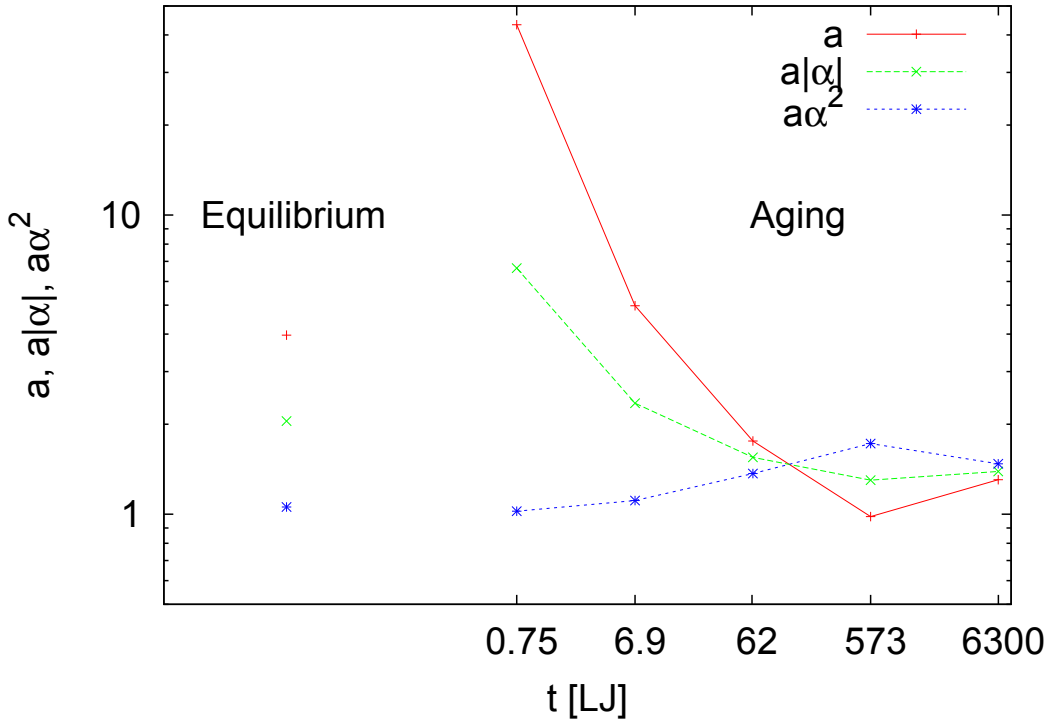

Figure 3.10: Skewness of the Gumbel fit a, as a function of time for the aging system (right part). Also shown is the skewness of the Gumbel fit for the equilibrium. In addition, $a|\alpha|$ and $a\alpha^2$ are shown.

consequence of the effective action of $\dot{\phi}_{\vec{r}}$ may be used in our case to explain the skewness of the PDFs provided $\dot{\phi}_{\vec{r}} \geq 0$. This is a theory of the glassy state and its predictions become more likely to be verified as we approach the glass transition. Therefore, it is not surprising that the tails in the equilibrium system, which is at a higher temperature are less skewed than the tails of the aging system, which is at a lower temperature. Similar skewness in PDF's of two time correlations were observed by Cipelletti *et al.* in concentrated colloidal gels [70]. They attributed the skweness to loss of correlation due to rare events involving large movements that are localized in time as well as space, i.e. dynamic heterogeneity. PDF's of two time correlations studied by Parsaeian and Castillo showed similar skewness [40, 41]. However, we notice that in the two time correlations studies, the skewness is on the low correlations, which characterize fast regions. A naive

analysis would suggest that we ought to be finding skewness towards the larger relaxation rates, instead of the skewness towards smaller relaxation rates that we find, however the highly nonlinear nature of the relation between $\dot{\phi}_{\vec{r}}(t)$ and $C_{\vec{r}}(t, t')$ might explain this discrepancy.

3.5.2 Power Spectra of $\dot{\phi}_{\vec{r}}$

We determine the power spectrum of the $\dot{\phi}_{\vec{r}}(t)$, for both the equilibrium system and the aging system, using the *Lomb Periodogram* [71, 72]. We use the Lomb periodogram because the time steps in the data are not evenly distributed. The Lomb periodogram is described by

$$P(\omega) \equiv \frac{1}{2\sigma^2}\left\{\frac{\left[\sum_j (h_j - \bar{h})\cos\omega(t_j - \bar{t})\right]^2}{\sum_j \cos^2\omega(t_j - \bar{t})} + \frac{\left[\sum_j (h_j - \bar{h})\sin\omega(t_j - \bar{t})\right]^2}{\sum_j \sin^2\omega(t_j - \bar{t})}\right\} \tag{3.46}$$

where $\omega = 2\pi f$ is the angular frequency, $\bar{h} = \frac{1}{N}\sum_i h_i$, σ is the standard deviation of the data $\{h_i\}_{i=1,\ldots,N}$, $\bar{t}$ given by the relation

$$\tan(2\omega\bar{t}) = \frac{\sum_j \sin(2\omega t_j)}{\sum_j \cos(2\omega t_j)} \tag{3.47}$$

makes $P(\omega)$ completely independent of shifts to t_j's by a constant, and we are not determining the $f = 0$ value because we explicitly subtract the time average of the data [71, 72].

Fig. (3.11) shows the power spectra we find for the two systems. In the equilibrium system the power spectrum rapidly decays to a constant level, and it is fit well by a Lorentzian

$$P_L(f) = \frac{A}{1 + (2\pi f t_0)^2} + B. \tag{3.48}$$

Here, A, B and t_0 are constants, with B the constant background at large frequencies, t_0 the characteristic time of the power spectrum. We remark that the values of the fit parameters depend on the cutoff frequency used when fitting. When fitting with all the frequencies,

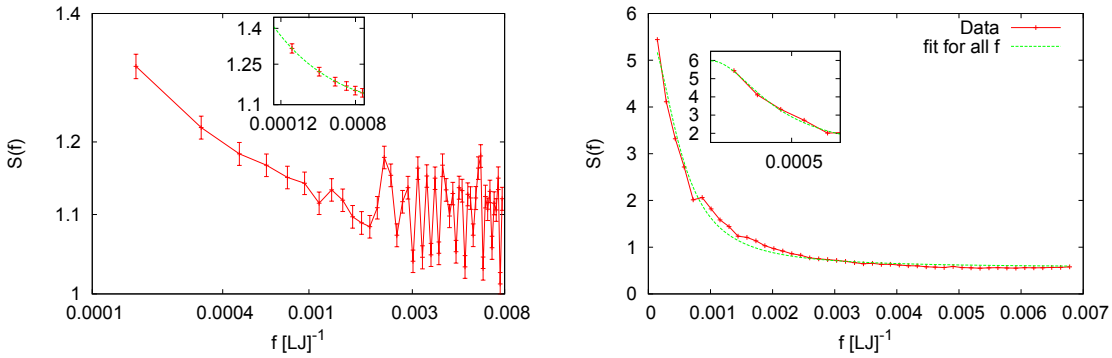

Figure 3.11: The Lomb periodogram in the aging system, with $N_{B_F} = 125$, $M = 100$ and $N_R = 1000$ (left panel) and the equilibrium system with $N_{B_F} = 216$, $M = 94$ and $N_R = 1000$ (right panel). The left panel is a log-log plot with an almost linear regime for the low frequencies, hence the insert is a power law fit $P(f) = Af^{\gamma} + B$ with $\gamma \approx -0.7$, $A \approx 4 \times 10^{-4}$ and $B \approx 1.1$, for the low frequencies. The insert in the right panel is a fit to a Lorentzian $P(f) = A/\left[1 + (2\pi t_0 f)^2\right] + B$ with $t_0 \approx 400[LJ]$, $A \approx 5.0$ and $B \approx 0.96$.

we find $t_0 = 300[LJ]$ whereas when considering only the frequencies up to $0.008[LJ]^{-1}$ (insert on right panel of Fig. (3.11)) we find $t_0 = 400[LJ]$. We note that $t_0 = 400[LJ] \approx 415[LJ] = \tau_\alpha$, where $\tau_\alpha \equiv \langle \dot{\phi} \rangle^{-1}$. In the aging system, we find a power spectrum that decays at frequencies up to $0.008[LJ]^{-1}$ and oscillates around a constant background at larger frequencies. The low frequency part of the spectrum is fitted by a power law

$$S \approx Af^{\gamma} + B. \tag{3.49}$$

Here A, B and γ are constants, with $\gamma \approx -0.7$. Power law spectral density has been observed in a variety of systems. In resistors made from semiconductors, metals, and semi-metals the noise on the voltage has a power law spectrum, with scaling exponents in the range $-0.8 \leq \gamma \leq -1.4$ [73]. Systems characterized by jumps in response to smoothly varying external forces (crackling noise), such as disordered ferromagnets and earthquakes, exhibit power law scaling in the noise statistics, with the power spectrum scaling exponent $\gamma = -1.77$ for the zero temperature Random Field Ising Model [74]. In

the case of disordered ferromagnets, the observed noise statistics are attributed to the presence of spin domains and domain wall propagation with rare new domain wall formation during the evolution of the system [74]. It should be noticed that in these systems, the power scaling of the spectral density is found at the high end of the observed frequency range [73, 74] whereas for our system the power law scaling is found at the lower end of the observed frequency range. We remark that power law scaling of the power spectrum is not expected to extrapolate to zero frequency because such an extrapolation would lead to a power spectrum that cannot be normalized. The main reason for the power law scaling remains unclear but it is tempting to think that its an artifact of greatly slowed down dynamics below the mode coupling critical temperature in which very slow (much slower than the average) regions that are rare cause a shift from a Lorentzian form.

3.6 Conclusions

In this chapter we have shown that a quantitative description of glassy relaxation in terms of local fluctuating phases and relaxation times is possible. On the one hand, starting from the case of exponential relaxation we presented a line of phenomenological arguments that shows how a local phase function $\phi_{\vec{r}}(t)$ can emerge in the description of the data, and how its time derivative can, under certain circumstances, be interpreted as a local fluctuating relaxation rate $1/\tau_{\vec{r}}(t)$. On the other hand, it has been shown that in a theoretical framework that postulates the presence of a broken symmetry under time reparametrizations, it is expected that as the dynamics becomes more glassy, fluctuations should be dominated by Goldstone modes - *i.e.* transverse fluctuations - which are described naturally in terms of the same local fluctuating phases $\phi_{\vec{r}}(t)$ [37, 38, 39]. Besides establishing a connection between the two points of view, we have also derived a practical method for extracting the phases $\phi_{\vec{r}}(t)$ from numerical or experimental data.

We have applied this method to two numerical simulation data sets, one corresponding to a system undergoing aging at a temperature slightly below the mode coupling critical temperature T_c and another one corresponding to a system in equilibrium at a temperature slightly above T_c. We have found that in both cases the results are robust with respect to changes in the number M of position snapshots used in the analysis, as long as M is not too small.

The time reparametrization symmetry framework predicts that for larger coarse graining regions and lower temperatures, transverse fluctuations should be dominant, and indeed, this is what we found in our results. For both systems, the ratio between the magnitude of the transverse fluctuations and the magnitude of the total fluctuations grows monotonically with the coarse graining size. For the smallest coarse graining sizes, longitudinal fluctuations dominate, but transverse fluctuations dominate for large coarse graining sizes. Also, as expected, the range of coarse graining sizes for which transverse fluctuations dominate is wider in the system that is in contact with a heat reservoir at a lower temperature than in the system that is in equilibrium at a higher temperature.

We have shown detailed results for the fluctuating phase $\phi_{\vec{r}}(t)$ and its time derivative $\dot{\phi}_{\vec{r}}(t)$, for a coarse graining size such that the transverse fluctuations capture slightly more than 60% of the total fluctuations. For this coarse graining size, we found that both in the equilibrium system and in the aging system, the time derivative of the local phase fluctuates rather strongly over timescales of the order of the instantaneous global relaxation times or shorter. These fluctuations are strong enough that the time derivative often takes negative values. The presence of negative values, although not surprising, makes an interpretation of $\dot{\phi}_{\vec{r}}(t)$ as a relaxation rate somewhat problematic. It is tempting to speculate that this interpretation may be more cleanly applicable for large enough coarse graining sizes, for which the total fluctuations are expected to be weak enough that $\dot{\phi}_{\vec{r}}(t)$ should always remain positive.

Since our method involves fitting the local two-time correlations $C_{\vec{r}}(t, t')$ by the expression $g[\phi_{\vec{r}}(t) - \phi_{\vec{r}}(t')]$, one of our results is the functional form for $g(x)$. In our fits we modeled this function as a stretched exponential $g(x) = q_{EA} \exp(-|x|^{\beta})$. Phenomenological arguments have been made that would indicate that the relaxation should be exponential for small enough coarse graining regions [8]. If this was the case, we should find the fitting parameter β approaching unity for smaller coarse graining sizes. Our results in this respect are inconclusive: although the fitting parameter β does approach unity as the coarse graining size is reduced, and even becomes larger than unity in the case of the aging system, this happens for a range of coarse graining sizes in which the fluctuations are mostly longitudinal, or in other words most of the fluctuations are "explained" by the fitting residuals and not by the fit itself.

We have also shown results for the PDFs and power spectrum of $\dot{\phi}_{\vec{r}}(t)$ for a coarse graining size such that the transverse fluctuations capture slightly more than 60% of the total fluctuations. For the aging system, we have shown PDFs for different times and have found significant changes as a function of time. The PDFs deviate from Gaussian distributions, with significant deviation observed in the aging system's PDFs. The tails of the PDF is less skewed in the equilibrium system, which is at a higher temperature, than the tails of the aging system, which is a glassy state at a lower temperature. The power spectra we found are substantially different between the two systems. In the aging system the power spectrum is fitted by a Lorentzian with a characteristic time scale approximately equal to τ_{α}, whereas the power spectrum in the aging system is fitted by a power law. The reason for power law scaling for the aging system's spectrum remains unclear.

4 C F W

In Chapter (2) we presented a detailed proof that p-spin models are time reparametrization invariant regardless of the range of the interactions. Using the renormalization group on the action of the Martin-Siggia-Rose generating functional, we showed that there are three families of stable fixed points in the limit of long time differences. The first family of fixed points corresponds to high temperature dynamics and the fixed points are not time reparametrization invariant. The second family of fixed points corresponds to a cross over between high temperature and low temperature dynamics and these fixed points are also not time reparametrization invariant. The third family of fixed points correspond to the low temperature dynamics that is described by the spin-spin interactions and these fixed points are time reparametrization invariant.

The results on the p-spin model are significant because of the connection between the dynamics of p-spin models and structural glasses. Combining this result with the growing evidence from simulations confirming predictions of the time reparametrization approach, it is tempting to speculate that the symmetry can also be found in models of structural glasses. In order to tackle such a problem we need to have a microscopic model of a structural glass and if we are to follow the prescription of the proof we have given here, then such a model should have quenched disorder. This is a challenge for structural glasses because the interactions between different atoms and molecules are not random and change over time as particles get displaced. To overcome the problem of quenched disorder, we could think of adding a fictitious term representing self generated frozen disorder in the theory. Such a term would have to be added with a tunable parameter so that at the end of the calculation we can systematically let it go to zero but still have its impact in the effective theory.

In Chapter (3) we presented the derivation of a method for extracting the local fluctuating phases of the time reparametrizations and showed that their time derivatives

can in some cases be interpreted as instantaneous relaxation times. We showed that the method works and used it to extract the phases in two data sets of molecular dynamics simulation of binary mixtures in which the constituent particles interact via the Weeks-Chandler-Andersen potential. One data set corresponds to a system in equilibrium and the other data set corresponds to an aging system. We proved that the results of the method are robust for both systems by showing that the local phases converge to a unique $\phi_{\vec{r}}(t)$ as the number of data snapshots is increased.

Our results also confirm the prediction that transverse fluctuations will be more dominant for larger coarse graining sizes and low temperatures. Therefore, the results are suggesting that time reparametrization symmetry is a symmetry of the low temperature glass state, since transverse fluctuations are the Goldstone modes of time reparametrizations. Detailed results on the $\phi_{\vec{r}}(t)$ and $\dot{\phi}_{\vec{r}}(t)$ show that there are strong fluctuations that push the time derivative to negative values, rendering its interpretation as a local relaxation rate problematic. The fits we have done for different coarse graining sizes give some support to the idea that local dynamics are exponential but our results are not conclusive because at these small coarse graining sizes, longitudinal fluctuations dominate. We have found that probability distribution functions of $\dot{\phi}_{\vec{r}}(t)$ are non Gaussian, with more deviation from the Gaussian form found in the aging system. For the equilibrium system we found a power spectrum that can be fit by a Lorentzian characterized by a time scale for fluctuations of $\dot{\phi}_{\vec{r}}(t)$ that is of the order of the alpha relaxation time. For the aging system, the spectrum we found is significantly different and the low frequency part is fitted with a power law.

Now that we have a method for extracting the time reparametrization fluctuations, we expect to apply it to other data sets of glassy systems. In these additional studies, it will be interesting to determine if the trend of exponential local dynamics can be found in more systems, and if we find such a trend, how can we explain it given the doubt cast on the

validity of the method by the dominance of longitudinal fluctuations at small coarse graining sizes. We will also be interested in quantifying the changes with time and temperature in the probability distribution functions of $\dot{\phi}_{\vec{r}}(t)$. In addition to power spectra analysis, we are interested in determining spatial correlations of $\dot{\phi}_{\vec{r}}(t)$.

R

[1] L. Leuzzi and T. M. Nieuwenhuizen, *Thermodynamics of the Glassy State* (Taylor and Francis Group, USA).

[2] C. A. Angell, Science **267**, 1924 (1995).

[3] P. G. Debenedetti, F. H. Stillinger, Nature **410**, 259 (2001).

[4] P. Jenniskens, D. F. Blake, Science **265**, 753 (1994).

[5] J. H. Crowe, J. F. Carpenter, L. M. Crowe, Annu. Rev. Physiol. **60**, 73 (1998).

[6] A. L. Greer, Science **267**, 1947 (1995).

[7] L. F. Cugliandolo, Arxiv: cond-mat/0210312v2, (2002).

[8] M. D. Ediger, Annu. Rev. Phys. Chem. **51**, 99 (2000).

[9] H. Sillescu, *J. Non-Crystal. Solids* **243**, 81 (1999).

[10] K. Binder and A. P. Young, Rev. Mod. Physics **58**(4), 801 (1986).

[11] I. M. Hodge, Science **267**, 1945 (1995).

[12] L. C. E. Struik, *Physical Aging in Amorphous Polymers and Other Materials*, (Elservier Amsterdam, 1978).

[13] K. Binder, W. Kob, *Glassy Materials and Disordered Solids* (World Scientific Publishing Co. Pte. Ltd, 2005).

[14] J. M. Rallison and E. J. Hinch, J. Fluid Mech. **167**. 131 (1986).

[15] D. R. Reichman and P. Charbonneau, J. Stat. Mech., P05013 (2005).

[16] P. G. debenedetti, F. H. Stillinger, T. M. Truskett, and C. J. Roberts, J. Phys. Chem. B **103**, 7390 (1999).

[17] T. Keyes, Phys. Rev. E **59**3, 3207 (1999).

[18] M. Schulz, Phys. Rev. B **57**18, 11319 (1998).

[19] S. Sastry, P. G. debenedetti, F. H. Stllinger, Nature **393**, 554 (1998).

[20] E. Vidal Russell, N. E. Israeloff, L. E. Walther, and H. Alvarez Gomariz, Phys. Rev. Lett. **81** 1461 (1998); L. E. Walther, N. E. Israeloff, E. Vidal Russell, and H. Alvarez Gomariz Phys. Rev. B **57** R15112 (1998); E. Vidal Russell and N. E. Israeloff, Nature **408**, 695 (2000).

[21] E. R. Weeks, J. C. Crocker, A. C. Levitt, A. B. Schofield, and D. A. Weitz,Science **287**, 627 (2000);

[22] E. R. Weeks, and D. A. Weitz, Phys. Rev. Lett. **89**, 095704 (2002).

[23] R. E. Courtland and E. R. Weeks, J. Phys.: Condens. Matter **15** ,S359 (2003).

[24] L. Cipelletti, H. Bissig, V. Trappe, P. Ballesta, and S. Mazoyer, J. Phys.: Condens. Matter **15**, S257 (2003).

[25] A. S. Keys, A. R. Abate, S. C. Glotzer, and D. J. Durian, Nature Physics **2007**, 260–264, (2007).

[26] W. Kob, C. Donati, S. J. Plimpton, P. H. Poole, and S. C. Glotzer, Phys. Rev. Lett. **79**, 2827 (1997).

[27] N. Lacevic, F. W. Starr, T. B. Schroder and S. C. Glotzer, *J. Chem. Phys.* **119**, 7372 (2003).

[28] C. Toninelli, M. Wyart, L. Berthier, G. Biroli, and J.-P. Bouchaud, Phys. Rev. E **71**, 041505 (2005).

[29] C. A. Angell, K. L. Ngai, G. B. McKenna, P. F. McMillan, and S. W. Martin, J. Appl. Phys. 88, 3113 (2000).

[30] J. P. Garrahan and D. Chandler, Phys. Rev. Lett. **89**, 035704 (2002).

[31] D. Chandler, and J. P. Garrahan, Annu. Rev. Phys. Chem. **61**, 191 (2010).

[32] X. Xia, P. G. Wolynes, Phys. Rev. Lett. **86**, 5526 (2001).

[33] V. Lubchenko, P. G. Wolynes, J. Chem. Phys. **121**, 2852 (2004).

[34] V. Lubchenko and P. G. Wolynes, Annu. Rev. Phys. Chem. **58**, 235 (2007).

[35] L. F. Cugliandolo, J. Kurchan, J. Phys. A **27**, 5749 (1994).

[36] L. F. Cugliandolo, J. Kurchan, Phys. Rev.Lett. **71**(1), 173 (1993).

[37] C. Chamon, M. P. Kennett, H. E. Castillo, and L. F. Cugliandolo, Phys. Rev. Lett. **89**, 217201 (2002).

[38] H. E. Castillo, C. Chamon, L. F. Cugliandolo, and M. P. Kennett, Phys. Rev. Lett. **88**, 237201 (2002).

[39] H. E. Castillo, C. Chamon, L. F. Cugliandolo, J. L. Iguain, and M. P. Kennett, Phys. Rev. B **68**, 134442 (2003).

[40] H. E. Castillo, Phys. Rev. B **78**, 214430 (2008).

[41] H. E. Castillo and A. Parsaeian, Nat. Phys. **3**, 26 (2007).

[42] A. Parsaeian, H. E. Castillo, Phys. Rev. E **78**, 060105(R) (2008).

[43] A. Parsaeian, H. E. Castillo, Phys. Rev. Lett. **102**, 055704 (2009).

[44] A. Parsaeian and H. E. Castillo, arXiv:0811.3190 (2008).

[45] G. A. Mavimbela, H. E. Castillo, J. Stat. Mech., P05017 (2011).

[46] K. E. Avila, H. E. Castillo, and A. Parsaeian, Phys. Rev. Lett. **107**, 265702 (2011).

[47] K. E. Avila, H. E. Castillo, and A. Parsaeian, *in preparation*.

[48] N. Goldenfeld, *Lectures on Phase Transitions and the Renormalization Group* (Addison-Wesley Publishing Company, USA, 1992).

[49] V. Cannella, and J. A. Mydosh, Phys. Rev. B **6**, 4220 (1972).

[50] C. A. M. Mulder, A. J. van Dyneveldt, and J. A. Mydosh, Phys. Rev. B **23**, 1384 (1981).

[51] ed. A. P. Young *Spin Glasses and Random Fields* (World Scientific Publishing Co, Singapore, 1998).

[52] T. R. Kirkpatrick, D. Thirumalai, Phys. Rev. B **36**, 5388 (1978).

[53] M. Campellone, G. Parisi, P. Ranieri, Phys. Rev. B **59**(2), 1036 (1999).

[54] M. A. Moore, Barbara Drossel, Phys. Rev. Lett. **89(21)**, 217202 (2002).

[55] C. Chamon, L. F. Cugliandolo, H. Yoshino, J. Stat. Mech, P01006 (2006).

[56] C. De Dominicis, L. Peliti, Phys. Rev. B **18**, 353 (1978).

[57] H. Sompolinsky and A. Zippelius, Phys. Rev. Lett. **47**(5), 359 (1981).

[58] H. Sompolinsky and A. Zippelius, Phys. Rev. B, **25**(11), 6860 (1982).

[59] A. Crisanti, and H. J. Sommers, Z. Phys. B-Condensed Matter, **87**, 341 (1992).

[60] A. Crisanti, H. Horner and H. J. Sommers, Z. Phys. B-Condensed Matter, **92**, 257 (1993).

[61] A. Atland and B. Simons, *Condensed Matter Field Theory* (Cambridge University Press, Cambridge, UK, 2010).

[62] M. Kardar, *Statistical Physics of Fields* (Cambridge University Press, Cambridge, UK, 2007).

[63] M. E. Peskin, D. V. Schroeder, *An Introduction to Quantum Field Theory* (Westview Press, USA, 1995).

[64] A. Zee, *Quantum Field Theory in a Nutshell* (Princeton University Press, USA, 2003).

[65] T. R. Kirkpatrick, P. G. Wolynes, Phys. Rev. A **35**, 3072 (1987).

[66] R. Bohmer et. al, J. of Non-Crystalline Solids, 235 (1998).

[67] A. Parsaeian, Ph.D thesis, Ohio University, 2009.

[68] W. Zwerger, *Phys. Rev. Lett.* **92**, 027203 (2004).

[69] C. Chamon, P. Charboneau, L. F. Cugliandolo, D. R. Reichmann and M. Sellitto, J. Chem. Phys. **121**, 10120 (2004).

[70] L. Cipelletti, H. Bissig, V. Trappe, P. Balletsa and S. Mazoyer, J. Phys.: Condens. Matter **15**, S257 (2003).

[71] N. R. Lomb, Astrophysics and Space Science **39**, 447 (1976).

[72] W. H. Press, S. A. Teukolsky, W. T. Vetterling and B. P. Flannery, *Numerical Recipes in Fortran 77*(Cambridge University Press, UK, 1996).

[73] M. B. Weissman, Rev. Mod. Phys. **60**(2), 537 (1988).

[74] A. Travesset, R. A.White and K. A. Dahmen, Phys. Rev. B **66**, 024430 (2002).

[75] D. S. Dean, 1996 J. Phys. A: Math. Gen. **29**, L613 (1996).

[76] A. Andreanov, G. Biroli, A. Lefevre, J. Stats. Mech.: Theory and Experiment, 1742 (2006).

A A: M -S -R F

A.1 From the Langevin Equation to the Generating Functional

A field theory description for the relaxation of an N-particle interacting system can be achieved in several ways. One possibility is to derive a field theory in a system with Newtonian dynamics, via a non-linear hydrodynamics approach [76]. Another possibility is to consider a system in contact with a thermal bath. In this case, the bath introduces noise in the microscopic equations of motion, resulting in stochastic dynamics (Langevin dynamics). De Dominicis and Peliti developed a formalism for determining the generating functional for a system with Langevin dynamics in terms of field variables [56]. It starts from the Langevin equation

$$\partial_t \phi_j(t) = -\frac{\delta H}{\delta \phi_j(t)} + \eta_j(t), \tag{A.1}$$

where H is the Hamiltonian, the $\{\phi_j\}_{j=1,\cdots,N}$ are the field variables and $\{\eta_j\}_{j=1,\cdots,N}$ are random variables representing the thermal noise, with zero mean and a variance proportional to the bath temperature ($\langle \eta_j(t) \rangle = 0$ and $\langle \eta_j(t)\eta_i(t') \rangle = 2T\delta_{ij}\delta(t-t')$). An alternative description of the dynamics of the Langevin equation is given by the generating functional,

$$Z_\eta[l] = \int D\phi J[\phi] \prod_{j,t} \delta\left(\partial_t \phi_j(t) + \frac{\delta H}{\delta \phi_j(t)} - \eta_j(t)\right) \exp\left(\int_{t_0}^{t_f} dt \sum_{j=1}^{N} l_j(t)\phi_j(t)\right), \tag{A.2}$$

where the $\{l_j(t)\}_{j=1,\cdots,N}$ are external sources and $J[\phi]$ is the Jacobian associated with the argument of the delta function,

$$J[\phi] = \exp\left(-\frac{1}{2}\int_{t_0}^{t_f} dt \frac{\delta^2 H}{\delta \phi_i(t)\delta \phi_j(t)}\right). \tag{A.3}$$

This term can in principle contribute to the action but will be ignored from now on[2]. Using a conjugate field $\hat{\phi}_j(t)$ we can write the delta function as an integral of an imaginary

[2] For harmonic systems this term only contributes a constant to the action and can therefore be dropped. Even in anharmonic systems this contribution is usually safely ignored

exponential. If we integrate over the noise we obtain the generating functional,

$$Z_\eta[l] = \int D\phi D\hat{\phi} \exp\left(L[\phi, \hat{\phi}] + \int_{t_0}^{t_f} dt \sum_{j=1}^{N} \left[l_j \phi_j + i\hat{l}_j \hat{\phi}_j \right] \right). \tag{A.4}$$

where we have omitted writing the time variables for simplicity and added an external source for the conjugate field. The action is given by

$$L[\phi, \hat{\phi}] = -i \int_{t_0}^{t_f} dt \sum_{j=1}^{N} \left[\hat{\phi}_j \left(\partial_t \phi_j + \frac{\delta H}{\delta \phi_j(t)} - iT\hat{\phi}_j \right) \right]. \tag{A.5}$$

This formalism developed in reference [56] has been used in references [40] and [76] and we use it in our work to determine the generating functional, of the system we study.

A.2 The Generating Functional as a Generator of Correlations and Responses

The correlation functions of ϕ_j's are obtained from the generating functional by taking derivatives with respect to the source l_j's [56]. The most general correlation function is given by

$$\begin{aligned} C_p(1, t_1; ...; p, t_p) &= Z^{-1}[0] \frac{\delta^p}{\delta l_1(t_1) \cdots \delta l_p(t_p)} Z[l, h]|_{l=h=0} \\ &= \langle \phi_1(t_1) \cdots \phi_p(t_p) \rangle \end{aligned}$$

The response functions are obtained from the generating functional by taking derivatives with respect to the physical external fields h_i's coupled to the auxiliary fields $\hat{\phi}_i$'s. The most general response function is given by [7]

$$\begin{aligned} R_p(0, t_0 | 1, t_1; ...; p-1, t_{p-1}) &= Z^{-1}[0] \frac{\delta^p}{\delta l_0(t_0) \delta h_1(t_1) \cdots \delta h_{p-1}(t_{p-1})} Z[l, h]|_{l=h=0} \\ &= Z^{-1}[0] \frac{\delta^{p-1}}{\delta h_1(t_1) \cdots \delta h_{p-1}(t_{p-1})} \langle \phi_0(t_0) \rangle|_{l=h=0}. \end{aligned}$$

The usual two time correlation and response functions are recovered by setting $p = 2$.

A B: T R G

B.1 Wilson's Approach to the Renormalization Group

The renormalization group (RG) is a theoretical framework for calculating the relationship between coupling constants at different length scales. To illustrate how it works, we consider the $\lambda\phi^4$ theory [63]. The generating functional of this theory is given by

$$Z = \int [D\phi]_\Lambda \exp\left(-\int d^dx \left[\frac{1}{2}(\partial_\mu\phi)^2 + \frac{1}{2}m^2\phi^2 + \frac{\lambda}{4!}\phi^4\right]\right), \tag{B.1}$$

where in the differential $[D\phi]_\Lambda = \prod_{|k|<\Lambda} d\phi(k)$, we have introduced a cutoff in the momentum to cure divergences that result from high momentum integrals. The first step is to divide the integration variables $\phi(k)$ into two groups. We choose a fraction $b < 1$ and use it to define high momentum degrees of freedom $\phi_>(k) = \phi(k) \Leftrightarrow b\Lambda \leq |k| < \Lambda$. In this construction the old ϕ becomes $\phi_< + \phi_>$ and the functional becomes,

$$Z = \int D\phi_< e^{-L[\phi_<]} \int D\phi_> \exp\left(-\int d^dx \left[\frac{1}{2}(\partial_\mu\phi_>)^2 + \frac{1}{2}m^2\phi_>^2 + \lambda V[\phi_<, \phi_>]\right]\right), \tag{B.2}$$

where $V[\phi_<, \phi_>] = \frac{1}{6}\phi_<^3\phi_> + \frac{1}{4}\phi_<^2\phi_>^2 + \frac{1}{6}\phi_<\phi_>^3 + \frac{1}{4!}\phi_>^4$. Integrating over the high momentum degrees of freedom gives,

$$Z = \int [D\phi]_{b\Lambda} \exp\left(-L_{\text{eff}}\right) \tag{B.3}$$

where the effective action $L_{eff}[\phi]$ contains the degrees of freedom $\phi(k)$ with $|k| < b\Lambda$. $L_{eff}[\phi] = L[\phi]$+corrections, where the corrections are powers of λ. They compensate for the removal of the high momentum degrees of freedom. The second step is to compare the original functional with the functional that results from integrating over the high momentum degrees of freedom. To do this we rescale momenta and distances according to $k' = k/b$, $x' = xb$ so that the original integration range, $|k'| < \Lambda$ is restored. We also rescale the field by some parameter $A(b)$ (i.e $\phi' = A(b)\phi$). The last step is to read off the effect of the high momentum integration. From this procedure, differential equations

called *flow equations* are obtained that describe the evolution of the mass and coupling constant as a function of the scale.

B.2 Renormalization Group Over the Time Variable

Chamon et. al [37, 38, 39, 40] recognized that Wilsons formalism can be implemented for the time variables in the Martin-Siggia-Rose generating functional for non-equilibrium dynamics problems, particularly for spin glass models [37, 38, 39, 40]. Furthermore, the cut-off is defined on short time differences, $\tau_0 < |t - t'|$. In the spin glass problem, the crucial degrees of freedom are two time fields $Q(t, t') \sim \langle \phi(t)\phi(t') \rangle$ instead of single variable fields $\phi(t)$. A detailed discussion of the method can be found in Ref. [40].

A C: E L R T N D

Here we present some extra details about the derivation of the method for extracting local phases from numerical or experimental data, which we omitted in Sec. 3.3. We start by considering the minimization of $\overline{\epsilon}(\{\phi_1, \cdots, \phi_M\}; \vec{\alpha})$, defined by Eq. (3.26). By using the definition of Φ_{ji} in Eq. (3.27), and explicitly writing the terms in the Taylor expansion $g^{(1)}(\phi_j - \phi_i; \vec{\alpha})$ we rewrite $\overline{\epsilon}$ to obtain

$$\begin{aligned} & \overline{\epsilon}(\{\phi_1, \cdots, \phi_M\}; \vec{\alpha}) \\ = \; & \eta^{-1}(M) \sum_{1 \le i < j \le M} \left(g\left(\Phi_{ji}; \vec{\alpha}\right) - \left\{ g\left(\Phi_{ji}; \vec{\alpha}\right) + g'\left(\Phi_{ji}; \vec{\alpha}\right) \left[(\phi_j - \phi_i) - \Phi_{ji} \right] + \cdots \right\} \right)^2 \\ = \; & \frac{1}{2\eta(M)} \sum_{1 \le i, j \le M} \left\{ g'\left(\Phi_{ji}; \vec{\alpha}\right) \left[(\phi_j - \phi_i) - \Phi_{ji} \right] + \cdots \right\}^2 \end{aligned} \tag{C.1}$$

where the terms omitted are of quadratic order in $\left((\phi_i - \phi_j) - \Phi_{ij} \right)$. In the last line we have allowed both $i > j$ and $i < j$ terms to appear in the sum, and we have defined $\Phi_{ii} \equiv 0$ so that $i = j$ terms are identically zero. We now impose the condition that all derivatives of $\overline{\epsilon}$ with respect to ϕ_k be zero,

$$0 = \frac{\partial \overline{\epsilon}}{\partial \phi_k} = \eta^{-1}(M) \sum_{i=1}^{M} g'^2\left(\Phi_{ik}; \vec{\alpha}\right) \left[(\phi_i - \phi_k) - \Phi_{ik} \right], \tag{C.2}$$

where we have used the fact that $g(-x) = g(x)$ and therefore $g'(-x) = -g'(x)$. Hence for $1 \le k \le M$, we have the minimization conditions:

$$\sum_{i=1}^{M} g'^2\left(\Phi_{ik}; \vec{\alpha}\right) \Phi_{ik} - \sum_{i=1}^{M} g'^2\left(\Phi_{ik}; \vec{\alpha}\right) \phi_i + \phi_k \sum_{i=1}^{M} g'^2\left(\Phi_{ik}; \vec{\alpha}\right) = 0 \tag{C.3}$$

We express the minimization conditions in terms of the equivalent matrix equation

$$\vec{\hat{w}} = \hat{A} \vec{\phi}, \tag{C.4}$$

with the definition of the M-component vector $\vec{\hat{w}}$

$$\hat{w}_k \equiv \sum_{i=1}^{M} g'^2\left(\Phi_{ik}; \vec{\alpha}\right) \Phi_{ik} \tag{C.5}$$

and the $M \times M$ matrix $\hat{A}$

$$\hat{A}_{ki} \equiv g'^2\left(\Phi_{ik}; \vec{\alpha}\right) - \delta_{ki} \sum_{j=1}^{M} g'^2\left(\Phi_{jk}; \vec{\alpha}\right). \tag{C.6}$$

The system of equations described by Eq. (C.4) is singular, since the nonzero vector $\vec{\phi}_0 \equiv (1, ..., 1)$ satisfies $\hat{A}\vec{\phi}_0 = \vec{0}$, which indicates that the rank of the matrix $\hat{A}$ is at most $M - 1$. In particular, any solution $\vec{\phi}$ of Eq. (C.4) can be modified by adding an arbitrary multiple of $\vec{\phi}_0$ to obtain another solution. This degeneracy is associated with the gauge symmetry that the problem has under the shift $\phi_k \to \phi_k + \rho$, which is a consequence of the fact that in Eq. (3.13) the phases appear in a difference. To eliminate this degeneracy, we impose the additional condition that the projection of the solution $\vec{\phi}$ on the direction of $\vec{\phi}_0$ should be zero, thus obtaining the gauge fixing condition of Eq. (3.28). By combining the gauge fixing condition with Eq. (C.4) above, we obtain a system of $M + 1$ equations with M unknowns:

$$\vec{\hat{w}} = \hat{A}\vec{\phi} \quad \text{and} \quad \vec{\phi}_0 \cdot \vec{\phi} = 0. \tag{C.7}$$

Since one of the equations is a linear combination of the others, the solution is well defined and unique. Hence, we omit the first equation, for $k = 1$, which is redundant, and solve

$$\vec{w} = \bar{A}\vec{\phi}, \tag{C.8}$$

where $\vec{w}$ and $\bar{A}$ are given by

$$\begin{aligned}
\bar{w}_k &\equiv \begin{cases} 0 & : \quad k = 1 \\ \hat{w}_k = \sum_{i=1}^{M} g'^2\left(\Phi_{ik}; \vec{\alpha}\right) \Phi_{ik} & : \quad k \neq 1 \end{cases} \\
\bar{A}_{ki} &\equiv \begin{cases} 1 & : \quad k = 1 \\ \hat{A}_{ki} = g'^2\left(\Phi_{ik}; \vec{\alpha}\right) - \delta_{ki} \sum_{j=1}^{M} g'^2\left(\Phi_{jk}; \vec{\alpha}\right) & : \quad k \neq 1. \end{cases}
\end{aligned} \tag{C.9}$$

which is the same as Eq. (3.31).

We now turn to the determination of the local phase fluctuations $\delta\phi_{i\vec{r}}$, which requires minimizing the expression for ϵ in Eq. (3.22). Here the derivation is very similar to the

previous case. We start by using the definition of $\delta C_{\vec{r}}(t,t')$ in Eq. (3.16) to rewrite ϵ as

$$\begin{aligned}&\epsilon(\{\delta\phi_{\vec{r}}(t_i)\};\vec{\alpha},\{C_{\vec{r}}(t_j,t_i)\})\\&=\frac{1}{2\eta(M)}\sum_{1\le i,j\le M}\left\{\delta C_{\vec{r}}(t_j,t_i)-g'(\phi(t_j)-\phi(t_i);\vec{\alpha})\left[\delta\phi_{\vec{r}}(t_j)-\delta\phi_{\vec{r}}(t_i)\right]\right\}^2.\end{aligned}\tag{C.10}$$

We then impose the condition that the derivatives with respect to all of the phase fluctuations $\delta\phi_{k\vec{r}}$ must be zero,

$$0=\frac{\partial\epsilon}{\partial\delta\phi_{k\vec{r}}}=-2\eta^{-1}(M)\sum_{i=1}^{M}\left[\delta C_{ki\vec{r}}-g'\left(\phi_k-\phi_i;\vec{\alpha}\right)\left(\delta\phi_{k\vec{r}}-\delta\phi_{i\vec{r}}\right)\right]g'\left(\phi_k-\phi_i;\vec{\alpha}\right).\tag{C.11}$$

This is equivalent to imposing, for $1\le k\le M$, the conditions

$$\sum_{i=1}^{M}g'\left(\phi_k-\phi_i;\vec{\alpha}\right)\delta C_{ki\vec{r}}=\delta\phi_{k\vec{r}}\sum_{i=1}^{M}g'^2\left(\phi_k-\phi_i;\vec{\alpha}\right)-\sum_{i=1}^{M}g'^2\left(\phi_k-\phi_i;\vec{\alpha}\right)\delta\phi_{i\vec{r}}.\tag{C.12}$$

This set of conditions can be written as the matrix equation

$$\tilde{w}_{\vec{r}}=\tilde{A}\delta\phi_{\vec{r}},\tag{C.13}$$

where

$$\tilde{w}_{k\vec{r}}\equiv\sum_{j=1}^{M}g'\left(\phi_k-\phi_j;\vec{\alpha}\right)\delta C_{kj\vec{r}}\quad\text{and}\quad\tilde{A}_{ki}\equiv\delta_{ki}\sum_{j=1}^{M}g'^2\left(\phi_k-\phi_j;\vec{\alpha}\right)-g'^2\left(\phi_k-\phi_i;\vec{\alpha}\right).\tag{C.14}$$

From here, the steps are almost identical to those for the determination of the global phases. Just as in that case, we have a degeneracy resulting from the shift symmetry under the transformation $\delta\phi_{k\vec{r}}\to\delta\phi_{k\vec{r}}+\rho_{\vec{r}}$, where $\rho_{\vec{r}}$ is time independent. We again modify the system of equations by imposing an additional constraint, given by Eq. (3.32), that removes the degeneracy. Here again we omit the redundant equation corresponding to $k=1$, and thus finally recover Eqs. (3.33) and (3.35).

C.1 Proof of the Orthogonality of δC^T and δC^L

In this section we prove Eq. (3.40). We start by applying the definition of the Euclidean scalar product in Eq. (3.38),

$$\left(\delta C^T|\delta C^L\right) = \frac{2}{\omega M(M-1)} \sum_{1\le i<j\le M} \sum_{\vec{r}} \langle \delta C^T_{\vec{r}}(t_j,t_i)\delta C^L_{\vec{r}}(t_j,t_i)\rangle. \tag{C.15}$$

We now insert the definitions of δC^T and δC^L, given by Eqs. (3.18) and (3.20), and obtain

$$\left(\delta C^T|\delta C^L\right) = \frac{1}{\omega M(M-1)} \sum_{1\le j,i\le M} \sum_{\vec{r}} \langle g'(\phi_j-\phi_i)\left(\delta\phi_{j\vec{r}}-\delta\phi_{i\vec{r}}\right)\left\{\delta C_{ji\vec{r}} - g'(\phi_j-\phi_i;\vec{\alpha})\left[\delta\phi_{j\vec{r}}-\delta\phi_{i\vec{r}}\right]\right\}\rangle, \tag{C.16}$$

where we have removed the restriction $j > i$. By using the symmetry of the terms under the exchange of indices $i \leftrightarrow j$, we rewrite this expression as

$$\left(\delta C^T|\delta C^L\right) = \frac{1}{\omega M(M-1)} \left\langle \sum_{\vec{r}} \sum_{j=1}^{M} \delta\phi_{j\vec{r}} \sum_{i=1}^{M} g'(\phi_j-\phi_i)\left\{\delta C_{ji\vec{r}} - g'(\phi_j-\phi_i;\vec{\alpha})\left[\delta\phi_{j\vec{r}}-\delta\phi_{i\vec{r}}\right]\right\}\right\rangle. \tag{C.17}$$

We now recognize that, by Eq. (C.11), the sum over the index i is zero, and therefore the whole expression is zero, which gives us the result that $\left(\delta C^T|\delta C^L\right) = 0$.

A D: G G D

In Ref. [69] Chamon *et al.* describe the main features of a generalized Gumbel distribution and two important limits of the distribution. The distribution is given by

$$P_a(x) = \frac{|\alpha| a^a}{\Gamma(a)} \exp\left\{a\left[\alpha(x - x_0) - \exp(\alpha(x - x_0))\right]\right\}, \tag{D.1}$$

where $\Gamma(a)$ is the *gamma* function. The parameter x_0 controls the center and the parameter α controls the width of the distribution. The distribution becomes a Gaussian of unit variance in the limit $a \to \infty$ while $\alpha^2 a = 1$, that is $|\alpha| \to 0$. Starting form the generalized distribution and taking this limit we get

$$\begin{aligned}
&\lim_{a\to\infty,\alpha^2 a=1} P_a(x) \\
&= \lim_{a\to\infty,\alpha^2 a=1} \frac{a^a}{\sqrt{a}\Gamma(a)} \exp\left\{a\left[\alpha(x - x_0) - 1 - \alpha(x - x_0) - \frac{1}{2}\alpha^2(x - x_0)^2 - O(\alpha^3)\right]\right\} \\
&= \lim_{a\to\infty,\alpha^2 a=1} \frac{a^a}{\sqrt{a}\Gamma(a)} \exp\left[-a - \frac{1}{2}\alpha^2 a(x - x_0)^2 + O(\alpha^3)\right] \\
&= \lim_{a\to\infty} \frac{a^a \exp(-a)}{\sqrt{a}\Gamma(a)} \exp\left[-\frac{1}{2}(x - x_0)^2\right] \\
&= \frac{1}{\sqrt{2\pi}} \exp\left[-\frac{1}{2}(x - x_0)^2\right],
\end{aligned} \tag{D.2}$$

where in the last step we have used Stiling's formula for the gamma function $\Gamma(a) \approx \sqrt{\frac{2\pi}{a}} a^a \exp(-a)$ for large a.

The other important limit is found when $a \to 0$ with $|\alpha| a = 1$, that is $\alpha = 1/a \to \infty$. Since we can have $\alpha < 0$ or $\alpha > 0$ and $x - x_0 < 0$ or $x - x_0 > 0$ we need to consider four cases when taking this limit. Before considering the four cases we note that the normalization factor goes to unity in this limit. First we consider the limit $a \to 0$ with $\alpha < 0$ and $x - x_0 < 0$:

$$\begin{aligned}
\lim_{a\to 0,\alpha<0,x-x_0<0} P_a(x) &= \exp[-(x - x_0)] \exp[-e^{\alpha(x-x_0)}] \\
&= \exp[-(x - x_0)] \times 0 = 0
\end{aligned} \tag{D.3}$$

where we have used the fact that the double exponential goes to zero given the signs of the exponents. The second case is given by the limit $a \to 0$ with $\alpha < 0$ and $x - x_0 > 0$. In this case the double exponential goes to unity and we have

$$\begin{aligned} \lim_{a\to 0,\alpha<0,x-x_0<0} P_a(x) &= \exp[-(x - x_0)] \\ &= \exp[sgn\alpha(x - x_0)]. \end{aligned} \tag{D.4}$$

Repeating this analysis for the other two cases in which $\alpha > 0$ we find that we can summarize the results of taking the limit $a \to 0$ with $|\alpha|a = 1$ as follows

$$\lim_{a\to 0,|\alpha|a=1} P_a(x) = \exp[(sgn\alpha)(x - x_0)]\theta[-sgn\alpha(x - x_0)]. \tag{D.5}$$

Therefore, the limit $a \to 0$ leads to exponential distributions starting or ending at $x = x_0$ depending on the sign of α.

Thesis and Dissertation Services